ROBUST MOLECUAR PREDICTIVE METHODS FOR NOVEL POLYMER DISCOVERY AND APPLICATIONS

DE-SC0017710

SHEETA GLOBAL TECHNOLOGY CORPORATION
PRINCIPAL INVESTIGATOR: CHENGYANG (RAYMOND) JIANG, PH.D.
RESEARCH ORGANIZATION: CALIFORNIA INSTITUTE OF TECHNOLOGY
PROFESSOR WILLIAM A. GODDARD, III
ANDRES JARAMILLO-BOTERO, PH.D.

PROJECT MANAGER: JOHN MA, PH.D
CONTACT INFORMATION
738 ARROW GRAND CIRCLE, COVINA, CA 91722
JOHN.MA@SHEETAGLOBAL.COM
(909)510-7819

PROJECT PERIOD: 08/27/2018 – 08/26/2020
REPORT SUBMISION DATE: 12/23/2020
REPORTING PERIOD: 08/27/2018 – 08/26/2020

Disclaimer

This report was prepared as an account of work sponsored by an agency of the United States Government. Neither the United States Government nor any agency thereof, nor any of their employees, makes any warranty, express or implied, or assumes any legal liability or responsibility for the accuracy, completeness, or usefulness of any information, apparatus, product, or process disclosed, or represents that its use would not infringe privately owned rights. Reference herein to any specific commercial product, process, or service by trade name, trademark, manufacturer, or otherwise does not necessarily constitute or imply its endorsement, recommendation, or favoring by the United States Government or any agency thereof. The views and opinions of authors expressed herein do not necessarily state or reflect those of the United States Government or any agency thereof.

20 YEAR SBIR/STTR DATA RIGHTS (2019)

Funding Agreement No DE-SC0017710

Award Date September 11, 2018

SBIR/STTR Protection Period: Twenty years from Award Date

SBIR/STTR Awardee: Sheeta Global Tech Corp.

This report contains SBIR/STTR Data to which the Federal Government has received SBIR/STTR Technical Data Rights or SBIR/STTR Computer Software Rights during the SBIR/STTR Protection Period and Unlimited Rights afterwards, as defined in the Funding Agreement. Any reproductions of SBIR/STTR Data must include this legend.

Table of Contents

1. Executive Summary

Polymeric materials are ubiquitous in modern society and they play an instrumental role in almost all industries, undoubtedly including the energy and environment sectors. Increased demand of energy and awareness to sustainability both necessitates the development of novel polymers with enhanced properties. Unfortunately, their structural and behavioral complexity render such discovery challenging and impeded. To address this problem, scientists are developing various computational modeling techniques and leveraging their power to depict the relationship between structural characteristics of polymers and their properties (such as rheological behaviors), and use such prediction to guide the design and syntheses of novel polymeric materials with enhanced performances.

Unfortunately, predicting the relationships between polymer structure and composition with rheological properties via atomistic modeling is still a major challenge because of the extended time and length scales involved. Studying dynamic shear viscosity and linear viscoelasticity using molecular models requires capabilities that have been elusive, including representation of large molecular weight chains with an effective internal scale capable of describing entanglement, shear-rates that are in the s^{-1} scale with accurate quantitative stresses, and chemically-realistic combinations of both homogeneous and heterogeneous systems.

Motivated by these unmet challenges, the overall technical objective of this DOE-STTR Phase II project is to develop robust molecular predictive methods for advanced polymer discovery and applications and especially for designing and demonstrating the "smart" polymer-based waterflooding enhanced oil recovery (EOR) process. In particular, we apply state-of-the-art molecular modeling methods developed by our academic partner, Materials Stimulation Center (MSC) at California Institute of Technology (Caltech), to facilitate and accelerate the experimental discovery processes. During the Phase I of this project, we had focused on development and demonstration of the molecular modeling methods to describe rheological properties of non-Newtonian polymer fluids, and to improve our fundamental understandings of shear-thickening mechanism and kinetics. In Phase II, we further apply the theoretical models to guide our experimental programs to improve our design of smart rheology modifier (SRM) polymers and their optimization for EOR. Specifically, we have three objectives in the Phase II study: (1) to further improve out computational modeling methods, coupling with the advanced machine learning algorithms; (2) to develop cost-effective and efficient SRM-flooding process suitable for EOR applications under typical reservoir conditions; and (3) to further explore the application of our molecular predictive models for innovative material discovery in other industrial applications.

The recent development of our multiscale predictive framework allows the successful prediction of rheological properties from the chemical structure for polymers of experimentally relevant molecular weights, and provides an in-silico machine learning engine for screening novel compositions and structures with optimized non-Newtonian response, required for both shear-

thinning and shear-thickening applications. Our framework provides: (1) procedures and tools for systematic coarsening from atomistic models and reverse mapping of coarse-grain models to atomistic, (2) unique ab initio methods to characterize the atomistic origin of colloidal and interfacial interactions and phenomena, (3) systematic structure and composition builders based on practical descriptors that drive rheological changes in polymer melts and diluted polymer mixtures, (4) a rheological properties engine capable of predicting viscosity in the zero-shear limit and under realistic dynamic conditions (for shear-rates commensurate with experiments) for large heterogeneous systems, (5) coarse-grain force fields with improved non-bond descriptions based on accurate quantum mechanics, (6) an in-silico screening machine learning engine that feeds from the systematic model builders to cover the descriptors search space, computes the rheological properties from converged trajectories spanning sub-milliseconds and ranks them for each structure/composition using an automated viscosity-vs-shear rate fitness function that can be tuned for shear-thickening, shear-thinning and other rheological responses.

2. Background Information

2.1 Polymer Flooding for Enhanced Oil Recovery

Applying EOR to the two-thirds of proved oil reserves left within reservoirs has been recognized as one of the realistic paths to fill the worldwide energy gap. Chemical EOR processes involve the injection of a fluid containing small amount of chemical additives into a reservoir to assist oil flowing to the production well. Improving volumetric sweep efficiency is considered an essential factor for the success of chemical EOR. Polymer flooding (P-flood) involves the addition of water-soluble, high molecular-weight (MW, typically >10 million Da) polymers, in order to thicken the injection fluid and improve the sweeping efficiency, known as "conformance control". Polymers used for this purpose are also referred to as fluid viscosifying agent (FVA). In some occasions, polymers (either crossed-linked or self-associated) are also included to divert the injection fluid to more oil-rich zones. Polymers used for this purpose are referred to as fluid diverting agent (FDA).

A number of polymer-augmented flooding EOR projects have been implemented in US since 1960's. However, mobility control alone does not ensure adequate microscopic displacement efficiency and may result in a low recovery rate. Manning et al. analyzed statistical data of field-wide projects and found the median recovery rate of oil was 2.91% OOIP.[1]Schurz et al. summarized results from 99 projects initiated during 1980-1989 and found that the projected median incremental oil recovery range is between 3.7% and 4.8%.[2]The main reason for the low oil recovery rate has been recognized as the inability to control the breakthrough of water in high permeability (high-K) zones,[3] which is commonly referred as "poor conformance". In other words, the injected displacing fluid preferentially flows through the most permeable zones of the

[1]Manning, R. K.; Pope, G. A.; Lake, L. W. *A Technical Survey of Polymer Flooding Projects*; Bartlesville, OK, 1983.
[2]Schurz, G. F.; Martin, F. D.; Seright, R.; Weiss, W. W. *Polymer-Augmented Waterflooding and Control of Reservior Heterogeneity*. In *New Mexico Tech Centennial Symposium*; 1989; pp 263–275.
[3] Reisberg, J. *Secondary and Tertiary Oil Recovery Process*. US3653440A.

reservoir, thus leading to the premature breakthrough of the displacing fluid at the production well. In consequence, the injected fluid will bypass the remaining oil regions such that only a small portion of oils can be swept out. Poor conformance control is a direct consequence of the loss of viscosity of polymer solutions under high shear rates.

One possible approach for improving the sweep efficiency of P-flood is to design special polymers, which when incorporated into stimulation fluids, could unusually increase the fluid viscosity under high shear rate experienced in the reservoir (a phenomenon known as the "shear-thickening") but return to base fluid viscosity upon reaching even higher shear regions of the injection and production wells. We term these polymer fluids as Smart Rheology Modifier (SRM) fluids. Such SRM fluid is promising for the application of EOR conformance control where the polymer solution will beneficially block the high permeability zone due to the thickening effect induced by shear.

Polyacrylamide (PAM) is a polymer formed from acrylamide (AM) subunits (-$CH_2CH(CONH_2)$-). As one of the few ultrahigh MW hydrophilic polymers, PAM has found wide applications in water treatment and oilfield operations, especially EOR flooding. In recent years, associative PAM-based polymers have drawn a great attention not only for their tolerance to salts and mechanical stability, but also the unique rheological properties induced by the intra/inter molecular interactions. The viscosification of the polymer solution can be achieved by ultrahigh MW, chain/coil expansion, and/or intermolecular 3D network in solution. "Shear thinning effect", the non-Newtonian behavior of fluids whose viscosity decreases under shear strain, is commonly observed in polymer solutions. This is particularly the case for the high-MW PAM and hydrolyzed PAM (HPAM)-based solution fluids. Such "shear-thinning" fluids are problematic when applied in EOR flooding in reservoirs with high heterogeneity. Because the shear strain in a high-k zone is higher than that in a low-k zone, if the fluid viscosity is reduced in the high-k zone, the flow rate will further increase, thus leading to the earlier breakthrough.

The prototypes of our "shear-thickening" polymers are the PAM/HPAM-based water-soluble polymer classes that involve additions of small portions of specially functionalized monomers. In order to carefully control the rheological behavior in the solution, one must combine molecular design knowledge with synthesis techniques to sensibly select the polymer backbone and structure, distribution, and percentage of special functional groups. The systematic elucidation of polymer structural and rheological relationships to flow behavior of SRM fluids in porous media will be essential for the development and implementation of the SRM-based EOR processes.

2.2 Molecular Modeling

Substantial advances have been made in manufacturing through intelligent systems for materials discovery, such as in the discovery of heterogeneous catalysts and thin films for energy applications (photovoltaics, fuel cells, batteries), where advanced Quantum Mechanics (QM) Density Functional Theory (DFT) methods are applied to model crystalline systems (< 300 atoms per periodic cell, dynamical times of < 20 picoseconds) for rapid screening of materials

compositions and crystal structural types. However, these standard approaches are generally not useful for polymer discovery, mainly because of the size and time scales involved in modeling amorphous polymer cells with linear or branched chains of high molecular weight and relatively long relaxation time.

Newtonian fluids are characterized by a single viscosity coefficient for a particular temperature, in dependent of the strain rate. Fluids whose viscosity changes as a function of the strain rate (the relative flow velocity) are called non-Newtonian fluids. Viscosity is important for pure liquids and solvated molecules, as it influences their rates of rotational diffusion and conformational change. It can be interpreted as the propensity of a fluid to transmit momentum perpendicular to the direction of momentum flow (shear direction). Since it is a kinetic property, not just purely thermodynamic, it offers a good opportunity for us to estimate it for simple fluids from our quantum chemistry based molecular dynamics (MD) potentials in molecular dynamics simulations. In addition, the experimental measurement of the fluid viscosity as a function of strain is quite straightforward, giving us a means to compare theory vs experiments, albeit the differences in scales as explained next.

Identifying the mechanisms that drive non-Newtonian behaviors in complex fluids with polymers, such as those expected in EOR applications, requires knowledge of the molecular composition and its long-term dynamics as a function of relatively low shear rates; seemingly juxtaposed goals need to be addressed. Shear-thinning non-Newtonian fluids, exhibit an increase in relative flow velocity that causes a reduction in viscosity, or thixotropy, for example, by stirring. Shear-thickening (or dilatant) non-Newtonian fluids on the other hand, show the opposite effect, rheopecty, or the increase in viscosity with relative deformation. We are particularly interested, in the anomaly of shear-thickening at high shear rates can be observed under certain conditions for high MW polymers dissolved in low-viscosity Newtonian solvents (e.g. water). Although the shear-thinning phenomenon is understood and accepted as an intra-molecular effect occurring because of the extension and orientation of the polymer chains in solution, there is no consensus in explaining the origin of shear thickening yet.

Consequently, it is imperative to establish a link between the molecular constituents and the macroscopic rheological properties. Doing so will enable optimal processing, design and application of polymeric materials for a number of applications, including EOR. The difficulty in realizing this comes from the wide range of spatial and temporal scales involved in the characterization of polymeric materials. A typical polymeric network, with 1 to 100 micrometers in size, can have a relaxation time on the order of microseconds to milliseconds, while bulk polymeric materials composed of these coils and networks on the length scale of millimeters to centimeters, can have relaxation times in the range of seconds, hours or even years. The multiple, disparate spatial and temporal scales and their interdependence, oblige us to adopt a multiscale modeling strategy.

Our approach addresses these challenges with a hybrid experimental-computational effort. This effort includes the use of a novel multiscale software screening framework to determine the molecular cues that drive shear-thickening in dilute polymer mixtures. It starts from a library of

potential polymer unit combinations that have been shown to drive non-Newtonian behavior in simple fluids.

Compared to experiments, computational simulations provide new atomistic insights and theoretical understanding connecting the dynamics of structure evolution and atomistic level interactions that provide critical cues to steer property-design and modifications. However, such computations face a dilemma: either to use high accuracy methods for restricted length and time scales, or simplified less accurate methods for large-scale systems that provide less detailed atomistic information. This is especially true for polymers, because polymer properties generally depend on nano or micro-scale configurations whose scales are beyond practical atomistic simulations. In general, characteristic time scales (τ) for atomistic bonds and angles are on the order of ~10-13 s while torsional time scales are τ~10-11s. Therefore, polymers with degrees of polymerization higher than their entanglement lengths require very long relaxation times, typically many orders of magnitude beyond the scale of atomistic simulations. This problem becomes worse at lower temperatures, near the polymer glass transition temperature, and for predicting system properties that depend on such long relaxation times (e.g. dynamic viscosity).

In order to alleviate this problem, molecular dynamics simulations can resort to coarse grain (CG) models that filter the high-frequency vibrational modes to enable longer integration timesteps, larger-scale models, and a smoother potential energy surface. CG models merge atoms groups so that the longer range interactions can be followed, while ignoring the high frequency inner-group interactions. This allows the CG models to simulate much larger space and time scale, at the expense atomistic level information. The development of CG molecular force fields has mostly been based on fits of the derived properties to experiment or to atomistic molecular dynamics (MD) distributions. These MD atomistic are in turn approximations to the true quantum mechanical potential energy surfaces of a particular system. Dissipative particle dynamics (DPD) and iterative Boltzmann inversion (IBI) strategies have traditionally been used to describe the coarse-grain dynamics. But, the accuracies of such CG models are limited by the inherent inaccuracy and limited transferability of the empirical parameters of the atomistic force fields.

Having covered the in-silico architecture proposed in prior reports, we now turned our attention to characterizing the non-linear viscosity behavior of polymer-based solutions as a function of shear strain; the center piece of our in-silico optimization of shear-thickening water-polymer mixtures. To this end, we focused on two tracks: 1) using off-the-shelf CG force fields to characterize non-Newtonian behavior in polymer mixtures with water[4], and 2) developing an entirely new method to improve the accuracy of CG representations[4,5,6].

[4] "In-silico Screening and Characterization of Non-Newtonian polymer-based fluids using Coarse-grained force-fields Parameterized from Quantum Mechanics", K. Kempfer, A. Jaramillo-Botero, D. Pantano, S. Lohele, W.A. Goddard III, in prep for submission to JPC.

[5] "Effect of structure on the rheological behavior of non-Newtonian polymer-solvent mixtures: in-silico based studies" Z. Mei, A. Jaramillo-Botero, X-H Ju, and W.A. Goddard III, in prep for submission to JPC

[6] "A coarse-grain force field based on quantum mechanics (CGq FF) for molecular dynamics simulation of poly(ethylene glycol)-block-poly (e-caprolactone) (PEG-b-PCL) micelles", Sadeghi, M., Moghbeli, M.R., Goddard, W.A. III, Phys. Chem. Chem. Phys.,2020, 22, 24028

For the first track, we used the Martini CG force field from Marrink*et al*[7] to model polyethylene (PE) at different degrees of coarsening (we report here on 4 backbone carbons per CG bead). Simplified atomistic models were compared to the CG representations using the OPLS 2005 force field. We built different topological structures, including linear and branched systems using the CG representation to evaluate the non-linear viscosity effects (particularly shear-thinning in base oil solutions) using dynamic shearing at different rates as well as viscosity in the limit of zero-shear, and to characterize other system properties (e.g. density, radius of gyration, thermal conductivity). We find that the topological effect on dynamic viscosity are indistinguishable from the linear chain polymer additive case, for low molecular weight additives, and we expect it will be the same effect for water-polymer shear-thickening systems, i.e. non-linear effects on viscosity will only become distinguishable for higher molecular weight additives.

For the second track, we developed a new coarse-grained (CG) molecular dynamics force-field methodology based on fitting to the quantum mechanics (QM) equation of state (EOS). In this method, all the nonbond interactions between representative beads are parameterized using a series of QM-EOS, which significantly improves the accuracy in comparison to common CG methods derived from atomistic molecular dynamics. We have validated it for for polyethylene (PE), polyacrylamide (PAM), and other polymers, as well as for compounds of those. This CG force-field has both higher accuracy and greater computational efficiency than the existing atomistic level force fields (e.g. OPLS). The nonbond components of the EOS were obtained from cold-compression curves on PAM crystals with rigid chains, while the covalent terms that contribute to the EOS where obtained using flexible chains. For describing hydrated systems or gels we developed water-polymer interaction parameters using the same method. We demonstrated that the new CG-PAM force field reproduces the EOS of PAM crystals, isolated PAM chains, and water-PAM systems, while successfully predicting such experimental quantities as density, specific heat capacity, thermal conductivity, zero-shear and dynamic viscosity, and melting point.

3. Tasks and Schedules

Table 1. Gantt chart for this DOE-STTR Phase II project.

[7]Marrink, S. J. et. al. 2004, J. Phys. Chem. B, 108, 750-760

Task	Description	Duration (Quarter)							
		1	2	3	4	5	6	7	8
Task 1	**Coarse-Grain Solvated Methods**								
Task 1-1	Modified FENE Model								
Task 1-2	NEMD Simulation								
Task 1-3	Improved CG Models								
Task 2	**First-Principle Copolymer Predictions**								
Task 2-1	Accurate QM/FF Methods								
Task 2-2	Machine Learning QSAR/QSPR								
Task 3	**Fine-Grain Chemometrics**								
Task 4	**SPA Polymer Synthesis and Test**								
Task 4-1	Monomers for SPA Polymer								
Task 4-2	Chemical Synthesis of SPA Polymer								
Task 4-3	Rheological Properties of SPA Polymer Solution								
Task 5	**Coreflood and Digital Coreflood**								
Task 5-1	Laboratorial Core Flooding								
Task 5-2	Digital Core Flooding								
Task 6	**SPA-EOR Process Development**								
Task 6-1	Reservoir Criterion								
Task 6-2	SPE-Flooding Process								
Task 6-3	Economic Assessment								

Task 1 – Improved Coarse-Grain Description of Non-Newtonian Polymer Fluids

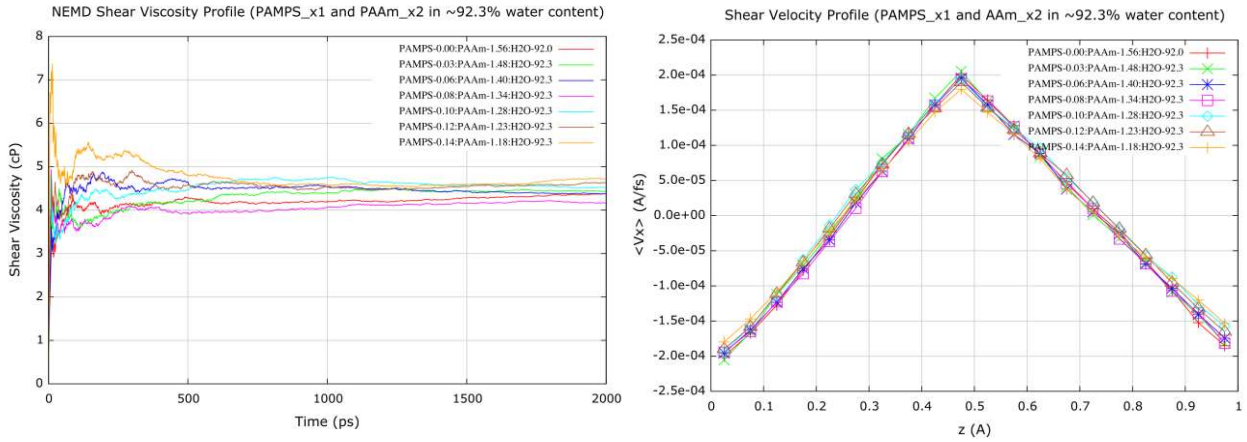

Figure 1.NEMD shear viscosity calculation of poly(2-acrylamido-2-methyl-propanesulfonic acid) (PAMPS) under different solvation environments using our atomistic Dreiding potential, shows the converged viscosity value (left) and the linear velocity profile (right).[1]

Task 1-1: Coarse-grain force fields with proper torsional polymer dynamics

The reason for starting with a coarse-grain model is that it allows us to explore higher length and time scales. As shown in Figure 1, we are able to predict the shear viscosity from fully atomistic models of our polymer mixtures, but the calculations are prohibitively expensive for the kind of in silico screening approach we developed for this application. An important decision in our *in-silico* screening strategy is to start with a simple (i.e. fast) coarse-grained MD model for generic

polymers, or solvated polymers. In this case, we opted for a modified finite-extensible non-linear elastic (FENE) model.[8] In the basic FENE model, monomers are lumped together into spherical beads, inter-connected through elastic springs. For dense polymeric systems, all the beads interact with each other through the Weeks-Chandler-Andersen (WCA) potential[9], which is a Lennard-Jones potential cut off at its minimum and shifted to zero. Therefore, the WCA potential is continuous and differentiable in the entire range of interaction,

$$V_{WCA}(r) = 4\varepsilon\left[\left(\frac{\sigma}{r}\right)^{12} - \left(\frac{\sigma}{r}\right)^{6} + \frac{1}{4}\right], \qquad r < r_{cut} = \sqrt[6]{2\sigma}$$

In addition, the bonded beads interact through the FENE potential[10],

$$V_{FENE}(r) = -\frac{1}{2}KR_0^2 ln\left[1 - \left(\frac{r}{R_0}\right)^2\right],$$

And we have added a bending potential to consider the polymer backbone stiffness appropriately,

$$V_{bend} = K_{bend}[1 - cos(\theta - \theta_0)]$$

where $\theta_0 = 180$, K is the bond strength (usually K = 30, to avoid bond crossing) and $R_o = 1.5\sigma$ is used as the maximum bond length. Here, when $r \geqslant r_{cut}$, $V_{WCA} = 0$ (Figure 2, black line), and $\sqrt[6]{2\sigma}$ and ε represent the non-bonded diameter and interaction strength of the polymeric beads, respectively. Since the FENE potential is attractive and the WCA potential repulsive, the combination of them forms an anharmonic spring (Figure 2). The equilibrium mean bond length is about 0.97 σ at a temperature of T = 1. For melts, the bead number density, is fixed to $\approx$ 0.85, and the system temperature is controlled by a Langevin thermostat with a weak friction constant of 0.5. σ and εserve as dimensional units of simulated, dimensionless quantities, thus, $\sigma = 1$ and $\varepsilon = 1$. Similarly, the bead mass, m, is also set to unity. r_{cut} is the cutoff distance for the V_{WCA} potential. By setting Boltzmann's constant, $k_B = 1$, the unit of time is given by $t = \sigma\sqrt{m/\varepsilon} = 1$. When increasing the bending stiffness, k_{bend}, from 0 to 2ε, the entanglement length, N_e, is reduced significantly, thus increasing the effective chain length. With this bending potential added into the FENE model, a scaling law between the entanglement length and the reduced polymer density was derived and found to be consistent with the experimental results on different polymer classes for the entire range, from loosely to tightly entangled polymers.[11] By taking m, σ, ε and k_B as fundamental quantities, all the other units can be defined (i.e. reduced Lennard-Jones, LJ, units).

[8] Kroeger, M. *Phys. Rep.***2004**, *390*, 453–551.
[9] Weeks, J.D.; Chandler, D.; Andersen, H.C. *J. Chem. Phys.***1971**, *54*, 5237–5247.
[10] Grest, G.S.; Kremer, K. *Phys. Rev. A***1986**, *33*, 3628–3631.
[11] Uchida, N.; Grest, G.S.; Everaers, R. J. Chem. Phys. 2008, 128, 044902:1–044902:6.

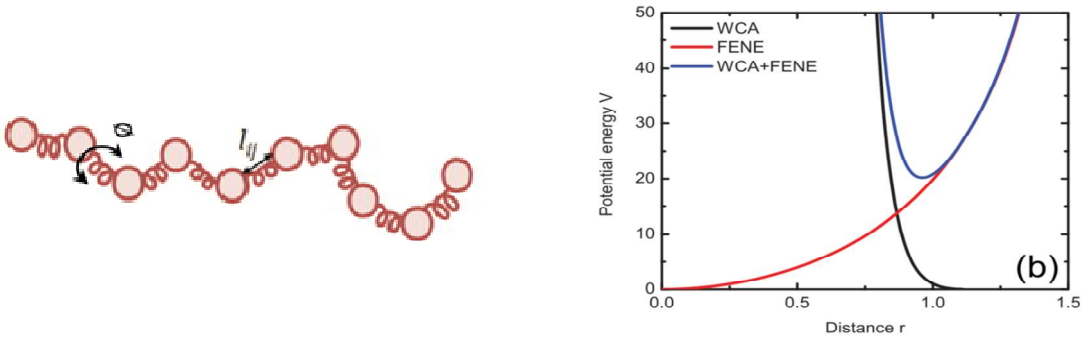

Figure 2. Depiction of (left) the extended FENE model used and (right) its potential functions.

The main advantage of the FENE model is that it avoids the computationally expensive long-range van der Waals (vdW) interactions between polymeric beads, as well as the square root operation involved in calculating the harmonic bond energy. Additionally, the coarse-grain description implies that several monomers are coarse-grained into one bead, which greatly reduces the degrees of freedom, and the Einstein frequency determining the MD time step is basically set by the WCA potential.[12] Therefore, simulation of the FENE model is extremely fast compared with all-atomistic simulations. This is ideal for our fast screening strategy.

Task 1-2: Long-term Non-Equilibrium Molecular Dynamics (NEMD) Shear-rate-dependent Viscosity

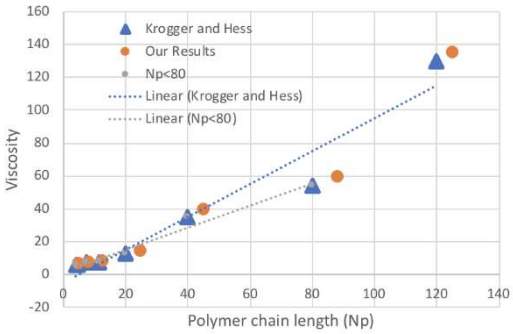

Figure 3. Plot of zero shear viscosity as a function of chain length. The line is a best fit to the viscosity in Krogger and Hess (and it matches for both unentangled, N_p<80, and entangled chains, N_p>80).

Using a simple bead-spring force field description of polymers, Kroger and Hess,[13] obtained the zero-rate shear viscosity, η_o, of unentangled and entangled polymer chains and the scaling law between chain length, N, and η_o in accordance with the prediction from the Rouse and tube models, i.e. linear $\eta_o \sim N$ for unentangled and cubic $\eta_o \sim N^3$ for entangled chains. This was

[12] Polymers 2013, 5, 751-832; doi:10.3390/polym5020751
[13] Kroger, M.; Hess, S. Phys. Rev. Lett. 2000, 85, 1128–1131.

confirmed using our models, for short unentangled polymers and for long polymers (N_p> 80) (Figure 3). Furthermore, adding the bending correction enables direct comparison of the MD results with real polymer chemistry and physics, and mapping between FENE chains and real polymers.[14] This is essential to our multiscale strategy.

The results of our NEMD simulations are reported in dimensionless units, reduced with respect to molecular parameters such as the Lennard-Jones potential parameters. This enables moderate values of the reduced strain rate in our NEMD simulations, which correspond to extremely high strain rates in real units, making nonlinear behavior apparent even for low molecular weight systems.[15] Nonlinear rheological effects are usually associated with experiments on polymer solutions and melts with much higher molar masses than the molecules considered in NEMD simulations. The reason being, that by introducing a strain rate reduced with respect to an appropriately chosen relaxation time, it is often possible to map results obtained for short chain molecules at high strain rates onto results that would be obtained for longer molecules at lower strain rates – case in point our dilute polymer mixtures that exhibit shear-thickening. In other words, we expect that our simulations contain features that are observed for long chain molecules at experimentally accessible strain rates.

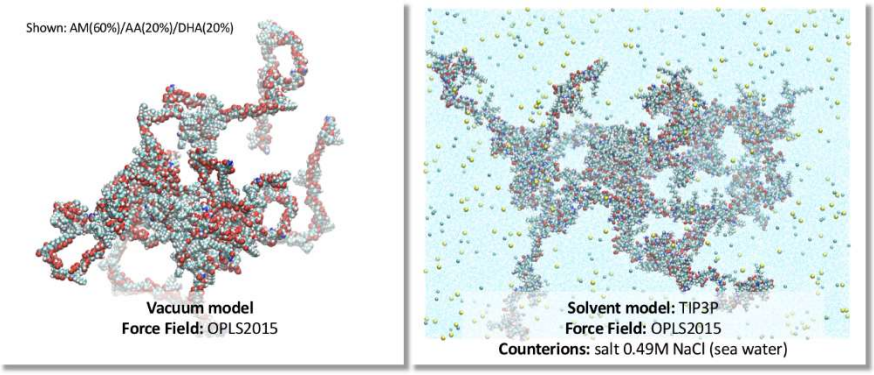

Figure 4.Fully atomistic co-polymer model for 60% acrylamide, 20% acrylic acid and 20% N,N-Dihexylacrylamide (left: vacuum, right: solvated).

In addition to the potential's fidelity, our strategy relies on the systematic generation of polymer models (linear and branched polymer and co-polymers) with chemical and structural features that have an expected influence on the non-Newtonian rheology of dilute polymer mixtures (i.e. chain length, side-chains, amphiphilicity, and group polarity). We use simple embedded rules in our bead model generator to account for these. For example, long linear alkane polymer components (including side-chains), will be represented with a hydrophobic bead, if polymer has areas where there is a partial positive or negative charge, it will include hydrophilic beads, if a monomer has a polar covalent bonds (i.e. atoms with significantly higher affinity for electrons, electronegativity) such as C-O, C-N and O-H bonds arrange asymmetrically, these will be

[14] Kremer, K.; Grest, G.S. J. Chem. Phys. 1990, 92, 5057–5086.
[15] J. Chern. Phys. 100 (1). 1 January 1994

represented as polar beads, if they are arranged symmetrically (e.g. carbon tetrachloride, CCl_4), it will be assigned a hydrophobic bead. These interactions are coded into the strength of our FENE pair potentials, for each possible interaction, i.e. polymer-polymer, phobic (apolar) polymer-solvent, philic (polar) polymer-solvent, solvent-solvent, etc. These are summarized graphically in Figure 4.

Task 1-3: Machine Learning in Compositional and Structural Search for Optimum Non-Newtonian Fluids

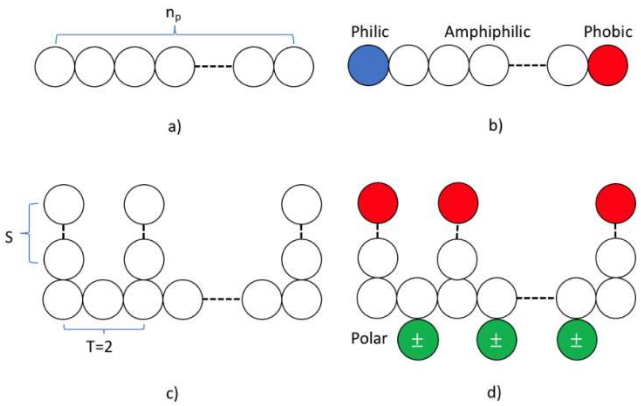

Figure 5. Different types of polymer structures and compositions [a) linear, b) amphiphilic, c) branched, d) polar of any combination from a-c)] may be generated automatically from the structural and chemical descriptor that relate our bead-spring FENE model structures to real polymers, including: chain length (Np), side-chain length (S), periodicity of sidechains (T), plus amphiphilic (philic or phobic) and polar (+/-) nature. Polarity in the context of our coarse-grain model in dealt with by modifying the attractive (opposites) or repulsive (equal) components of the force field pairwise parameters.

A special feature of this representation is that it allows us to embed transient bonds and control their lifetime. This is a useful tool for describing telechelic associating polymers (e.g. amphiphilic surfactants), or even cross-linkers, which are capable of forming transient bonds with the (attractive) end beads of polymers. Telechelic associating polymers have been shown to induce interesting non-Newtonian rheologies, including shear-thickening.[16] These structural and chemical characteristics are embedded into our evolutionary structure generation cycle, through parameters that are coded into the alleles of our chromosome population (in the language of genetic algorithms), within step 1 of the strategy described above.

Our initial design, considers chromosomes with the following real-encoded parameters (that evolve within the ranges specified above):

N	L/B	A	Np	PB	NB	Rho	ST	SL

[16] Eur. Phys. J. E 17, 115–118 (2005)

Figure 6: Chromosomic word format.

These structural and chemical characteristics are embedded into our evolutionary structure generation cycle, through parameters that are coded into the alleles of our chromosome population (in the language of genetic algorithms), within step 1 of the strategy described above. The starting structural parameters and descriptors (in beads and LJ units) in our in our coarse-grain silico screening were:

- (N) Beads per monomeric backbone unit, N=1-20
- (L) Linear or (B) branched polymer/co-polymer
- (A) Number of amphiphilic polymers/co-polymers (e.g. surfactants), A=(0.001-0.02)N
- (Np) Degree of polymerization, n_p=10-500
- (PB) Positive polar beads per polymer chain, PB=(0.01-0.20)N
- (NB) Negative polar beads per polymer chain, NB=(0.01-0.20)N
- (Rho) System density, rho=0.1-0.84
- (ST) Side chain periodicity, ST=2-10 (equivalent to monomer length)
- (SL) Sidechain length, SL=1-10

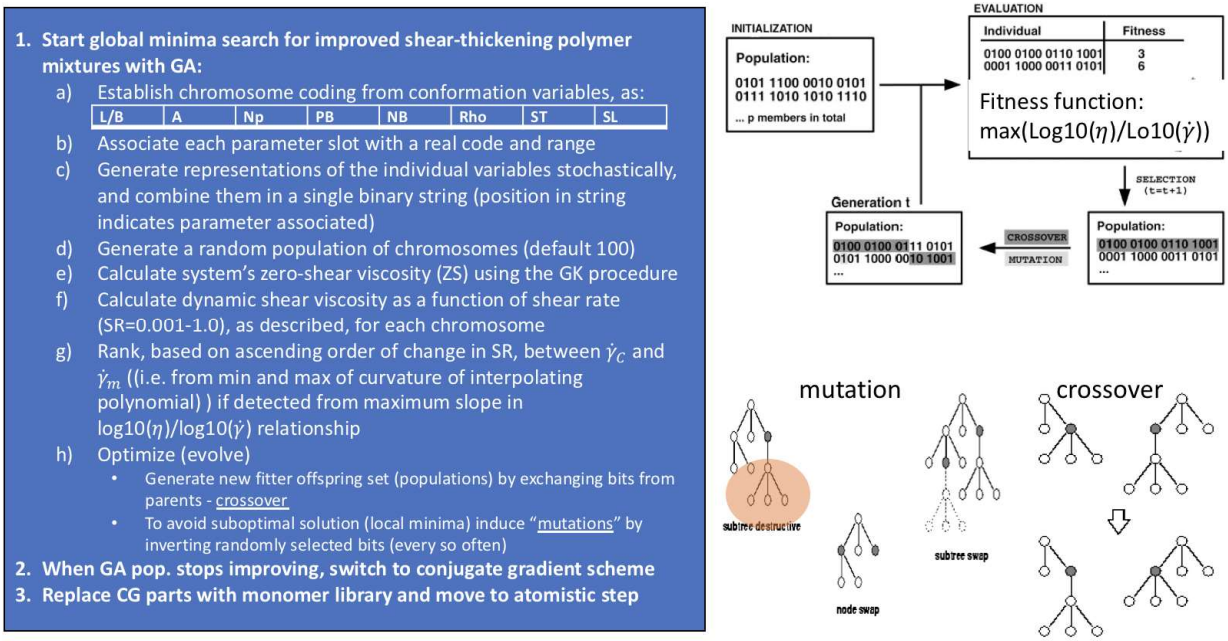

Figure 7. Evolutionary scheme for optimizing shear-thickening structures from coarse-grain descriptors.

The machine learning procedure, already validated by us in a different application[17], implemented in C and coupled to a python structure generation script, for systematic generation of coarse mixture structures is described in Figure 7.

Task 2 – Full Atomistic Scale Polymer Compositions from Coarse-Grain Best-Performers

Task 2-1: Coarse-grain to Atomistic Mapping from Accurate QM and FF Methods

The uniqueness of our atomistic mapping approach lays in the use of new polarizable PQEq[18] and ReaxFF reactive[19] force fields capable of predicting the charges and polarizations dynamically (the first time this has been done for polymer dynamics). Once we obtain the best performers from a GA population, we map the resulting structures onto an atomistic description, and characterize the molecular level cues that will serve to further correlate their performance as 'smart polymers'. Among these atomistic level metrics, we include: localized stress fluctuations, stress correlations, stress relaxation, stress tensor and strain history, electrostatic interactions and electrokinetic resistance, local polarizations, finite temperature shear elastic constants, normal shear velocity profiles, radial distribution functions, radius of gyration of polymers, free-energy, entropy, and others. These are computed using our breakthrough technologies, as described next.

For this, we have developed accurate QM and reactive polarizable FF methods to predict thermodynamic and physicochemical properties, including densities, chemical and mechanical stabilities (including entanglement length), bonded and non-bonded interactions between chain groups, solubilities and compatibility with different solvents, hydrophobicity-hydrophilicity, and effects from copolymers and additives. These provide needed information by experimentalists to select the most promising variations to synthesize and characterize before experiments. These *in-silico* studies enable the discovery of new promising polymer compositions.

We will use these QM-based FF methods to generate input data to perform Quantitative Structure-Activity Relationships (QSARs) and Quantitative Structure-Property Relationships (QSPRs). This will be focused on finding meaningful mathematical relationships between the molecular structure and energy output, using our methods as chemometric (featurization) tools to characterize the physicochemical response of our predicted shear-thickening compositions. The fundamental hypothesis behind the use of QSAR/QSPR methods is that changes in molecular structure are reflected in changes in observed viscosity, as a function of temperature and shear rate.

Task 2-2: Machine Learning and QSAR/QSPR

Non-Newtonian fluids have complex stress-strain rate relationships and their apparent viscosities depend on transient shear rate. Unfortunately, QM and RMD methods are incapable of reaching

[17] Journal of Chemical Theory and Computation, 2014, 10 (4), pp 1426-1439. DOI: 10.1021/ct5001044
[18] The Journal of Chemical Physics 146(12), DOI10.1063/1.4978891
[19] J. Phys. Chem. A, 2001, 105 (41), pp 9396–9409

the length and time scales needed to describe the transition to shear-thickening or shear-thinning, i.e. given that critical shear rate $\dot{\gamma}_c$ for dilute polymer mixtures in fluids for EOR are in seconds. To address this problem, our strategy involved using fast-screening coarse-grain long-term non-equilibrium molecular dynamics (NEMD) simulations, along with machine learning and big data analytics techniques, to predict how polymer fluid compositions and structures can drive structural reorganization and shear-rate dependent viscosity during flow modulation, and their effect on macro rheological properties.

We instantiate the search from a random population of polymer mixtures, built considering different structural and chemical cues (co-polymerization ratios, polymer lengths, side chains, polarity, etc.). We seed our evolutionary algorithms with information from candidate polymers, for which we already have experimental evidence of shear-thickening response, and evolve these using the components and rules. The population is ranked according to the fitness function (slope of shear-thickening regime, estimated from macroscopic viscosities from zero shear viscosity). The highest performing coarse-grain models obtained from our previous studies are then mapped onto different atomistic structures. Since we're interested in the primary mechanisms (structural or chemical) that drive shear-thickening, we expect this would be a much cleaner and faster way to develop new generation polymer fluids for EOR. Since the mapping from our coarse-grain models to atomistic counterparts is not 1:1 (i.e. it is a non-deterministic problem), we use this step to further characterize atomistic properties of all possible mappings, in order to identify highly correlated variables with shear-thickening or shear-thinning.

We will use supervised learning in a QSAR/QSPR framework, to extract the complex relationships between the molecular structure and the properties of interest in 'smart' polymers for EOR (in this case validated the experimentally obtained cues, described in sections below). This will allow us to build a reliable data set of shear-thickening components (from our own results, and from others) whose molecular structures and properties are reasonably well-defined, together with their measured macroscopic properties of interest, i.e. ΔS, ΔG, G", G', R_g, crosslinking/telechelic degree, polarization, electro-kinetics, and others vs our fitness function, the slope of $\mathrm{Log}_{10}(\eta)$ vs $\mathrm{Log}_{10}(\dot{\gamma})$) obtained from our CG models. This will be our training data. **Instead of using linear regression models within the QSAR/QSPR framework, that would not capture the complex non-linear relations between structure and properties in 'smart' polymers, we will use an evolutionary/genetic algorithm scheme and a non-linear predictor based on our accurate QM and reactive molecular dynamics and free-energy methods, as described below.**

Even though these machine learning methods hold great promise as a general means of developing models for relationships that have no known analytic forms, these tend to require data of sufficient quality, quantity, and diversity, which ostensibly limits the application to fields in which large, organized, and/or plentiful datasets are available, or can be produced. In the case of polymer mixtures for EOR, the dataset of high performing materials is rather small (a few hundred). To overcome this, we will generate a test population of candidates from the results of the CG steps, mapped onto atomistic models. This would be similar to those implemented in

other chemical tools by our group, e.g.GARFfield, except that here, we will use chemometric data to improve the quality and diversity of our test set, while improving overall convergence. In a sense, this will constrain the search space, when evolving a structure in the test population set (e.g., mutation or crossover). These fine level descriptors will be used to describe the training and test population entries.

Task 3 – Fine-Grain Chemometrics Using Our Reactive and Polarizable First-Principles Based FFs

The coarse-grain simulation results provide close indication of structures/compositions that exhibit shear-thickening events. These are then used to convert the best performing candidates to equivalent atomistic level structures, and to derive detailed thermodynamic, mechanical and chemical metrics that are highly correlated to shear-thickening behavior. This step deals with the individual monomers and the fine-grain polymer interactions. We have not implemented a systematic approach to address this step in Phase I, but the idea is to use our thermodynamics, mechanical and chemical correlation metrics associated to shear-thickening, to screen for new monomer components or changes to existing chemical groups, that could result in improved performance.

Task 4 – SRM Polymer Synthesis and Tests

The unique rheological properties of SRM polymer solutions are originated from the special functionalized monomer groups embedded into the high molecular-weight hydrophilic PAM-based polymer backbones. From our Phase-I studies, we have successfully identified and synthesized a couple of SRM candidates and demonstrated their technical feasibilities to be used in the SRM-flooding operation. We propose to perform more comprehensive experimental study in Phase II.

Task 4-1: Monomer Selections for SRM Polymers

The shear-thickening polymer will be based on the well-established PAM-based polymer manufacturing process with the addition the specifically selected monomers, which give rise to the "shear-thickening" phenomenon. In order to carefully control the rheological behavior in the solution, one must combine molecular design knowledge with synthesis techniques to intelligently select the polymer backbone and the structure/distribution/percentage of the special functional monomers. From our Phase-I studies, we have screened a number of SAP candidates and tested their shear-viscosity responses. We have learned that there is an optimal monomer concentration ratio in the molecular structure of SRM. Furthermore, we also discovered that when the special functional group containing both hydrophobic and hydrophilic counterparts (i.e., surfactant-like feature), the viscosity of associated PAM-based copolymers could be significantly boosted. In this task, we plan to further explore a number of different parameters, including

varying monomer concentration, additional additives, and new monomer candidates. The cost and the commercial availability of the selected monomers will also be considered.

Task 4-2: Chemical Synthesis of SRM Polymers

Several of laboratory PAM/HPAM synthesis routines have been well-established. We selected the free radical copolymerization as our main synthetic routines. In comparison with other polymerization processes, such as cationic/anion polymerization, condensation polymerization or ring-opening polymerization, this free radical copolymerization process is mature, cost-effective, and scalable. Among a number of radical copolymerization processes, the gel polymerization has the advantages of rapid reaction and convenient post-processing compared to common solution, dispersion or emulsion polymerization.

Task 4-3: Rheological Properties of SRM Polymers

As a SRM solution is injected into a reservoir, the shear rate, which is related to flow velocity will change substantially from near well-bore region to in-depth reservoir, as well as from high permeability zones to low permeability zones. One of the most important features of our developing SRM polymer flood is the unique viscosity-shear profile, which we denoted as the "shear thickening effect". That is, the viscosity of polymer fluid will increase, rather than decrease, in the high-K zone, such that to redirect more fluids into the low-K zones where more residual oils are in. Therefore, continuously checking the rheological properties of the selected SRM candidates as functions of shear rate, temperature, pressure, salinity, and polymer concentration are important. Both BrookField and Anton Paar (MCR-302) rheometers, which had been applied in our Phase-I studies, will be used in this subtask to compile a complete data set of viscosity of polymer solutions.

Task 5 – Core Flood and Digital Core Floods

The strength of SRM in improving sweep efficiency stems from its distinct flow behavior in porous media which is governed by the rheological and retention behaviors of SRM. The rheological properties of SRM solutions measured by conventional rheological instruments (Task 4) that produce pure shear flow need to be extrapolated to predict the pressure-to-flow relationship in porous media. Preliminary sand-packed core flood tests had been carried out in the Phase-I program as a demonstration and validation of the SRM-flooding process. Extensive laboratory core flood tests, including advanced computer-aided "Digital core flood" studies, will be carried out Phase-II, with a main object to establish the relationship between the characteristics of the rocks (permeability, relative permeability, saturation change, formation damage, etc.) and the rheology of the SRM fluids for different reservoir conditions.

Task 5-1: Laboratorial Core Flooding Tests

Laboratorial core flood testing forms the basis of the development and deployment of EOR technologies, allowing reservoir engineers to simulate reservoir-scale oil production curve from measurements made on individual pieces of reservoir cores, or man-made cores. The special core flooding system is an advanced, modular, computer-controlled setup configured for liquid permeability, water flooding, and polymer flooding under unsteady state conditions, at confining pressure up to 7,000 psi, pore pressure up to 6,000 psi, and temperature up to 180°C, which cover all encountered reservoir conditions. This system also features automated data acquisition, manual and semi-automated operation via a PC-based graphic user interface to digitally control the valves directing the flowing fluid and pump delivery system. Back pressure regulators are also on-site for the maintenance of pressure in core flood test system. Commercially available sandstone cores without clay/carbonate contents, such as Berea cores, will be used. The main advantage of working with the synthetic core is that it provides a uniform permeability and is more chemically inert.

Figure 8. Multi-core flooding system.

Task 5-2: Digital Core Flooding Studies

In-depth understandings of the flow of multiple fluid-phases in the subsurface are of great importance for the development of the SRM-flooding processes. A digital core flooding study is based on the advection-reaction-dispersion (ARD) equation to describe the reactive transport models

$$\frac{\partial C}{\partial t} = -v\frac{\partial C}{\partial x} + D_H\frac{\partial^2 C}{\partial x^2} - k_s\frac{\partial S}{\partial t}$$

where C is the concentration of shear-thickening polymer in the solution (mol/m^3), t is the time (s), v is the pore water flow velocity (m/s), x is the distance (m), D_H is the hydrodynamic dispersion coefficient (m^2/s), which can be expressed as $D_H = D_e + \alpha_L * v$, with D_e being the effective diffusion coefficient, and α_L being the dispersivity (m); S is the concentration of the shear-thickening polymer ($\partial S/\partial t$ indicates the change in concentration with respect to time due to reactions), and k_s is the rate of polymer loss due to adsorption and/or degradation. Based on

this model, we can build a digital core (dimension 181.5 x 33.373 x 33.373 mm) with multiple 1-D channels having different porosity and permeability, i.e. for low-K (porosity = 0.22 mD, permeability = 400 mD), whereas for three different channels of parameters, 0.25/2000, 0.30/4000, and 0.35/10000, respectively. The constraint conditions in the injector are set as MAX STW = 7.95 m^3/day, MAX borehead pressure (BHP = 160 kPa), and in the producer is set as min BHP =101 kPa. The duration of waterflood is 4.77 days. Figure 9 shows a few fluid properties, e.g., Darcy Velocity (left) and Shear-Rate (Right) determined from the calculation.

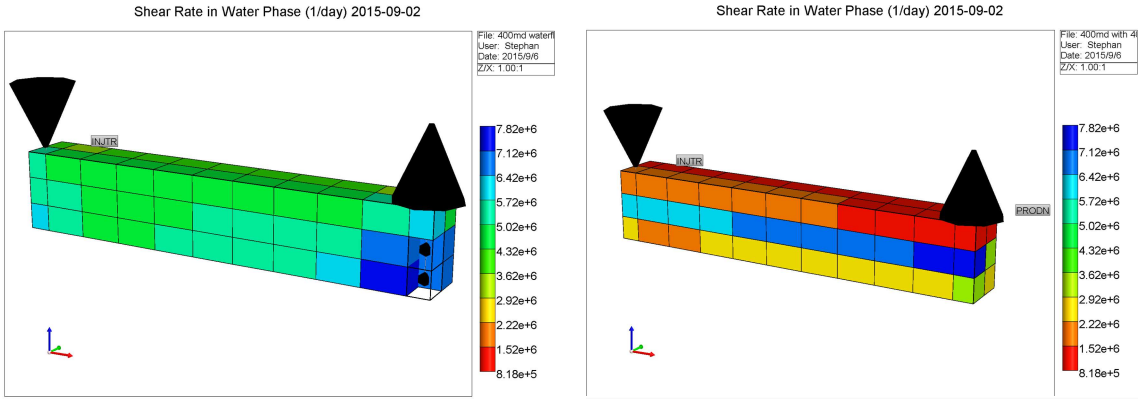

Figure 9. Calculated Darcy Velocity and Shear Rate of SRM-containing solution transport in a digital core (1-D channel).

We will continuously apply this digital core flooding method to determine and compare the flow properties of different SRM-containing fluids. We also plan to apply the MATLAB Reservoir Simulation Toolbox (MRST), which is a free open-source software package for reservoir modeling and simulation, developed by the Computational Geosciences group in the Department of Mathematics and Cybernetics at SINTEF Digital, and Heriot-Watt University, NTNU, TNO and TU Delft. The software consists of a minimal core module offering basic data structure and functionality, as well as different add-on modules for various specific purposes.

Task 6 – SRM-Flooding Process Development and Engineering Suggestion

Task 6-1: Establish Reservoir Selection Criterion for the SRM-flooding Process

One important objective of this Phase II study is to develop and optimize the SRM-Flooding process as an advanced EOR method for improving oil recovery from domestic mature oil fields. In this subtask, we shall combine our laboratorial core flooding results with reservoir conditions of the targeted oil fields to establish certain reservoir screening and selection criterion of the SRM-flooding process. Various field information including the oil reserve, production history, and reservoir conditions, etc. will be considered. Our initial target is the Illinois Basin, a Paleozoic depositional and structural basin in the Midwest of U.S. underlying most of the state of Illinois and extending into southwestern Indiana and western Kentucky. There are more than 1000 oilfields with ~ 14.1 billion barrels of OOIP in the Illinois Basin, and only 20~40% of that has been

recovered by the primary recovery (peaked in 1908) and the secondary water-flooding (in 1960s). Therefore, the Illinois Basin has a substantial amount of unrecovered oil. In addition, because it is dominated by very mature water-flooded reservoirs with small pattern spacing containing light crude oil, it has particularly high potential for chemical tertiary EOR applications. We plan to work with industrial partner, Paladin Geological Services, who has been very active in bring advanced and innovative formation evaluation services to domestic oil producers, especially in the Oklahoma, Illinois, Kentucky, and Texas regions.

Task 6-2: Engineering Processing

The engineering field implementation of the SRM-flooding process could be very similar to that of the conventional polymer-flooding pumping processes, since it is basically the injection of the simple polymer compound solution. Nevertheless, a number of technical and engineering issues of the SRM-flooding deployments will be considered. (1) Compared to the regular HPAM polymer, shear-thickening polymers will have stronger tendency to form association due to the addition of the special functional groups. This might potentially impact the injectability of the SRM-solution. One possible solution is to design the shear-viscosity profile of the SRM solution such that shear-thickening effect occurs only within the range that the SRM solution will experience in the subterranean formations. Another possible solution is to include certain additive chemicals (such as nanoparticles or surfactants) to prevents the early associations of the shear-thickening polymers. Industrial standard filtration tests will be conducted to ensure that the SRM solutions pass at least 3.0 micron pores, preferably 1.2 micron ones. (2) The surfactant-like feature of the shear-thickening polymers could potentially increase their interaction with rock materials, in particular when the shale/carbonate content is high. Besides, other chemicals additives required during EOR such as clay stabilizer, scale inhibitor and corrosion inhibitors may also have different interactive behaviors with shear-thickening polymers from traditional PAM and HPAM. Therefore, the compatibility of shear-thickening polymers with rock materials and common additives will be tested. (3) One of key technical issues in chemical EOR process is the oil-water demulsification (separation) of the produced fluids. This is a particular concern in the SP and ASP process when the residual surfactant after flooding still emulsify the oil with water. Here again, the surfactant-alike features of SRM polymers might post some additional difficulties on the oil-water demulsification. Thermal and mechanical degradation of the SRM polymer during SRM-flooding processes will be studied to determine the residual polymer/surfactant contents and their emulsification potentials.

Task 6-3: Economic Assessment

The scale-up production of the selected polymer candidates provides cost uncertainty, because SGTC is not a commercial-scale chemical producer. Therefore, we will closely work with our industrial partner, ChemEOR Inc. who is among the leading oilfield chemical suppliers in North America. Currently, ChemEOR has the polymer manufacturing facilities to annually produce over

40,000 tons of regular HPAM and 15,000 tons of functionalized HPAM polymers for well stimulation and oilfield water-treatments. Once our SRM polymer prototypes are defined, we will work with ChemEOR to secure the raw material supplies and manufacturing processes.

4. Details of Progress and Status

4.1Non-Newtonian Rheological Properties from Off-the-shelve CG Force Fields

4.1.1 Polyethylene

We have been developing a systematic scheme to build coarse-grain (CG) polymeric descriptions with higher accuracy. To improve accuracy, the focus has been on obtaining the proper angular/torsional distributions by controlling the bending stiffness of the polymeric backbone and side chains, and enabling model reversibility between CG and atomistic. Reversibility allows us to validate the coarser descriptions against those at the finer grain level of detail, e.g. bead models against fully atomistic descriptions that have been tested on specific polymeric compositions, and can be generalized to others, and to fine tune the CG parameters for improved accuracy (Figure 10).

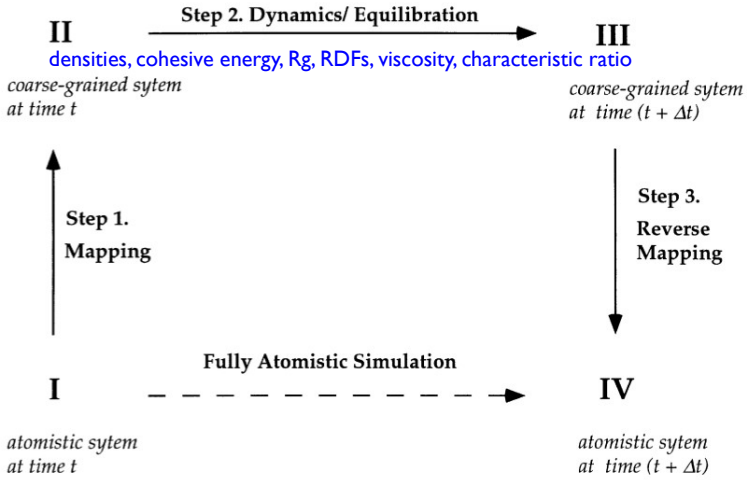

Figure 10.*Atomistic to Coarse-grain forward/reverse mapping*

The degree of reversibility for a particular model will depend on many variables, including the mapping choice (e.g. structural, phenomenological), the amount and type (e.g. structural, chemical-compositional, physical-dynamical) of information reduction/loss when coarsening, and on how (if at all) that information can be reconstructed/estimated when reverse mapping back to the atomistic (e.g. averaging, center of mass placement, etc.). The possibilities are endless, but ideally, transformations should minimize data loss.

The following results focus on an amorphous polyethylene melt system of 4 chains, each with 200 monomer units. We start with an atomistic model characterized via molecular dynamics (MD) at 300K using a standard Dreiding force field.[20] The system is then coarse-grain mapped, based on structural cues (2 types of beads, either composed of 3 CH_2 groups or 2CH_2 and a CH_3 group), and characterized using the same force field functional forms with adjusted coefficients (for bonds, angles and non-bond terms). Finally, we show how the same coarse-grain description can be characterized with improved performance, using a modified FENE+CWA+angle force field.

Important advantages may be derived from the CG models, when comparted to their fully atomistic counterparts. Since several monomers are coarse-grained into one bead, this greatly reduces the degrees of freedom and therefore the model's computational complexity, and at the same time, high-frequency vibrational modes are filtered, hence the Einstein frequency determining the MD time step may be reduced significantly. The latter allows longer overall timescales to be reached, much larger models that can appropriately capture important structural characteristics that affect polymers (e.g. entanglement), and a smoother potential energy surface to traverse during dynamics. A further set of advantages that we bring from our use of the FENE potential description, is that it avoids the computationally expensive long-range van der Waals (vdW) interactions between polymeric beads, when compared to the Dreiding potential description, as well as the square root operation involved in calculating the harmonic bond energy. Therefore, simulation of the FENE model is extremely fast compared with all-atomistic simulations. This is ideal for our fast screening strategy. These are all critical advantages in reaching the very long system relaxation times expected in polymer dynamics modeling, that would otherwise be impeded by the rather short characteristic time scales of atomistic bonds and angles.

All molecular mechanics (MM) and MD calculations were done using the LAMMPS parallel molecular dynamics simulation code.[21]

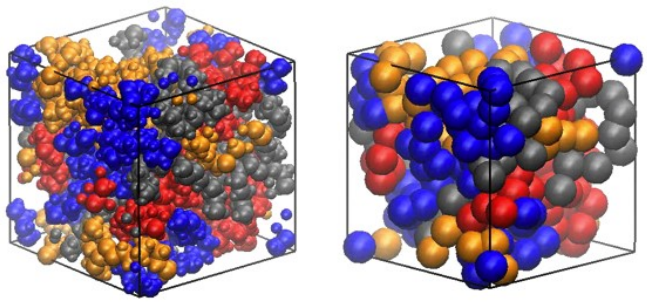

Figure 11. *(left) atomistic model of PE (4 chains of 100 monomers each), (right) coarse-grain description of the same PE system*

[20] Mayo et al, *J. Phys. Chem.*, **1990**, *94* (26), pp 8897–8909
[21] https://lammps.sandia.gov, originally developed by Plimpton, S. J Comp Phys, 117, 1-19 (1995)

We built an atomistic model of a polyethylene melt, from 4 chains of 100 monomers each, in atactic conformation using the Schrodinger polymer building tools[22]. Using a standard set of parameters for Dreiding, the system was minimized in total energy, using a conjugate gradient method with energy difference and RMS force convergence criteria set to 1e-6 in both cases, and then equilibrated at 300K using an NPT ensemble at 1 atmosphere, until volume convergence was confirmed.

We then performed systematic mapping of the PE, using two types of beads, a terminal bead (T=CH_2-CH_2-CH_3) and a central bead (M=CH_2-CH_2-CH_2). We chose bead positions that lead to rigid bonds, single peaked bond Gaussian distributions with height/width associated to bond strength (peak multiplicity leads to bond/angle potential interdependence), and all beads to be spherical in order to avoid anisotropic potentials. The CG bead center was placed at the central carbon of the 3-monomer sequence (i.e. 2nd carbon in the chain), equivalent to the center of mass for an ideally linear conformer configuration. Total bead mass, was the sum of individual atomic masses per bead, i.e. T=43.089 and M=42.081 amu. Beads within a chain were connected using a spring-like force, and described with the same Dreiding harmonic bond functional yet with adjusted coefficients (force constant and equilibrium distance, R_o). Angles and non-bond terms were adjusted, as shown in Table 2.

Table 2. *Adjusted Dreiding-like force field for coarse-grain PE*

Interaction	Form	Parameters
Bond	$E = \frac{1}{2}k_b(r_b - r_0)^2$	k_b = 6.96 (TT), k_b = 6.16 (TM, MM) kcal/mol Å^2 r_0 = 3.65 (TM), r_0=3.64 (MM) Å
Angle	$E = \frac{1}{2}k_\theta(\theta - \theta_0)^2$	k_θ = 1.09 (TMT), k_θ = 1.19 (TMM, MMM) kcal/mol θ_0 = 175.5 (TMT), θ_0 = 175 (TMM), θ_0 = 173 (TMM) degree
Nonbonded	$E = \left(\frac{27\varepsilon}{4}\right)\left[\left(\frac{\sigma}{r}\right)^9 - \left(\frac{\sigma}{r}\right)^6\right]$	ε = 0.469 (TT), ε= 0.444 (TM), ε = 0.42 (MM) kcal/mol σ = 4.585 (TT), σ = 4.5455 (TM), σ = 4.506 (MM) Å r_c = 15 Å (truncation radius)

Using the same system bead mapping, we also prepared a FENE model for dynamics characterization. In the basic FENE model, monomers are lumped together into spherical beads, inter-connected through elastic springs. For dense polymeric systems, all the beads interact with each other through the Weeks-Chandler-Andersen (WCA) potential[23], which is a Lennard-Jones potential cut off at its minimum and shifted to zero. Therefore, the WCA potential is continuous and differentiable in the entire range of interaction,

$$V_{WCA}(r) = 4\varepsilon\left[\left(\frac{\sigma}{r}\right)^{12} - \left(\frac{\sigma}{r}\right)^{6} + \frac{1}{4}\right], \qquad r < r_{cut} = \sqrt[6]{2\sigma}$$

[22] https://www.schrodinger.com/
[23] Weeks, J.D.; Chandler, D.; Andersen, H.C. J. Chem. Phys. 1971, 54, 5237–5247.

In addition, the bonded beads interact through the FENE potential[24],

$$V_{FENE}(r) = -\frac{1}{2}KR_0^2 ln\left[1 - \left(\frac{r}{R_0}\right)^2\right],$$

In this work, we have introduced an additional bending potential, to control the polymer backbone stiffness,

$$V_{bend} = K_{bend}[1 - cos(\theta - \theta_0)]$$

where $\theta_0 = 180$, K is the bond strength (usually K = 30, to avoid bond crossing) and $R_o = 1.5\sigma$ is used as the maximum bond length.Here, when $r \geqslant r_{cut}$, $V_{WCA} = 0$, and $\sqrt[6]{2\sigma}$ and ε represent the non-bonded diameter and interaction strength of the polymeric beads, respectively. Since the FENE potential is attractive and the WCA potential repulsive, the combination of them forms an anharmonic spring. The equilibrium mean bond length is about 0.97 σ at a temperature of T = 1. For melts, the bead number density, is fixed to $\approx$ 0.85, and the system temperature is controlled by a Langevin thermostat with a weak friction constant of 0.5. σ and εserve as dimensional units of simulated, dimensionless quantities, thus, $\sigma = 1$ and $\varepsilon = 1$. Similarly, the bead mass, m, is also set to unity. r_{cut} is the cutoff distance for the V_{WCA} potential. By setting Boltzmann's constant, k_B = 1, the unit of time is given by $t = \sigma\sqrt{m/\varepsilon} = 1$.

When increasing the bending stiffness, k_{bend}, from 0 to 2ε, the entanglement length, N_e, is reduced significantly, thus increasing the effective chain length.

Yet another simplification that we have applied to the FENE description, which allows us to perform calculations with improved computational efficiency, was the use of reduced LJ units in LAMMPS. This meant measuring energy in units of "eps" and length in units of "sigma", which simplifies the LJ potential in V_{WCA} to:

$$V_{WCA}^*(r) = 4\varepsilon\left[\left(\frac{1}{r^*}\right)^{12} - \left(\frac{1}{r^*}\right)^6 + \frac{1}{4}\right]$$

andfundamental quantities like m, σ, ε and $k_B$can be set to 1. This allows dimensionless analysis, and stabilization ofnumerical solutions through the normalization of independent variables. Of course, once we have performed all calculations, the results can then be transformed into real units, using a straightforward conversion (see units in LAMMPS).

The LAMMPS parameters for the FENE+CWA+angle solution, expressed in real units (i.e. mass = grams/mole, distance in Angstroms, time in femtoseconds, energy in Kcal/mole, force in Kcal/mole-Angstrom, and temperature in Kelvin) are summarized below:

Masses
1 43.089 # T
2 42.081 # M

Pair_coeff* * 0.75 4.5

Bond Coeffs

[24]Grest, G.S.; Kremer, K. Phys. Rev. A 1986, 33, 3628–3631.

1 0.5 5.5 1.0 3.5 # T-M
2 0.5 5.5 1.0 3.5 # M-M

Angle Coeffs
1 10 175 # T-M-M
2 10 173 # M-M-M

All models, i.e. atomistic with standard Dreiding, CG with adjusted Dreiding-like potential, and FENE+CWA+angle, were characterized during 1 ns of NPT dynamics, after volume had converged, in terms of:

- individual chain radius of gyration (Rg) (Figure 12)
- bond distributions (see Figure 13)
- angle distributions (see Figure 14)
- radial distribution functions (RDF), for full system (see Figure 15) and per chain

The timestep used for all CGdynamics calculations was 20fs and 1fs for the atomistic models.

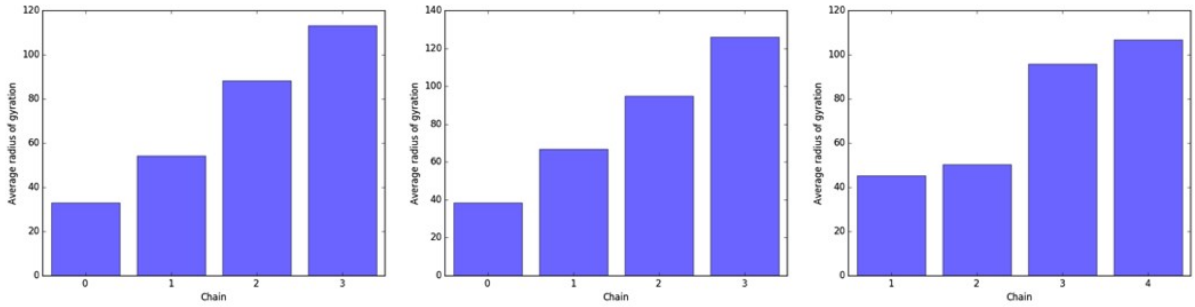

Figure 12.*Rg for (left) atomistic with Dreiding, (middle) CG Dreiding-like, and (right) CG with FENE+CWA+angle potential*

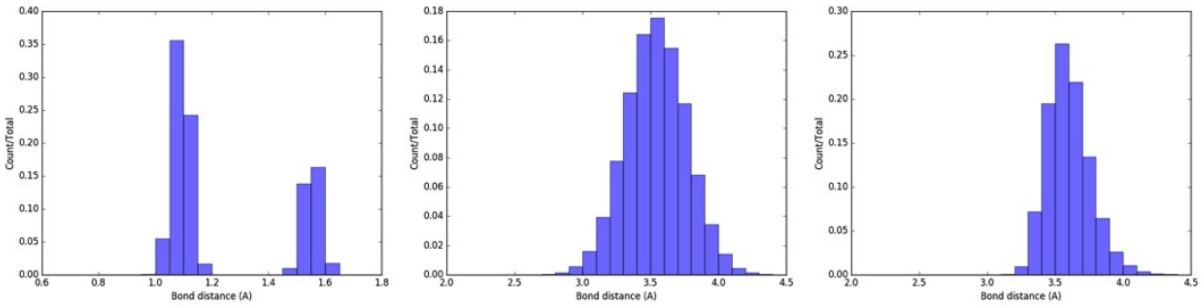

Figure 13. *Bond distributions for (left) C-H and C-C atomistic with Dreiding, (middle) CG M-M Dreiding-like, and (right) CG M-M with FENE+CWA+angle potential*

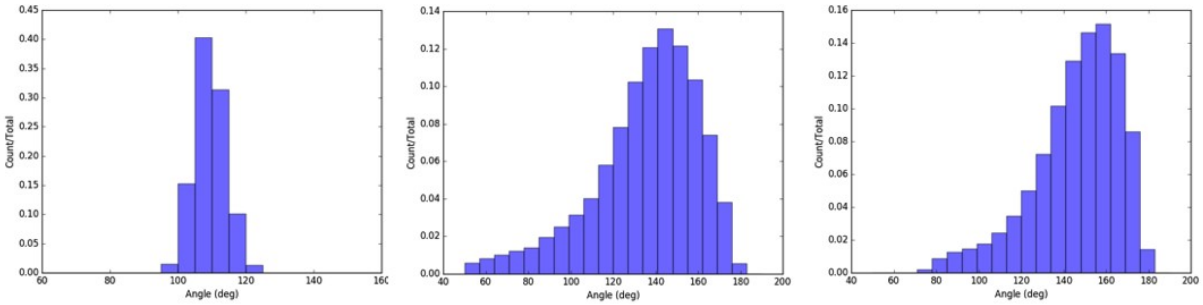

Figure 14. *Angle distribution for (left) atomistic with Dreiding, (middle) CG Dreiding-like, and (right) CG with FENE+CWA+angle potential.*

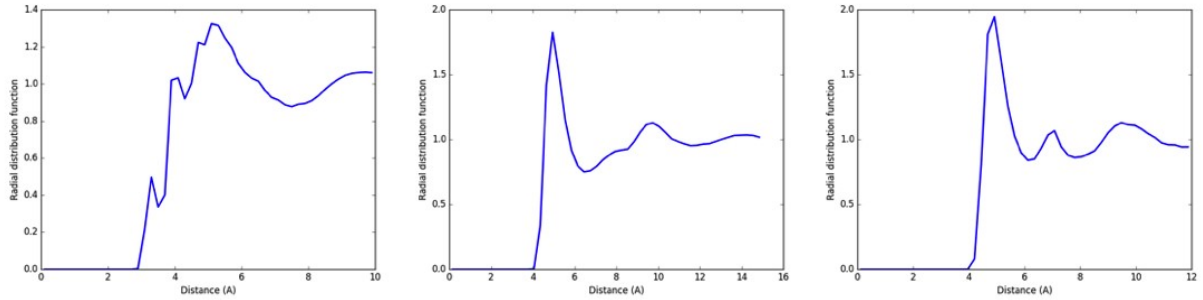

Figure 15. *RDF for (left) atomistically averaged C-C and C-H with Dreiding, (middle) CG M-M Dreiding-like, and (right) CG M-M with FENE+CWA+angle potential*

All systems were evolved dynamically starting from the initial atomistic backbone conformation. The procedure involved 5 compression-decompression cycles, between 300-800-300K in temperature, and a final equilibration run during 1ns. The resulting atomistic system density was 0.707 g/cm^3, the Dreiding-like system density was 0.9154 g/cm^3 and the FENE+CWA+angle system density was 0.8616 g/cm^3, all of which are within the experimental range. With the bending potential added into the FENE+CWA model, we were able to reproduce polymer density in a consistent manner with the experimental results; otherwise the densities obtained were overestimated.

Results in real units, demonstrate an accurate representation of our CG models, when compared to the atomistic Dreiding characterization and a significantly reduced computational cost. Furthermore, our CG models can be easily mapped back onto the atomistic models, which will allow us to explore the individual chemical compositions in additives and additive mixtures with enhanced non-linear viscosity regimes.

We are have also characterized the viscosity of octadecane $CH_3(CH_2)_{16}CH_3$ chains, based on these CG models, based on a higher-level CG mapping (one CG bead per 4 consecutive CH_2), with a harmonic bond form between beads (see Figure 16) fitted to the distribution of C1-C5, C2-C6 etc.

distances using a Gaussian fit from a Boltzmann inversion scheme. The resulting Dreiding like bond coefficients are K = 2.434, r_o = 4.97. This will serve as our base oil mixture, when characterizing viscosity index enhancing additives.

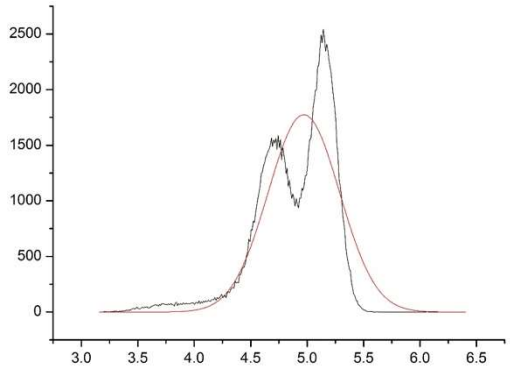

Figure 16. *CG model bond distribution for 1 bead = 4CH_2*

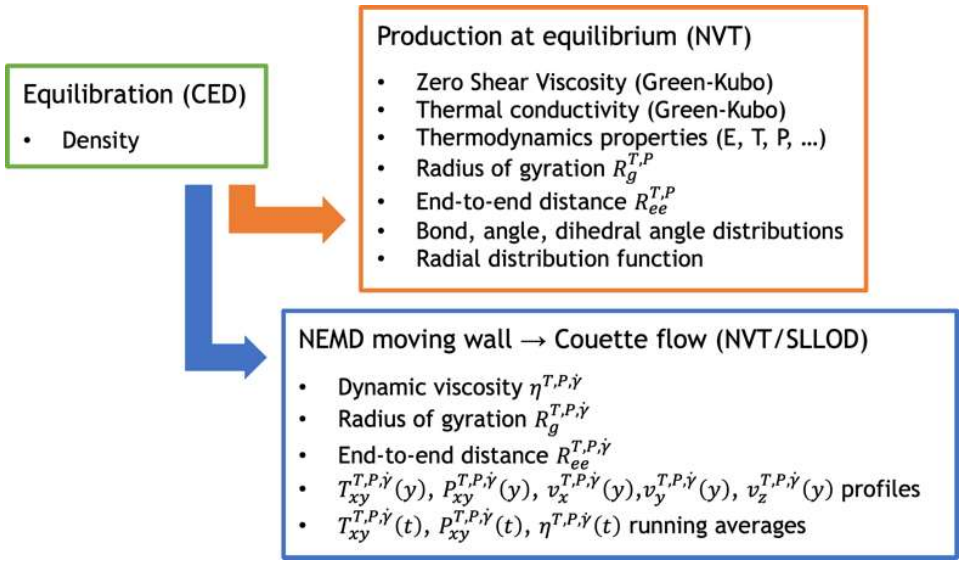

4.1.2 Polyacrylamide[4]

In order to prepare realistic polymer systems, we used the cohesive energy density procedure reported by Belmares*et al*[25] and prepared our model systems for characterization of the rheological and structural properties as summarized in the figure above, from a minimum of 5 statistically independent configurations per different temperatures and pressures. Timestep was set at 20 fs for the Maritini calculations and 1fs for the OPLS. T = 40^{0}C - 100^{0}C - 180^{0}C (Nose-Hoover thermostat), P = 1 atm - 0.25 GPa - 0.5 GPa - 0.75 GPa - 1 GPa (Nose-Hoover barostat),

[25]Belmares, M. et al. 2004, J. Comput Chem, 25, 1814–1826

Equilibration = 3 ns using Cohesive Energy Density (CED) procedure, 10 compression-expansion cycles from 0.5 g.cm-3 up to 1.4 g.cm-3 where performed per case, which include energy minimzation, an annealing cycle NVT 300 K -> 800 K -> 300 K (0.2 ns), an increase in system density by 0.1 g.cm-3. The systems were then heated via NVT @300 K -> Target temperature (0.1 ns), equilibrated using NPT dynamics at target temperature / target pressure (0.4 ns), and then ran a further production time using NVT dynamics at target temperature / target pressure (0.1 ns).

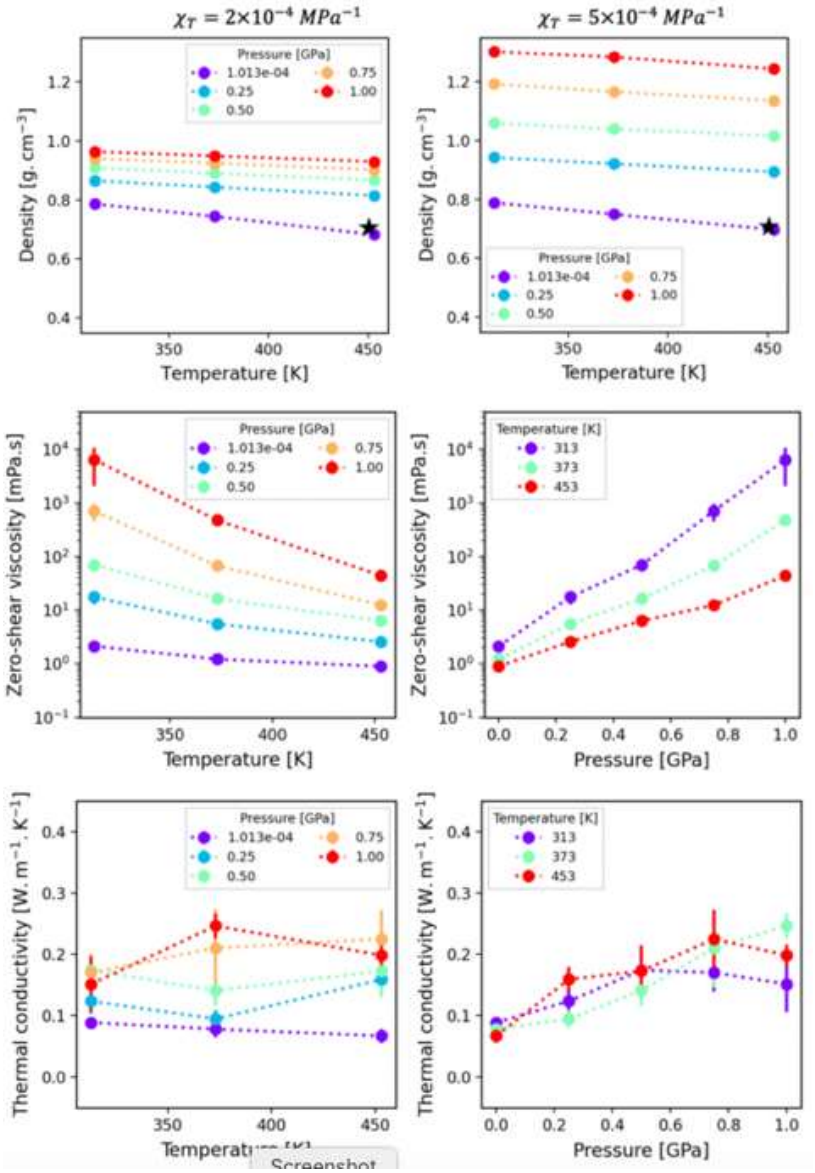

Figure 17. Density, zero-shear viscosity and thermal conductivity of PAM as a function of temperature and pressure, computed from the CG force field

Good matches were found between the OPLS and Martini cases for density vs T.

Viscosity as a function of temperature and pressure were then evaluated, as well as thermal conductivity (figures to the left), using the CG models.

Dynamic viscosity as a function of shear rate was finally obtained using the CG models, demonstrating acceptable agreement between our CG models and experimental values.[26]

In general, we find that Green-Kubo methods are faster than low shear rate NEMD simulations, simulation time increases by 100 when decreasing the shear rate by one decade, user-imposed minimum sampling window N_s leads to plateau above $10^9 s^{-1}$, and minor dependence with temperature and small dependence with pressure. Furthermore, we were able to explore with the CG models, structural dependencies on the viscosity of an additive on a base oil system as a function of shear-rate (figure below), most of which show a shear-thinning regime.

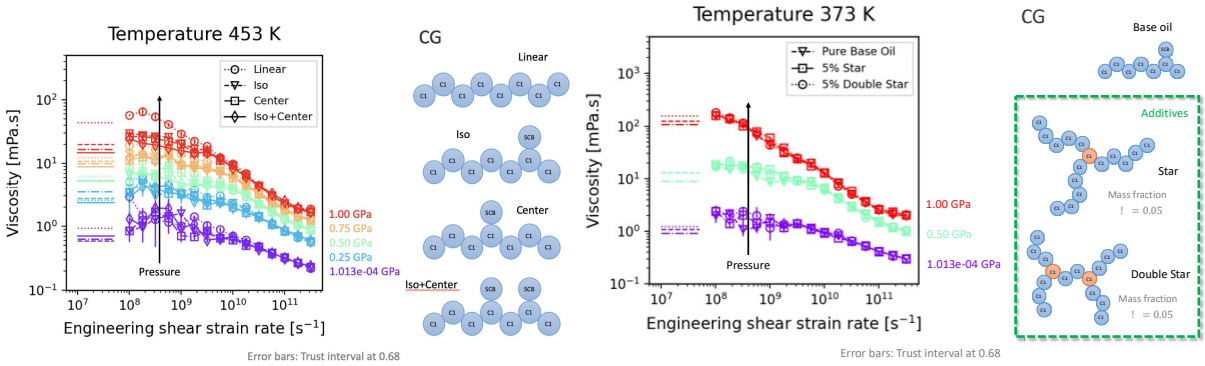

Figure 18. Pressure has a significant effect on viscosity while short side-chain branching has minor effect, a) independent from the site of side chain along back bone, and b) star topologies. All structures have a shear-thinning behavior at high strain rates.

From Figure 19, we find that the topological effect is indistinguishable from the linear chain polymer additive case, for low molecular weight additives, and we expect it will be the same effect for water-polymer shear-thickening systems, i.e. non-linear effects on viscosity will only become distinguishable for higher molecular weight additives. We are currently performing simulations on larger molecular weight polymer additives while maintaining the wt% percent ratio between the additive and the base solution (water and oil).

[26]Kim J. M. et al. 2008, J. Non-Newtonian Fluid Mech. 152, 168–183, and Wohlfarth C., Wohlfarth B. 2002, Pure Organic Liquids, 18B

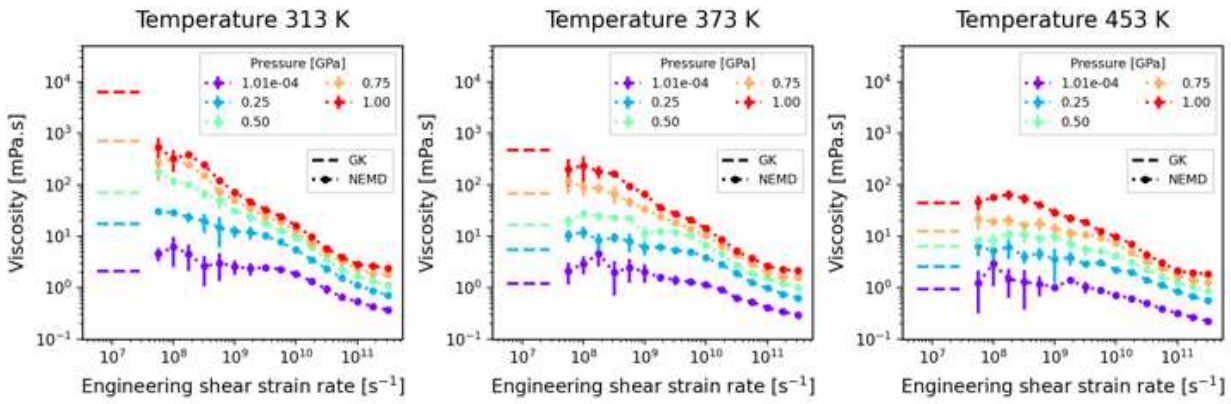

Figure 19. Equilibrium and non-equilibrium viscosity obtained from the CG force field as a function of temperature show higher accuracy at higher temperatures, where the dynamic viscosity approaches the zero-shear limit from the Green-Kubo approach.

Our CG force fields show good weak scaling (speedup for a scaled problem size with respect to the number of processors), which means we should be able to reach the time and length scales necessary to drive shear-rates down and system sizes up in order to explore these non-linearities further (assuming enough compute power is available).

4.2 Long-Term NEMD Shear-Rate-Dependent Viscosity

We have now implemented a general code to perform systematicequilibrium zero-shear viscosity and NEMD viscosity calculations, both for the atomistic and CG models. The latter is based on the Green-Kubo approach, for which the macro-algorithm is given as:

1. Equilibrate @T, using NVE ensemble plus Berendsen thermostat @T
2. Define distinct components of symmetric traceless stress tensor
3. Compute, average and dump pressure tensor component auto-correlations, S (every 5 iterations and a correlation length 400-800, depending on the system) – make sure diagonal components of computed autocorrelation is larger by factor 2-2/d (d=4/3 for 3D and d=1 for 2D systems, Daivis and Evans, J.Chem.Phys, 100, 541-547, 1994)
4. Then compute eta as,

$$\eta = \frac{V}{k_B T} \int_0^\infty dt \langle P_{xy}(0) P_{xy}(t) \rangle$$

The NEMD implementation code is based on the following macro-algorithm:

1. Equilibrate @T, using NVE ensemble plus Berendsen thermostat @T
2. Induce a flow gradient or momentum flux (*J*) by physically shearing the unit cell, and monitor the transverse velocity (*V*) of the polymer fluid
3. Compute the viscosity as (assuming flux in z direction and x transverse):

$$J_z(p_x) = -\eta \frac{\partial V_x}{\partial z}$$

NOTE: The direct NEMD (and the reverse-NEMD methods) require longer times to converge, and for now we need to confirm a linear shear velocity profile to trust the viscosity values have converged. This is particularly difficult for heterogeneous polymer fluids.

The overall method involves:

a. Confirm zero-shear viscosity for each system (Green-Kubo approach), if available from experiments or calculations, both atomistic and CG cases.

b. Compute and validate the dynamic shear viscosity for the system of interest using the NEMD approach coded in the scripts provided

c. Using the CG model, run full viscosity calculations over the range of shear-rates (0.00001-1.0 if possible, using engineering strain), i.e.

c.1. equilibrate the system at 300K

c.2. apply a shear deformation to the simulation box and integrate the SLLOD equations of motion at a controlled T and V, at a shear-rate relative to the perpendicular direction. This requires that the bead velocities should be remapped to the sheared box at every timestep.

c.3. monitor the velocity profile in the fluid mixture (should be consistent with the applied shear strain rate, i.e. linear (this is critical, otherwise we can't trust the viscosity)

c.4. monitor the off-diagonal component of the pressure or stress tensor, Pxz to determine the momentum flux (J) in units of momentum per area per time.

4.3 Compositional and Structural Search for Optimum Non-Newtonian Fluids

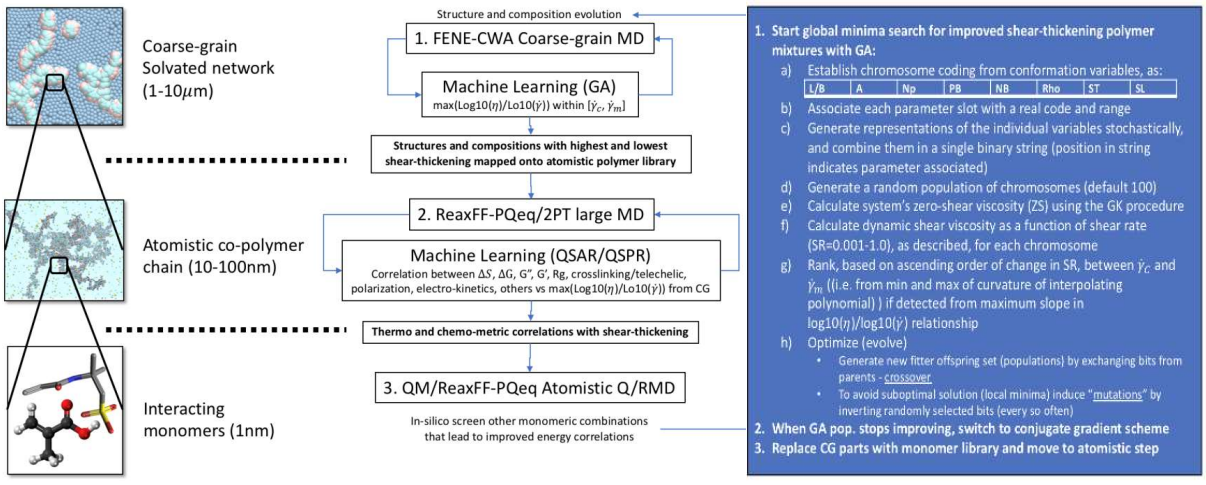

Figure 20. Methodology for in silico multiscale screening for enhanced non-Newtonian fluid mixtures in EOR. The methodology incorporates unique and breakthrough technologies from the group at CALTECH.

Our progress here has been in the development of a systematic structure building software framework to explore, using an evolutionary scheme, characteristic conformational cues and the effect of additives on shear-thickening/shear-thinning responses and viscosity index at the level of a coarse-grain description. The framework has been coded using Python (scipy), coupled to a MM/MD engine in LAMMPS via dynamically linked modules.

To test our prototype polymeric additive structure-screening framework, we used the Dreiding-like cg force field described before, on a system composed of 1 additive molecule and 100 solvent molecules (5-bead linear chain). The additive's structure/topology evolution was limited to the following structural/topological descriptors, in the GA chromosome representation (chromosome format AN:AL:BF:BL): degree of branching (AN), additive length (AL), branching frequency in beads (BF), branch length (BL).

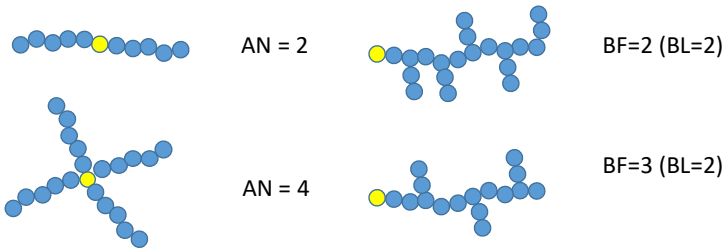

Figure 21. Structural descriptors for additive generation

From an initially random population (size 200) of (additive) chromosomes, we compute the (fitness function) shear-viscosity of the system within a shear-rate range of 0.0001-1.0 s^{-1} for every set of parameters per chromosome and rank the results based on the maximum slope in the log-log of viscosity and shear-rate. After a few evolutionary cycles (population of chromosomes is evolved based on best performers) convergences is established when fitness function error does not change more than 0.1%.

Initial evaluation			GA iteration *n*	
Structure vector	**Fitness Function**		**Structure vector**	**Fitness Function**
(4,14,1,0)	0.190481		(3,15,1,1)	0.235292
(3,15,3,3)	0.136452		(4,16,1,0)	0.138267
(3,40,1,2)	0.112344		(4,40,4,2)	0.121271
(3,18,2,0)	0.102548		(3,14,2,0)	0.071369
(4,23,4,3)	0.090338		(2,15,3,4)	0.068462
(3,17,1,1)	0.088697		(4,16,4,3)	0.065891
(4,16,1,1)	0.080643		(4,14,3,3)	0.059769
(4,36,2,0)	0.073484		(4,36,2,0)	0.054128
(4,13,3,3)	0.061054		(2,24,4,4)	0.050615
(3,22,5,2)	0.058614		(4,14,3,0)	0.049079
:	:		:	:

Figure 22. GA results from a chromosome with ranges AN:2-4 AL:1-25 BF: 1-5 BL: 0-5

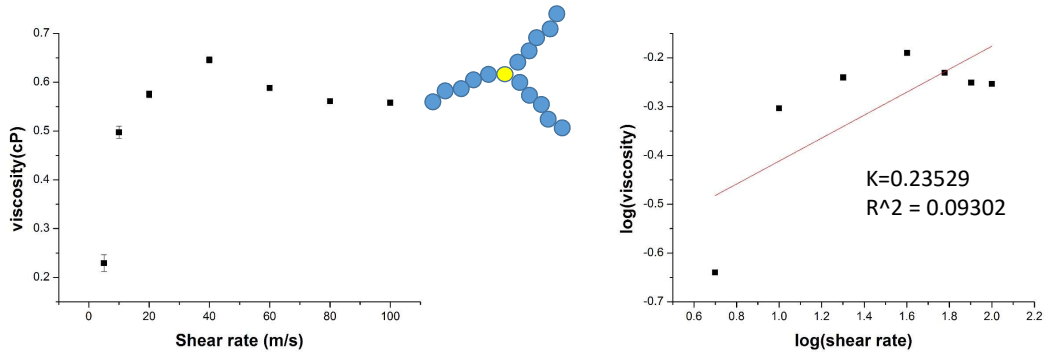

Figure 23. Non-linear viscosity response of (3,15,1,1) additive.(lateral branches not depicted for simplicity)

Our focus at this time is on finding structural effects on the non-linear viscosity response of polymeric additives to shear-rate. We will then add focus to compositional factors. This will allow us to reduce the search space for experimental validation.

The overall methodology so far is:

a) Our initial design, considers chromosomes with real-encoded parameters (that evolve within the ranges specified). These topological characteristics are embedded into our evolutionary structure generation cycle, through parameters that are coded into the alleles of our chromosome population (in the language of genetic algorithms). Initially, we consider a single additive molecule per volume of oil (at some specific wt% concentration), with the following descriptors: (N) Beads per monomeric unit, N=1-10, (Np) Degree of polymerization, Np=10-500, (Nb) Degree of branching (monomer unit), Nb=0-5, (BT) Branching periodicity (monomer unit), BT=2-10, (BL) Branching length (monomer unit), BL=1-10, (SBb) Degree of sub-branching (monomer unit), SBb=1-10, (SBT) Sub-branching periodicity (monomer unit), SBT=2-10, (SBL) Sub-branching length (monomer unit), SBL=1-10. Further descriptors that will be added, involve chemical interactions, such as: (A) Number of amphiphilic units, A=(0.001-0.02)N, (PB) Positive polar beads per polymer chain, PB=(0.01-0.20)N, (NB) Negative polar beads per polymer chain, NB=(0.01-0.20)N

b) The preferred approach, instead of hardwiring to a specific solution, is to write a simple flat file parser that takes the chromosome word and runs a python-driven moltemplate structure generator, force-field setup and lammps input scripts.

A few challenges have arisen here, an important one has been the need for an accurate screening function. Currently we're using slope of the log(eta)/log(strain_rate), which has proven tricky to systematically discriminate between normal viscosity oscillations (within our error bars) as a function of strain rate and true non-Newtonian regimes.

4.4 Coarse-grain to Atomistic Mapping from Accurate QM and FF Methods

Progress has been made in the following three aspects:

1. Systematic atomistic-CG mapper (a2cg). Stage two of this builder will include chemical descriptors (polar groups). The a2cg module involves the following steps (Figure 24):

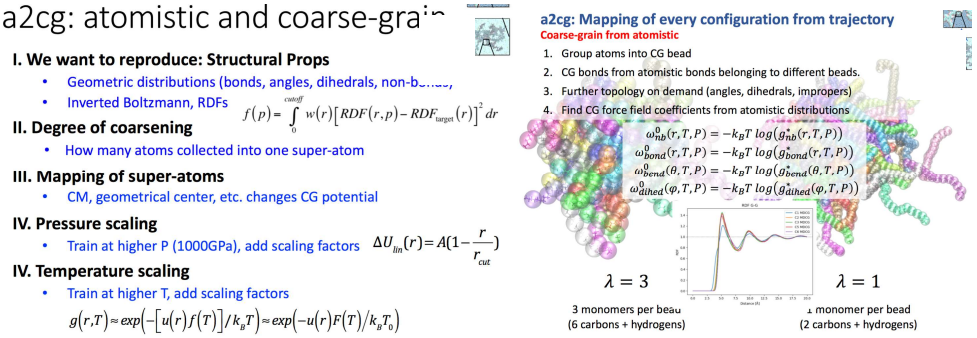

Figure 24. (left) Steps in a2cg, and (right) variable degree of coarsening as a function of pressure, temperature, and atomic bond, angle, and torsion distributions.

2. A CG-level (cg-gen) topological builder (Figure 25), including multiple descriptors (degree of branching, degree of polymerization, branching frequency, branch length, and others).

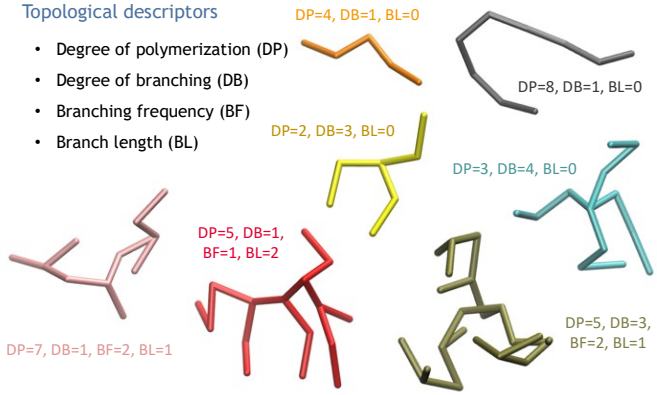

Figure 25. Systematic cg-gen topological builder used for screening large-scale coarse-grain models of complex systems. Stage 1 only includes topological descriptors (graph adapted from Kempfer, Jaramillo-Botero, etal).

The cg-gen builder now reads the CG force field parameters from a file and a polymer model file, as exemplified below (Figure 26),

```
[ajaramil@fermion]:more ff.builder
#  course grain force field parameters for PE (dreiding like)

# number of types
# keyword value
num_of_types   2

# mass
# type keyword value unit
0   mass   43.089   g/mol
1   mass   42.081   g/mol

# bond
# type1 type2 keyword value unit
0   1   k_bond   6.96   kcal/mol A^2
1   1   k_bond   6.16   kcal/mol A^2
0   1   r_0            3.65   A
1   1   r_0            3.64   A

# angle
# type1 type2 type3 keyword value unit
0   1   0   k_theta   1.09     kcal/mol
0   1   1   k_theta   1.19     kcal/mol
1   1   1   k_theta   1.19     kcal/mol
0   1   0   theta_0   175.5   degree
0   1   1   theta_0   175.0   degree
1   1   1   theta_0   173.0   degree

# non-bond
# type1 type2 keyword value unit
0   0   epsilon   0.469     kcal/mol
0   1   epsilon   0.444     kcal/mol
1   1   epsilon   0.42      kcal/mol
0   0   sigma     4.585     A
0   1   sigma     4.5455    A
1   1   sigma     4.506     A
```

```
[ajaramil@fermion]:more descriptor.builder
# descriptor of polymers
# keyword value
num_of_chains          50
branch_frequency       20
ave_linear_length      100
ave_branch_length      20
density                 0.7
sigma                   1.0     # for gaussian random
random_seed        123456
```

Figure 26 (left) example force field descriptor notation file for cg-polyethylene, and (right) cg-polymer model descriptor file for systematic cg-gen.

We are currently supporting chemical groups (cg bead Dreiding-like energy definitions) for polyethylene, polyacrylamide, and PEO. These cg force field parameters were obtained from equilibrated atomistic molecular dynamics distributions, at different temperatures (300-600K) and pressures (1-1000atm). Cg-gen produces and output file ready to run with LAMMPS (as exemplified below in Figure 27), which can be viewed using any molecular visualizer, as shown in the inset figure. Cg-gen grow particles stochastically along the polymer backbone or side-chains, calculating the non-bond energy of insertion, from the previous insertions, using a cutoff-based connectivity list to reduce computational costs.

```
# Model of polymers:
# Number of chains = 50, Branch frequency = 20, Average linear length = 100, Average branch length = 20
# Density = 0.7, Random seed = 167585, Random sigma = 1.0, Total cancels = 232, Time used = -1 hours  52 minutes  49 seconds.
# Total non-bond energy = -32987.9364, Total non-bond energy between different chains = -22680.0724, Tangle rate: 68.75 %

     10451   atoms
     10401   bonds
     10626   angles

         2   atom types
         3   bond types
         6   angle types

       0.0000     101.4517 xlo xhi
       0.0000     101.4517 ylo yhi
       0.0000     101.4517 zlo zhi

Masses

         1 43.0890
         2 42.0810

Atoms

         1     1     1      52.2015      90.2911      89.0255
         2     1     2      49.8787      88.0982      90.7914
         3     1     2      47.9410      85.5452      92.5169
         4     1     2      46.3176      83.1301      94.7035
         5     1     2      44.7319      80.3976      96.5115
         6     1     2      43.6441      77.3501      98.1784
         7     1     2      43.0575      74.1694      99.8484
         8     1     2      42.3323      71.2834     101.9447
         9     1     2      41.7533      68.7331     104.4766
        10     1     2      41.3248      66.5804     107.3804
        11     1     2      40.5655      64.7985     110.4622
```

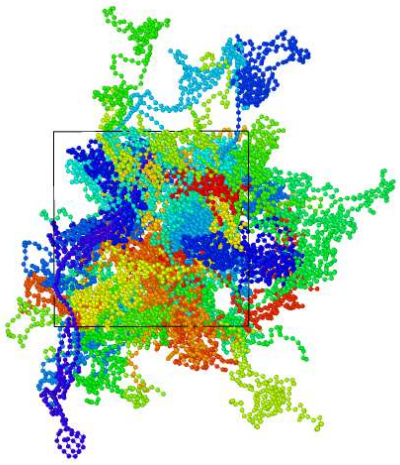

Figure 27. cg-gen output example, color-coded polyethylene chains in a cubic unit cell at a density of 0.7g/cc (Zheng, Jaramillo-Botero et al.)

3. Atomistic and CG-level simulation engines for computing structural and rheological properties is ready (zero shear, dynamic viscosities as a function of shear-rate for atomistic and cg systems, now incorporating changes in pressure, temperature and chemical - polarity/amphiphilicity). The focus here has been on validating the rheological and structural prediction molecular dynamics engines, and in embedding systematic convergence criteria within the in-silico screening framework (Figure 28) to make simulation times independent of model system complexity and size. We can now routinely screen viscosity vs shear-rate, as shown below (using a cg-description), and we expect to meet experiments in the shear-rate timescales within the next quarter of this effort.

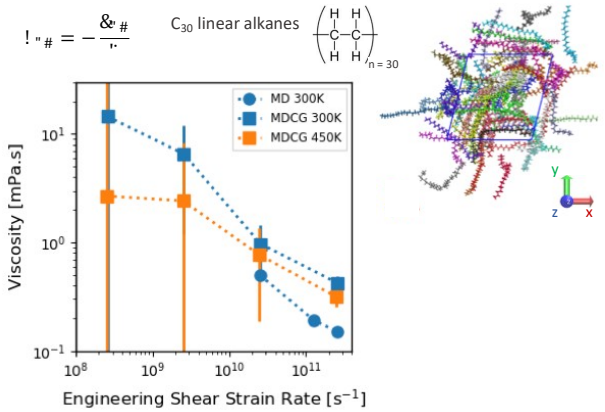

Figure 28. Viscosity vs shear-rate for a fully atomistic system and its CG equivalent (at 300 and 450K) match existing data for polyethylene. Shear-rate limited by atomistic timescales. Current timescales in the CG-only simulations down to $10^{6\text{-}7} s^{-1}$

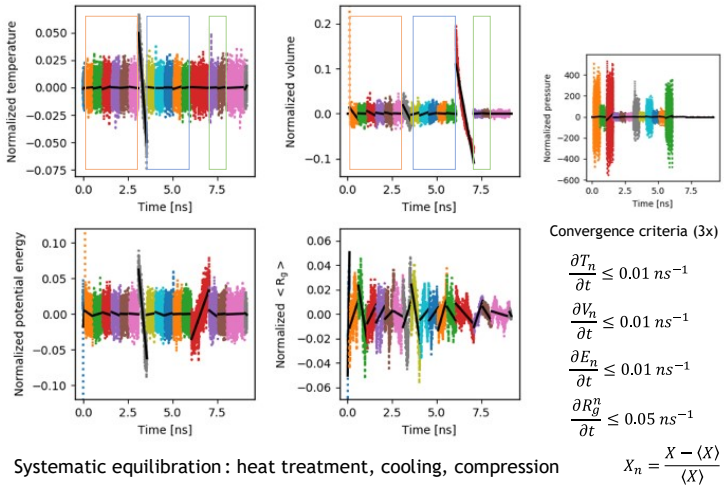

Figure 29. Systematic convergence criteria set for system-independent convergence in the in-silico screening framework (Kempfer, Jaramillo-Botero et al.)

Before we move fully into the CG-atomistic-mapping, we will be deploying production runs within the integrated framework at the CG level, i.e. in-silico screening using an evolutionary algorithm to automatically generate topologies from the cg-gen code using the topological and chemical descriptors, to determine the best performers in terms of shear-thickening compositions and structures. Best performer will have the best positive slope in the non-linear viscosity as a function of shear-rate. These will then be validated against the experimental cues.

As the next step, reverse mapping cg2a, requires an optimization step to guarantee conformational and structural mapping at the atomistic level.

4.5Parameterization of QM-CG-PAM Force Field[4,5]

4.5.1 Setup

All quantum mechanics (QM) computations for the EOS of PAM crystals were performed using the Vienna Ab initio Simulation Package (VASP) at the level of Density Functional Theory (DFT) with the PBE flavour of the Generalized Gradient Approximation and including the Grimme-Becke-Johnson D3 dispersion corrections. We showed recently that this PBE-D3 DFT leads to accurate EOS for molecular crystals up to 100 GPa or higher. We generated the QM EOS as cold-compression/expansion curves and then mapped onto CG models using our coarse-grain model depicted in Figure 30.

We considered two crystal configurations:

- CRY1 contains hydrophilic-hydrophilic and hydrophobic-hydrophobic interaction configuration.
- CRY2 contains hydrophilic-hydrophobic interaction configuration.

From CRY1 we generate two EOS: on for hydrophilic-hydrophilic interaction and one for hydrophobic-hydrophobic

From CRY2 we generate one EOS: for hydrophilic- hydrophobic interactions.

These EOS were crystals obtained by compressing and stretching along the lattice directions without changing the intrachain bond distances angles or chain-orientation.

Figure 31 and Table 2 show the QM-geometry-optimized PAM crystals. Every crystal contains 2 chains times 4 monomers.

To fit these QM EOS, we describe the nonbond interactions between the beads using Morse two-body potentials (**Equation 1**).

$$E_{vdW} = D_0\{\exp[-2\alpha(r-r_0)] - 2\exp[-\alpha(r-r_0)]\} \qquad (1)$$

Here we considered EOS chosen to emphasize different CG interactions.

The CG level calculations were performed using the LAMMPS Molecular Dynamics Simulator.[24] The parameters for the nonbond interactions (refeed to here as van der Waals, vdW) were adjusted to fit the five QM EOS. QM energies were obtained for all the chains while keeping the chains rigid during the lattice parameter changes.

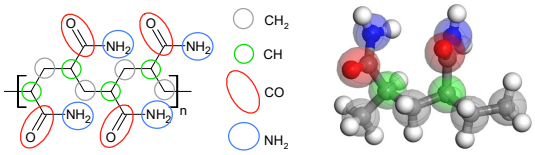

Figure 30. Coarse-grain mapping scheme for polyacrylamide (left) and atomistic representation (right). The beads are located at the center of mass of the corresponding atomic groups.

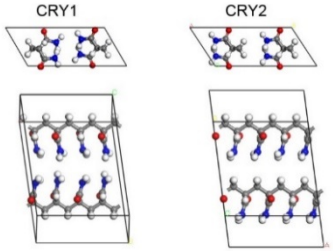

Figure 31. Optimized crystal structures of polyacrylamide. CRY1 has hydrophilic-hydrophilic and hydrophobic-hydrophobic interaction. CRY2 has only hydrophilic-hydrophobic interactions. The upper figures show perpendicular to the chain axis. The lower figures show the side view. Grey = carbon, red = oxygen, blue = nitrogen, white = hydrogen.

Table 2. Optimized lattice parameters of polyacrylamide crystals. Units are Angstrom and degree.

Structure	*a*	*b*	*c*	*α*	*β*	*γ*
CRY1	10.25	13.63	6.15	123.64	94.05	97.26
CRY2	10.24	13.52	6.01	119.74	90.85	97.92

In order to obtain accurate valence interactions, EOS target on a 10-monomer model is calculated using the DFT-PBE-D3 level based on the deformation of a sampling fragment in the chain(**Fig. S1 (a)**). The energy-deformation relationship is shown in (**Fig. S1 (b-g)**). Every EOS is an independent bond-stretching or angle-bending without any changing of other bonds or angels.

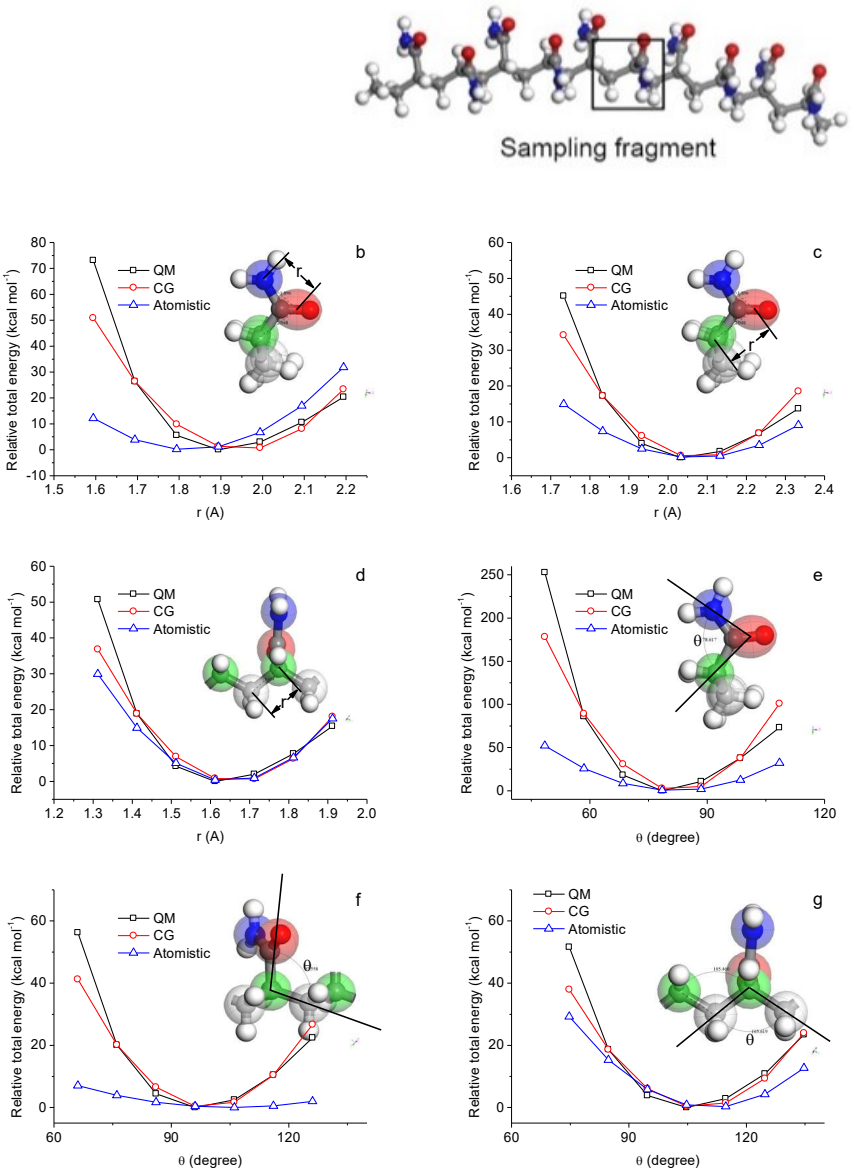

Figure 32. Fragment sampling (a) and the bond-stretching and angle-bending EOS (b-g).

Then we used QM to examine the energies for stretching the bonds and for bending the angles using PBE-D3. There were fitted to obtain Harmonic potentials (**Equation 2** and **3**) for the bonds and angles of the CG-PAM. The fit is shown in Figure 32.

$$E_{bond} = K_B(r - r_0)^2 \qquad (2)$$

$$E_{angle} = K_A(\theta - \theta_0)^2 \qquad (3)$$

We also derived nonbond vdW interaction parameters between water and PAM based on QM calculations at DFT-PBE-D3 level. The force field used for water is the SPC-E water model[25], which contains three charge sites but only one van der Walls site (centred at the oxygen atom). Our coarsening of the water-PAM interactions uses the bead located at the oxygen as the vdW site for the water molecule. For the water-water interactions we use the original SPC-E model. To obtain explicitly interaction parameters between the water bead and the PAM beads, we built gas models of isolated acrylamide monomers with a single water molecule adsorbed at various sites. the nonbond parameters for water-PAM were obtained by considering the correlations of the water bead-PAM bead distances and QM energies.

4.5.2 Parameterization of Van der Walls interactions

To obtain EOS of the PAM crystals, the deformations were done by increasing one cell parameter at a time. This helps identify which group pair is responsible for the change in energy. All pairs of non-bond interactions contribute to each EOS, so it's unlikely that a single set of parameters agrees with all the QM-EOS at once. However, a good initial guess of the parameter set can be obtained from the corresponding deformation. As Figure 33 shows, the EOS a, b, c, d and e mainly involve NH_2...NH_2, CH_2...CH_2, NH_2...CH_2, CO...NH_2 and CO...NH_2 non-bond interactions. we obtained the non-bond parameters (Table 3) for the beads as best fit possible over all 5 QM-EOS.

Table 3. Optimized Morse parameters for the CG-PAM non-bond interactions.

Non-bond interaction	D_o (kcal mol^{-1})	α	r_o (A)
CH_2-CH_2	0.1141	1.4170	4.2771
CH_2-CH	0.1141	1.4170	4.2771
CH_2-CO	0.3258	1.3083	4.0052
CH_2-NH_2	0.3327	1.2306	4.4548
CH-CH	0.1141	1.4170	4.2771
CH-CO	0.3258	1.3083	4.0052
CH-NH_2	0.3327	1.2306	4.4548
CO-CO	0.9307	1.1995	4.4345
CO-NH_2	0.9503	1.1218	3.8019
NH_2-NH_2	0.9702	1.0441	3.9663

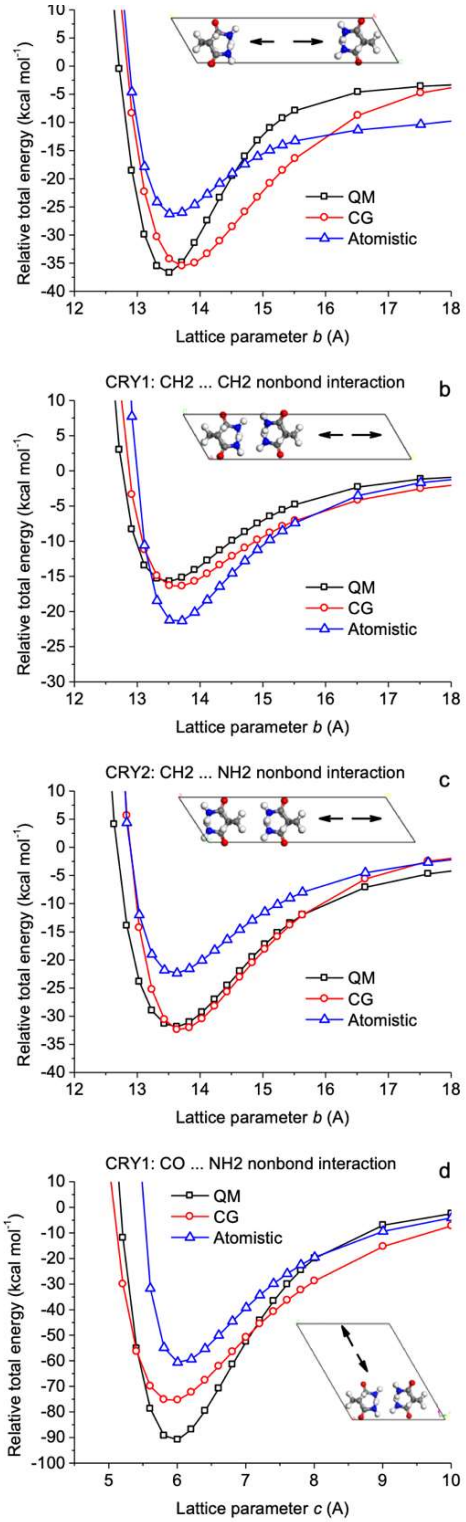

Figure 33.Five EOS according for changing various cell parameters for PAM crystals while keeping the chains rigid. The arrows represent the stretching directions of the crystals.

4.5.3 Validation of optimized CG-PAM force field

Using our CG-PAM model for a system of 20 chains each with 100 PAM monomers, we carried out MD with our optimized QM-CG-PAM force field to physical properties which we compared to experimental data and to an atomistic force field (OPLS).[26] To obtain an equilibrated polymer model, we built the initial structure at a low density (0.6 g/cm^3) followed by a series of "compress-quench" iterations that increases the density slowly until it reaches a desirable density (1.3 g/cm^3), as shown inFigure 34. 800 K was found to be a proper top temperature for quenching the CG-PAM. We suggest using the melting point as the target quenching temperature. This procedure allows the chains to entangle optimally with each other.

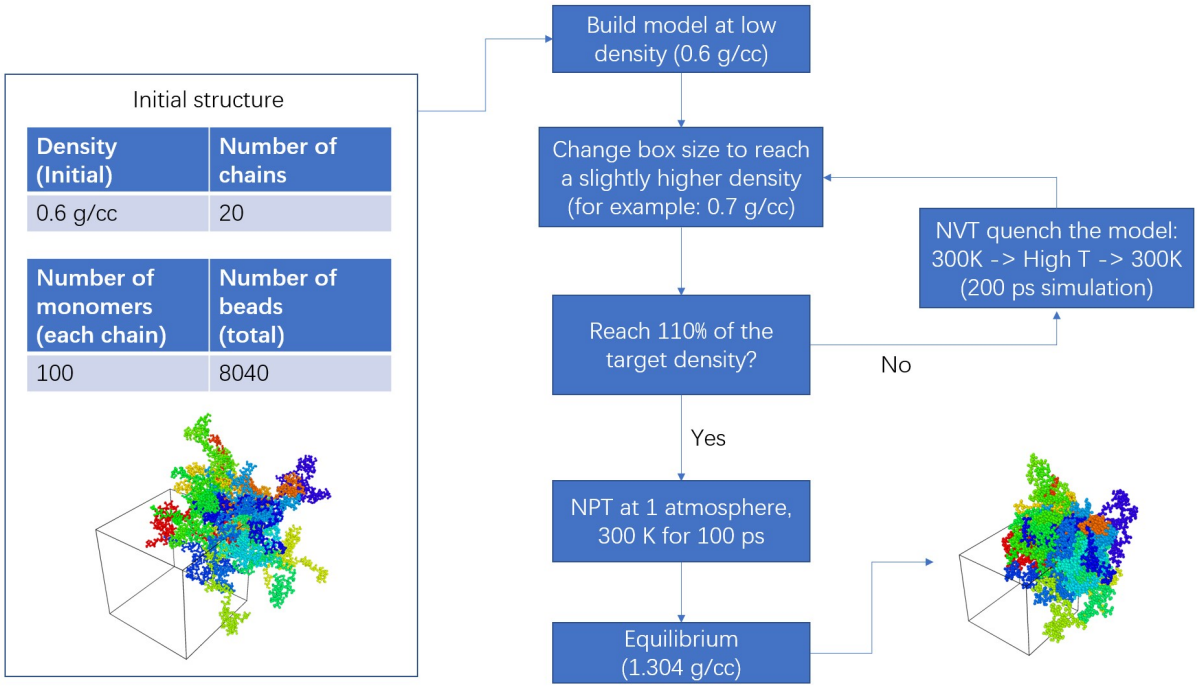

Figure 34. The construction and equilibrium procedure of the CG-PAM model.

We integrated the isobaric molecular dynamics ensemble equations of motion for the CG-PAM model using a 5 fs integration timestep with a Nose-Hoover thermostat (damping time of 500 fs) and a Nose-Hoover barostat (pressure damping time of 5 ps). The NPT simulations were performed for 1 ns at various temperatures in the range of 300-750 K and pressure of 1 atmosphere to obtain such experimental observables as density, heat capacity, and melting temperature.

We built and simulated an equivalent-sized PAM atomistic model using the OPLS force field for comparison.[26] A timestep of 1 fs, a temperature damping time of 100 fs and a pressure damping time of 1 ps were used for the atomistic simulations, while other settings remained the same as those in the CG model.

Using our optimized water-PAM interactions, we simulated aqueous gel models consisting of PAM and water with concentrations of 40, 60 and 80 % PAM by weight. These were built and

relaxed using the same procedure as for pure CG-PAM. The amount of CG-PAM was kept constant at 20 chains each with 100 monomers, while the amount of water molecules was set to 2000, 5300 and 11900 to reach the PAM weight concentrations of 40, 60 and 80%, respectively. The water-water interactions used the SPC-E water model. Together with our optimized CG-PAM force field and water-PAM interactions, the observables including density, specific heat capacity and thermal conductivity for 3 concentrations were obtained by 1 ns NPT dynamics simulations. The same simulations were performed on atomistic models using the OPLS force field for comparison. All dynamics for PAM aqueous gels were done at 300 K and 1 atmosphere pressure using the NPT ensemble, Nose-Hoover thermostat and barostat with 1 fs timestep, 100 fs temperature damping time and 1 ps pressure damping time.

We then carried out simulations using CG-PAM to shear these systems using a SLLOD deformation scheme in non-equilibrium molecular dynamics (NEMD) simulations.

Both our CG force field and the atomistic OPLS force field lead to good minimum-energy lattice parameters, which means they both lead to good densities. The main problem is the depth of the energy curves. The atomistic OPLS force field overestimates the hydrophilic interactions (by 35%) but underestimates the hydrophobic ones (by 39 to 58%). By contrast, our CG force field agrees much better with QM for the binding energy (2 to 17% deviation). This implies that the CG force field should be more accurate than OPLS for energy-dependent properties, such as melting point, heat capacity and thermal conductivity.

Due to the important applications of PAM as a water thickener, we calculated three EOS related to rheology. These EOS are for validation not parameter optimization. In Figure 35(a), both the CG and OPLS force field show barriers 60% lower than the QM-predicted EOS. The CG and the OPLS force field underestimate the friction between the chains having hydrophilic-hydrophilic contacts and hydrophobic-hydrophobic contacts. Otherwise the CG force field is in good agreement with the QM friction EOS and slightly better than OPLS (Figure 35(b) and (c)).

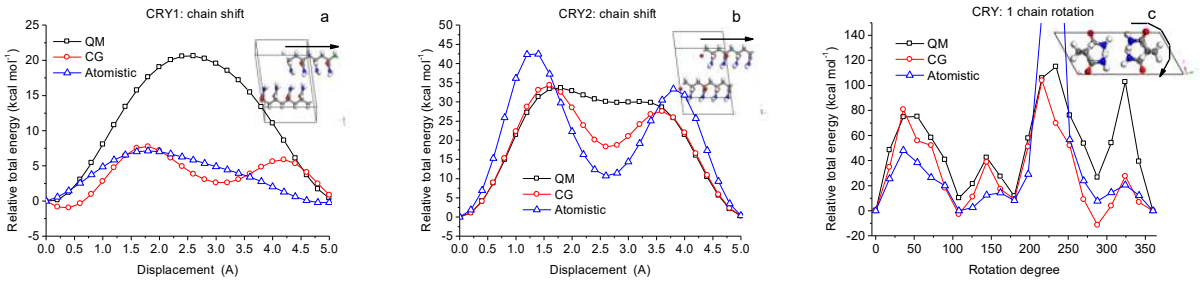

Figure 35. EOS for translation a single one chain in CRY1 (a) and CRY2 (b) and the EOS of rotation of one chain in CRY1 (c).

The non-bond interactions parameters between water and CG-PAM were developed for aqueous gel simulations, using the QM EOS of the water-monomer adsorption structures. Again, the atomistic OPLS force field overestimates the hydrophobic interaction and underestimates the

hydrophilic interactions. Sometimes these deviations cancel each other, but still probably there may be errors for energy-dependent properties. By fitting to the QM-predicted EOS, the optimized CG force field are more accurate than OPLS in reproducing the potential energy curve, represents an improvement for aqueous PAM gel models and simulations.

4.5.4 Validation against experimental observables

The best validation of a simulation method is to compare with experiment. First, we focus on the melting point, an important index for polymers. The NPT dynamics simulations for CG-PAM and atomistic PAM were performed at various temperatures to obtain the time-averaged density and potential energies as functions of temperature. Since the temperature dependence of the properties change at the phase transition, we located the melting points at the turning points of these functions. Figure 36 shows the estimated melting points by CG-PAM (517-530 K) and atomistic PAM (553 K). Comparing with the experimental melting point 519-523 K, the CG-PAM model is more accurate.[27] Notice that the densities of both CG-PAM (1.304 g/cm^3) and OPLS PAM (1.307 g/cm^3) are in good agreement with experiment (1.30 g/cm^3), but their thermal expansion behaviours are slightly different. The OPLS model for PAM has a lower density at high temperatures. This is probably caused by the underestimate in vdW well depths for hydrophilic groups.

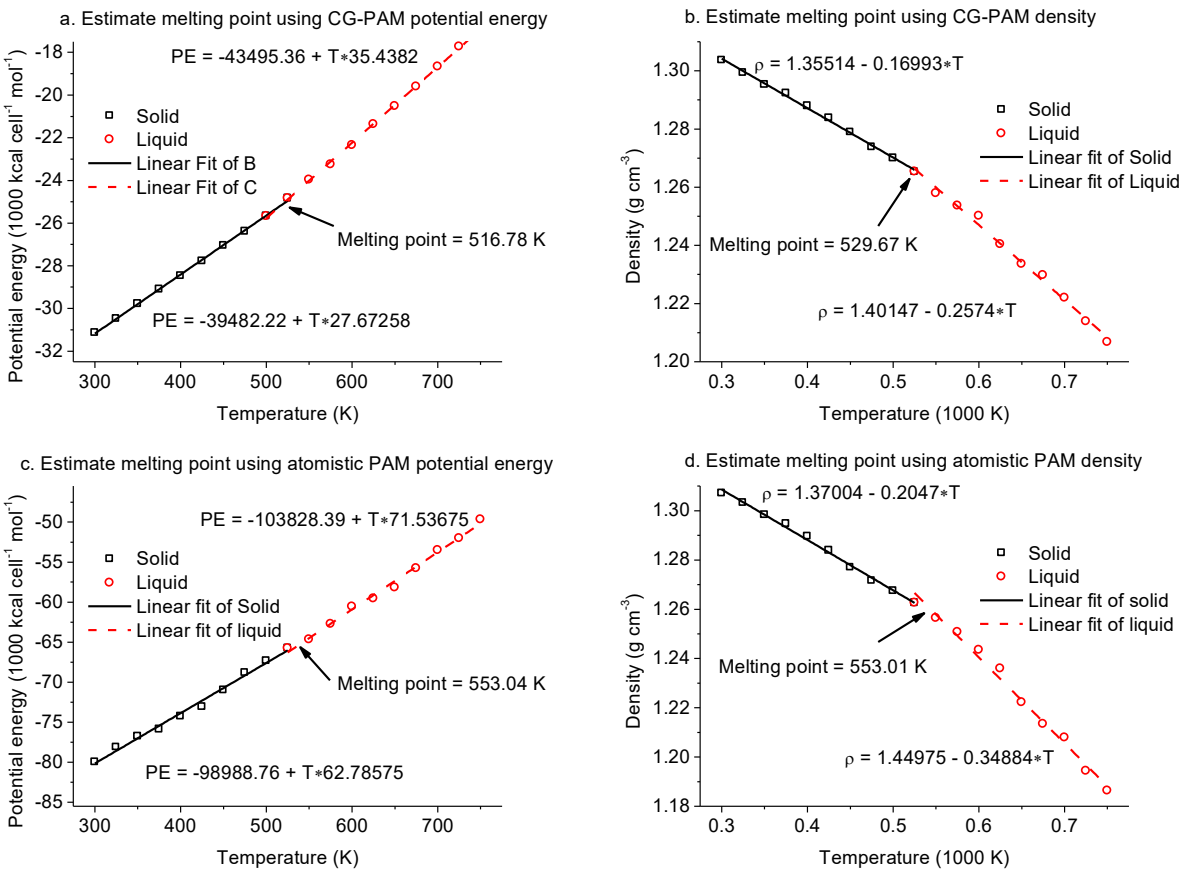

Figure 36. Estimated melting point using the turning points in the temperature dependence functions of potential energy and density. The experimental melting point of PAM is 519-523 K.[27]

The second validation is heat capacity. The time-averaged enthalpies at different temperatures were calculated, leading to the specific heat capacities (C_p) shown in Figure 37. The OPLS PAM model shows 1.5 times larger C_p than experiment. This may be because of the too-weak hydrophilic interactions. In contrast, the C_p of CG-PAM model (1.45 kJ kg^{-1} K^{-1}) agrees roughly with experiment (1.75 kJ kg^{-1} K^{-1}).[28] We find similar behaviours for the aqueous PAM gel at 300K as shown in Figure 37(b).

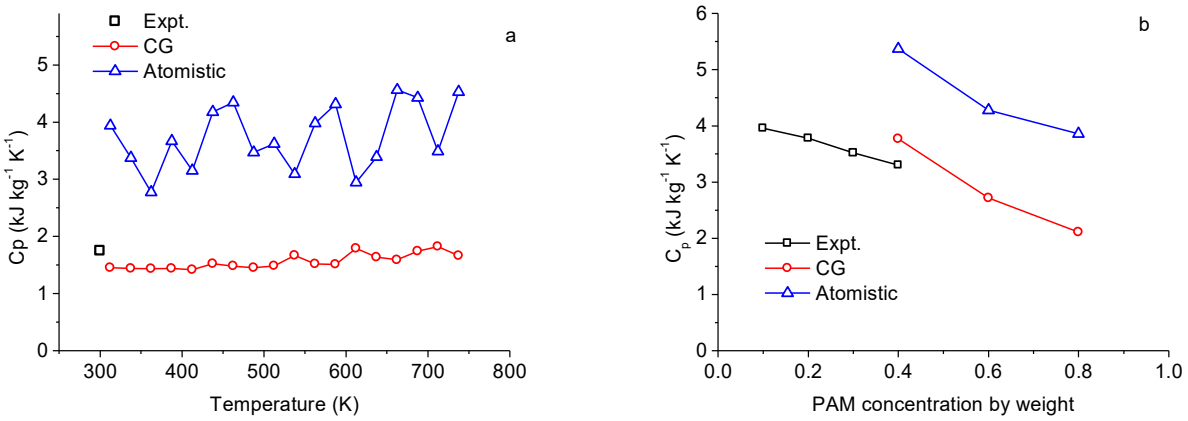

Figure 37. Temperature dependence of specific heat capacities for pure PAM (a) and concentration dependence of specific heat capacities under 300 K for aqueous PAM gel (b).

The remaining validations focus on the concentration dependence of density and thermal conductivity. Figure 38(a) shows that the density of CG-PAM aqueous gel (1.123 g/cm^3) agrees with experiment (1.138 g/cm^3) at a concentration = 0.4. In contrast, the OPLS model leads to 10% larger density at the same concentration. The reason may be the inaccurate water-PAM non-bond interactions.

The thermal conductivities were calculated using the Green-Kubo (GK) formulation which averages the auto-correlation of the heat flux. Both CG and OPLS models produce thermal conductivities higher than experiment[28], but the CG model shows better accuracy than the OPLS model.

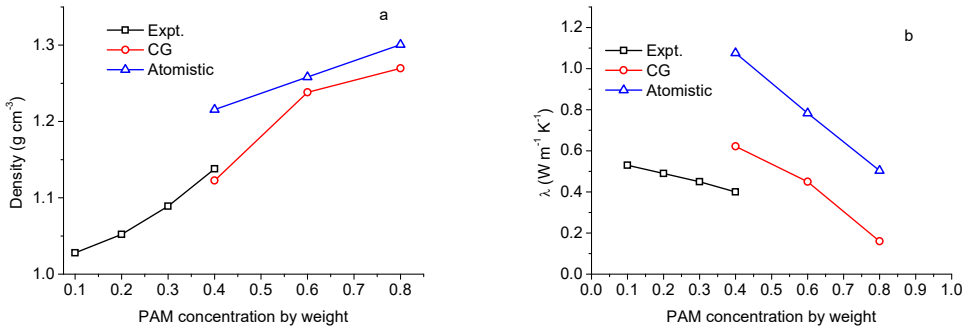

Figure 38. Concentration dependence on density and thermal conductivity for aqueous PAM gel under 300 K.

From the above validations, this QM based CG-PAM force field provides good accuracy for large scale length-time simulations. The accuracy improvement arises from parameterizing directly to QM, and the scale capability is extended by the coarsening. For same size of polymer models, the

CG model has a larger mass with reduced interaction terms than the atomistic model. This CG model allows us to use longer timesteps to simulate larger models. Comparing with the OPLS atomistic forcefield, our CG-PAM force field uses 2/5 the number of interacting units to represent the atomistic model. We have tested that the simulations are stable at 0-1500 K for timesteps of 5 to 10 fs, which is 5 times longer than the OPLS (usually 1-2 fs). On the whole, the computational efficiency of CG-PAM model is 12.5 times that of atomistic model.

4.6 Syntheses of SRM Polymers

4.6.1 Monomers

Based on the position of hydrophobes in the polymer chain, associating polymers with potential shear-thickening capabilities can be classified into following categories:

- telechelic polymer where hydrophobes are located at chain ends;

- comb copolymer where hydrophobes are evenly distributed in the chain;

- bunched copolymer where hydrophobes are sparsely clustered in the chain (unlike block copolymers where hydrophobes are clustered into long sections)

- random copolymer where hydrophobes are randomly distributed in the chain;

- random copolymer with spacer where hydrophobes are attached to the chain through molecular connectors;

- hydrophobic alkali-swellable emulsion.

Considering the materials cost and convenience of manufacturing, we have established that polyacrylamide (PAM) modified with rationally selected surface-active or hydrophobic functional monomers will be our technical route towards the manufacturing of associating polymers with shear-thickening properties. Via controlling percentage of hydrophobes and the reaction conditions, we can alter the resultant modified PAM-based copolymer all the way from block to comb structure, and to random structure. In order to maximize solubility and rheological tunability of these SRMs, random distribution of discrete hydrophobes is desired.

PAM-based SRMs can be synthesized both in one step and through post-polymerization functionalization in order to incorporate hydrophobes. The advantage of incorporatinghydrophobic groups into PAMafter the polymerization processis that commercially available polymerscan be used as starting material. However, such advantage is unfortunately overshadowed by the disadvantagethat reactions involving viscous polymer solutionsare not easily carried out due to the problemsassociated with mixing and reaction homogeneity. As a result, we focus on surface-active or hydrophobic monomers containing vinyl groups so that they can be incorporated into the PAM chains *in situ* during polymerization.

The candidates of these functional monomers can be classified by whether they contain hydrophilic spacers, which are usually short polyethylene oxide (PEO) blocks. In both categories, the most common candidates are hydrophobically modified acrylamides and acrylates, which are more likely to be compatible with acrylamide in terms of solubility and reactivity.

4.6.2 Gel Polymerization

Both amphiphilic monomers, ionomers and aromatic monomers can be incorporated into the PAM backbone through the one-step co-polymerization with acrylamide and sodium acrylate monomers. Several parameters are carefully controlled and frequently tuned in order to achieve polymer products with desired molecular weight, linearity, water solubility, monomer distribution and reaction yield, including:

(1) molar ratios of monomer;

(2) amount of water (i.e., reciprocal of monomer concentration), which should be high enough to ensure dissolution of monomers and mitigate uncontrolled chain propagation during polymerization, but low enough to ensure proper reaction rate and reduce water content in the resultant gel product;

(3) types of initiators (peroxides, azo compounds, etc.) that are compatible with the desired reaction temperature;

(4) amounts of initiators that should be high enough to trigger the reaction but low enough to achieve high molecular weight;

(5) reaction temperature that should be high enough to trigger the reaction but low enough to avoid uncontrolled reaction acceleration and temperature overshoot (since the polymerization processes are strongly exothermic);

(6) solution pH which will affect the forms of ionomers and reactivities of certain monomers;

(7) chain transfer agents which are introduced to avoid branching, control overall molecular weight and improve the solubility of products;

(8) types and dosage of surfactants that solubilize some of the otherwise water-insoluble monomers.

Other experimental factors such as stirring and degassing of reaction mixtures should also be carefully controlled and optimized.

Specific to monomers with long hydrocarbon chains and/or aromatic groups, surfactants are necessary as solubilizing agent, and the polymerization process virtually resembles the emulsion polymerization (Figure 39). The amount of surfactants need to be sufficient to not only solubilize all the non-hydrophilic monomers but also form free micelles that can accommodate the free radicals generated *in situ* and the monomers diffused from the emulsion droplets, serving as microreactors for chain propagation. In this sense, the types of concentrations of the surfactant,

which determines the sizes and numbers of the micelles, are crucial to the molecular weight and monomer distribution of the final modified PAM products. It is also noted that for gel polymerization, the resultant products actually contain the original surfactants since the product is processed via desiccation rather than precipitation, and these surfactants may have complicated effects on the rheological behaviors of the polymer.

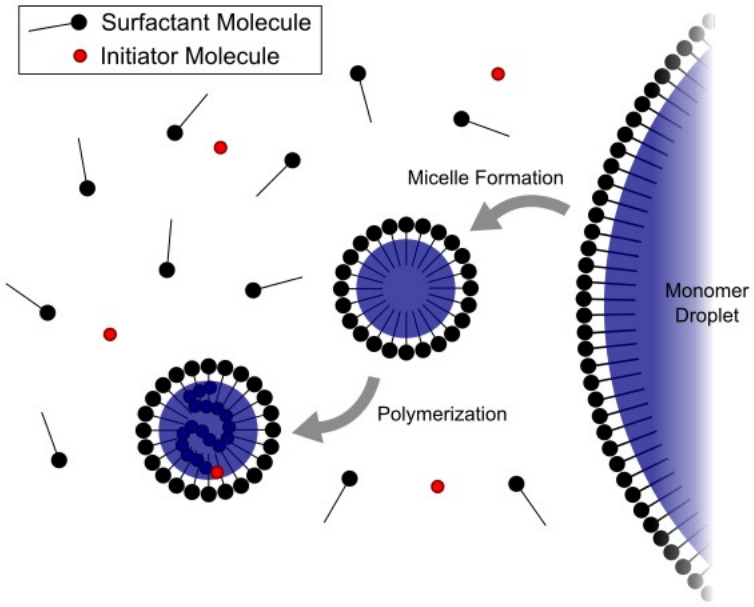

Figure 39. Schematic illustration of emulsion polymerization.

4.6.3 Post-synthesis Modification

Introduction of special molecular interactions (electrostatic attraction/repulsion, van der Waals force, π-π stacking, etc.) via the incorporation of special vinyl monomers does have its limitations. The availability and cost of monomers with desired structures as well as their compatibility with the synthetic protocol of PAM in terms of factors such as solubility and reactivity can all pose restrictions towards the introduction of expected interactions. In particular, the vastly diverse reactivity of monomers with structures dissimilar to acrylamide (AM) can lead to the inability to control the unit distribution of molecular weight of the resultant polymer products.

In order to overcome such difficulties, post-synthetic modification has been proposed to allow the introduction of a wide range of chemical moieties and functional groups (Figure 40). In short, the carboxyl group on the partially hydrolyzed PAM is first activated by 1-ethyl-3-(3-dimethylaminopropyl)carbodiimide hydrochloride (EDC) to form the isoacylurea intermediate, which further reacts with N-hydroxysuccinimide (NHS) to yield the NHS ester, a more stable intermediate which can be stored for prolonged time. When this NHS ester intermediate undergoes the attack of primary amine, a nucleophile, acyl substitution reaction occurs, giving

rise to the final product of modified PAM accompanied with the departure of NHS. With such methodology, PAM whose nitrogen is functionalized with arbitrary chemical moieties can be obtained as long as the corresponding primary amine is available.

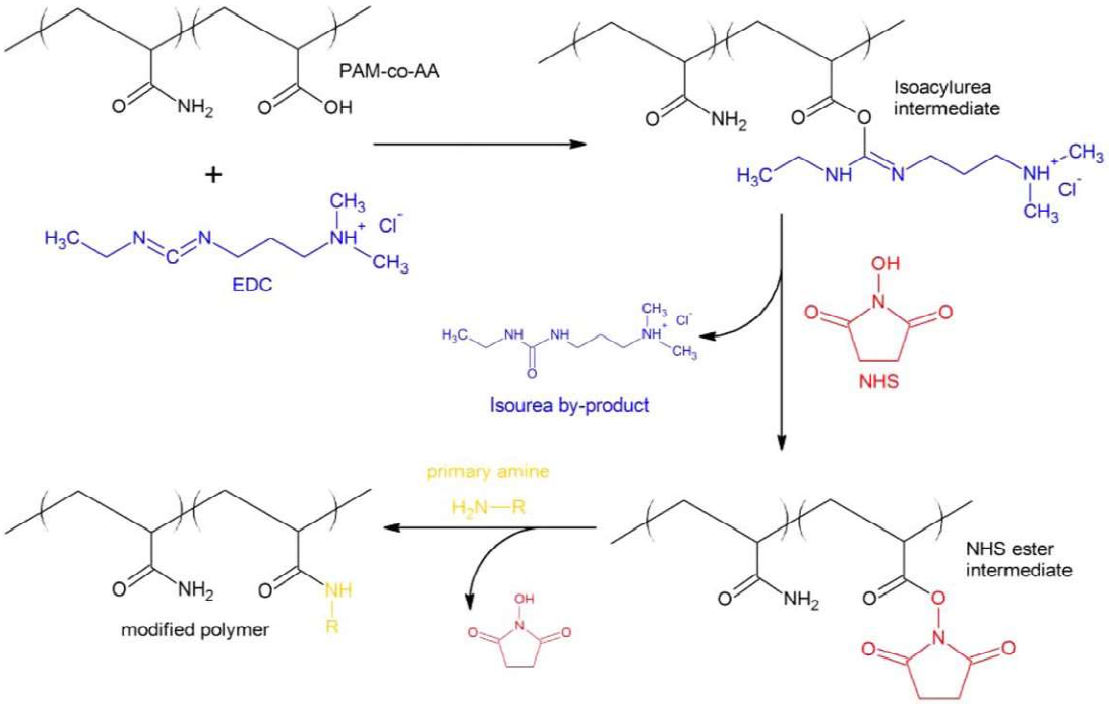

Figure 40. Post-synthetic modification of partially hydrolyzed PAM.[27]

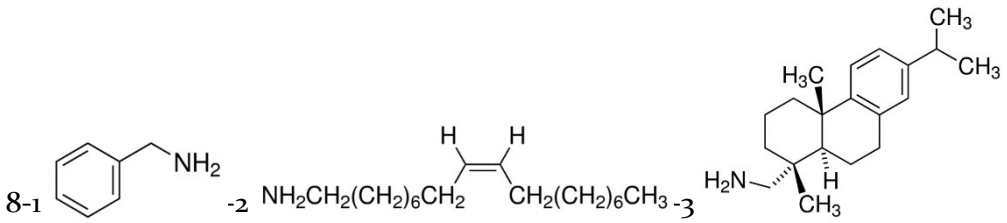

Figure 41. Common amphiphilic amines.

In order to introduce hydrophobic interactions to tune the rheological behavior of PAM, primary amines with relatively bulky aliphatic or aromatic tails are used for post-synthesis modification, such as benzylamine (8-1), oleylamine (8-2) and dehydroabietylamine (8-3, main component of rosin amine). To assist with the dissolution of relatively high concentration of amines with bulky tails, small amount of amphiphilic solvents such as tetrahydrofuran (THF) or 1,4-dioxane are sometimes added.

Typically, the three steps for the post-synthesis modification can be completed consecutively

[27] da Silveira, K.C. *et al.J. Appl. Polym. Sci.* **2015**, *132*, 42797.

within a single container. Partially-hydrolyzed PAM is first dissolved in water, and the addition of EDC, NHS and primary amine follows, each step separated by vigorous stirring for several minutes. As is discussed before, some amines are first dissolved in THF or 1,4-dioxane before they are added to the polymer solution.

One drawback of such approach is that as the molecular weight of partially-hydrolyzed PAM increases, the maximum concentration achievable decreases due to the excessively high solution viscosity, and this limits the throughput of the approach. One possible solution is to use acrylamide emulsion (a water-in-oil emulsion with extremely high concentration of PAM in the internal aqueous phase) as the source of PAM instead.

4.7 Rheological Properties of SRMs

Rheological properties of SRM polymers under specific conditions (shear rate, temperature, etc.) determine their actual performances during chemical flooding. In the previous progress report, we showcased our investigation into intrinsic properties of SRM polymers, such as cationic and anionic charge density, the effect of diacetone acrylamide (DAAM) monomer, and hydrophobic side chains attached through post-synthesis modification. Throughout Quarter IV and Quarter V, we continue our investigation with a shift of focus onto external factors, mainly the presence of salt and surfactant.

4.7.1 Effect of Salt

As will be further discussed in Section 4.5, we have found out that the presence of salt plays a key role in modifying the rheological properties of SRM polymers, and we consider this finding a major breakthrough achieved during this Phase II study that bears significance in the eventual commercialization of our technology, especially its deployment to chemical flooding operations.

First of all, it should be noted that the effect of salt is not universal. For traditional hydrolyzed polyacrylamide (HPAM), salt merely serves to compress the electrical double layer of the polymer colloid, reduce its hydrodynamic radius, and decrease the overall viscosity. For example, the viscosity of a 2000 ppm solution of 10% hydrolyzed HPAM decreases monotonically with the increase of ionic strength (Figure 42).

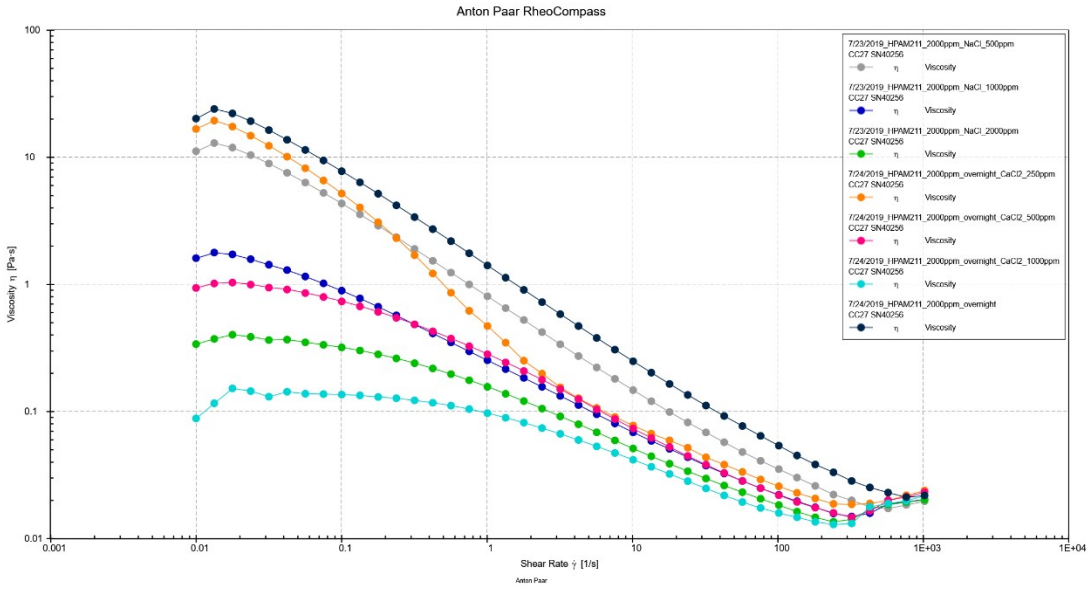

Figure 42. Rheology of HPAM solution under various salinity (black, grey, blue, green curves: increasing NaCl concentration) and hardness (black, orange, pink, cyan curves: increasing $CaCl_2$ concentration).

On the other hand, suitable salinity serves to enhance the abnormal rheological behaviors, especially the shear-thickening property of hydrophobically-modified PAM solutions. For example, 2000 ppm solution of a proprietarily-formulated SRM-1382 polymer possesses typical pseudoplastic characteristic when no salts are present, but the Newtonian and dilatant behavior starts to manifest itself and become more pronounced as the concentration of NaCl increases (Figure 43). In other words, salinity serves as a positive rather than negative factor to promote the viscosity of polymer solutions when hydrophobic side chains exist. It is notable that we can consistently reproduce such salt-induced shear-thickening behavior using different batches of SRM-1382 polymer, although the performance can be slightly different on a quantitative standard due to the variation in polymer synthesis and sample preparation.

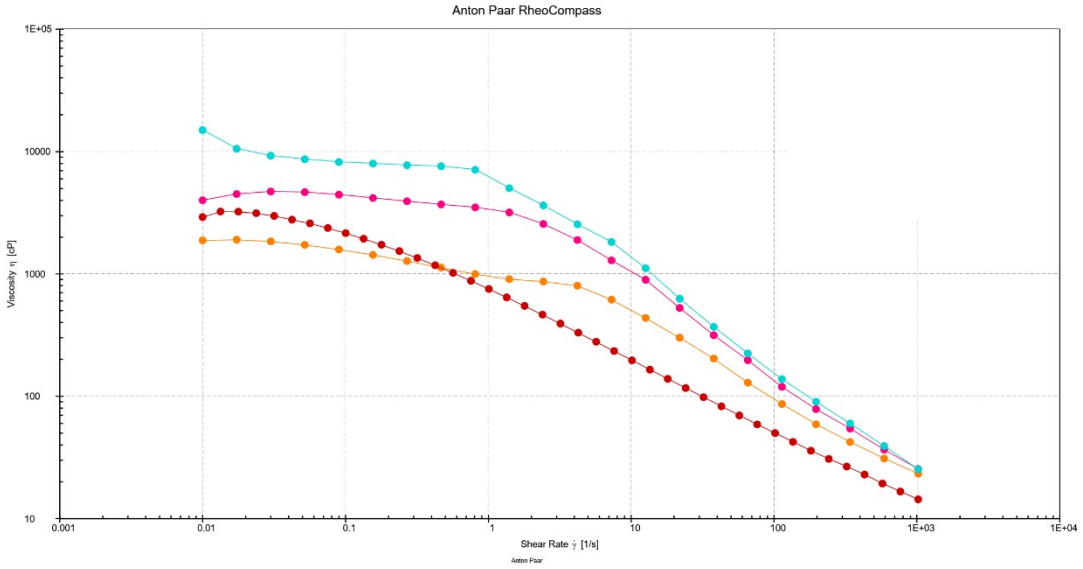

Figure 43. Rheological behaviors of SRM-1382 solution under various NaCl concentrations (red - 0 ppm; orange - 500 ppm; pink - 1000 ppm; cyan - 2000 ppm).

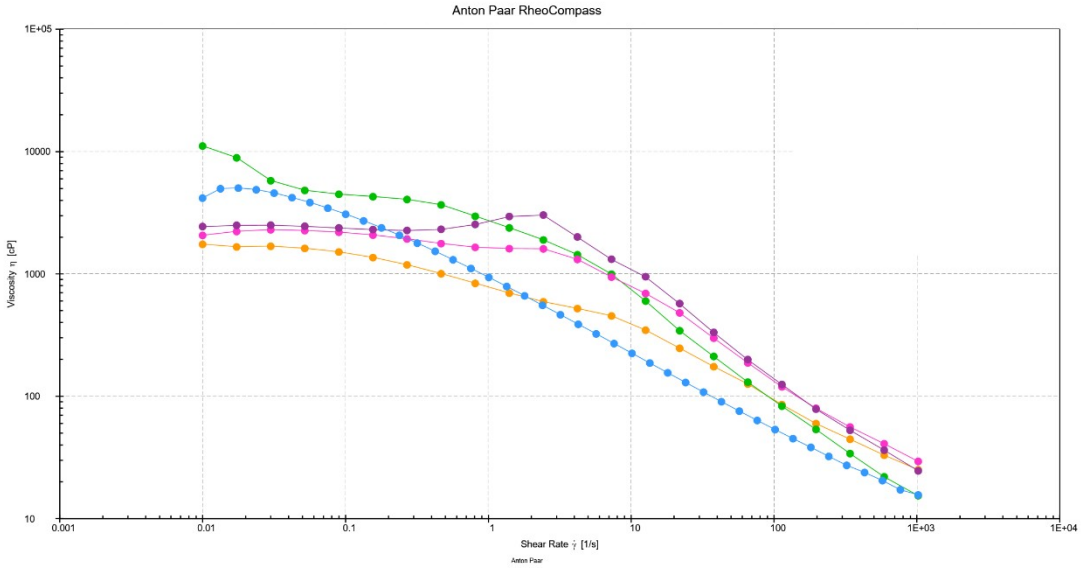

Figure 44. Rheological behaviors of another batch of SRM-1382 solution under various NaCl concentrations (blue - 0 ppm; orange - 500 ppm; pink - 1000 ppm; purple - 2000 ppm; green - 10000 ppm).

It is also noteworthy that even the presence of suitable concentration of divalent cations (such as Ca^{2+}) can significantly promote the shear-thickening behavior of hydrophobically-modified PAM (Figure 45). Contrary to most scenarios where the presence of divalent cations are strongly undesirable as they cause agglomeration of polymers and loss of viscosity, Mg^{2+} and Ca^{2+} can actually enhance the performance of hydrophobically-modified PAM under medium to high shear rate, a highly desirable feature for flooding and other operations where the purity of water cannot be guaranteed due to technical and/or economical reasons.

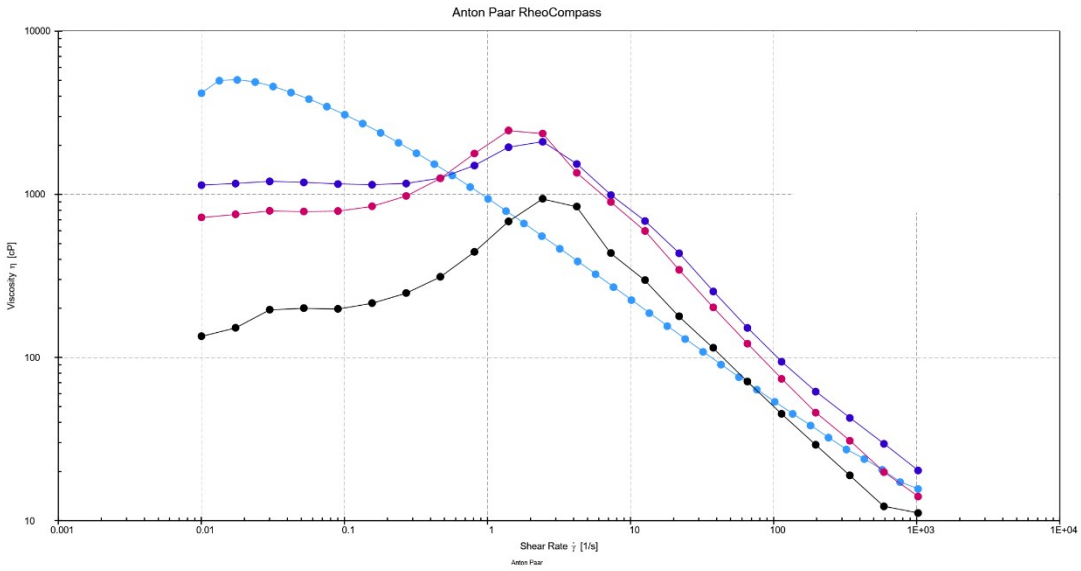

Figure 45. Rheological behaviors of SRM-1382 solution under various $CaCl_2$ concentrations (blue - 0 ppm; indigo - 500 ppm; fuchsia - 1000 ppm; black - 2000 ppm).

Upon observing such unusual salt-induced shear-thickening phenomenon, we have briefly investigated the underlying mechanisms that govern such behavior. Three possible mechanisms are put forward:

-Ionic or coordinative binding that bridges polymer chains;

- Charge screening that leads to proximity of polymer chains;

- Higher solution polarity that promotes hydrophobic interactions.

Control experiments indicate that the first hypothesis, namely specific ionic bonding between ions and polymer chains, is not responsible for the abnormal viscosification as equally concentrated monovalent cations (Na^+, K^+, Li^+, NH_4^+) and anion (Cl^-, NO_3^-) give rise to almost the same rheological curves of SRM-1382 solution (Figure 46).

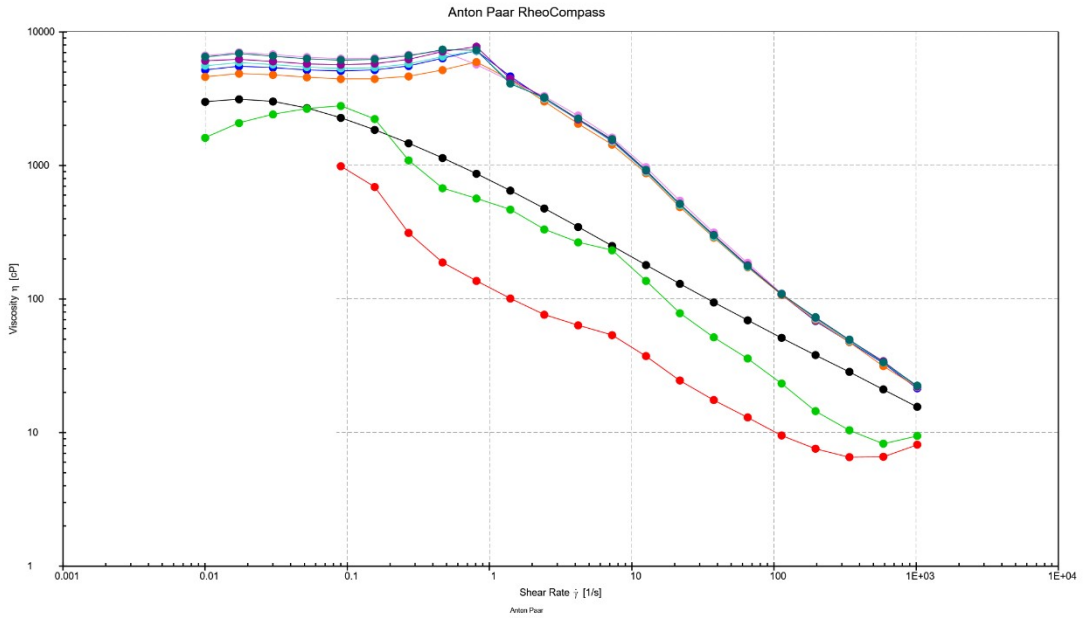

Figure 46. Rheological behaviors of SRM-1382 polymer in water (black curve) or various 40mM salt solutions (pink - NaCl; blue - $NaNO_3$; orange - KCl; cyan - KNO_3; purple - $LiNO_3$; dark green - NH_4NO_3; red - $CaCl_2$; grass green - $MgCl_2$).

On the other hand, charge screening which leads to the neutralization of polymer surfaces is partly confirmed through the measurement of apparent ζ-potential, or more precisely, Donnan potential. Such measurements indicate that the surface potential of 10%-hydrolyzed HPAM polymer coils approaches zero when more salts are added to the solution (Figure 47). As such, the electrostatic barrier between polymer coils is reduced with increasing salinity and interaction of hydrophobic side chains between different coils are more likely.

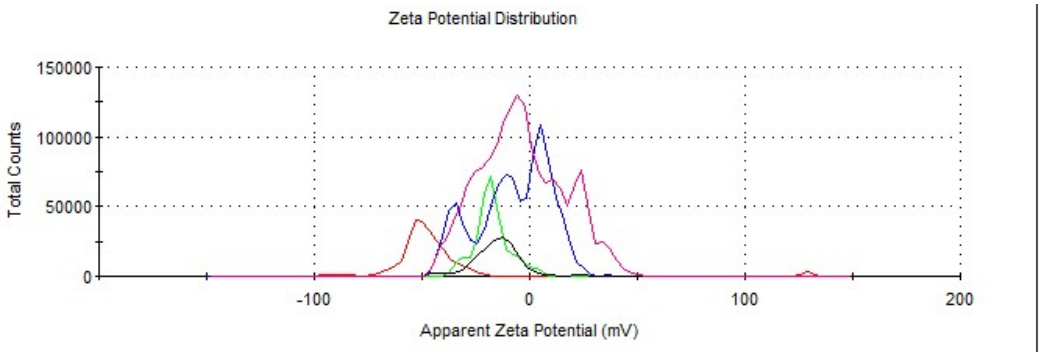

Figure 47. Donnan potential of HPAM polymer coils in water under increasing NaCl concentration (red - 0 mM; green - 5 mM; blue - 10 mM; black - 20 mM; pink - 40 mM).

Besides charge screening, increase of solution polarity offers another cogent and more comprehensive explanation to the shear-dependent viscosification under elevated salinity. As is observed in many previous examples (Figure 43, Figure 44 and Figure 45), compared with the

solution viscosity of polymer SRM-1382 in pure water, its viscosity under lower salinity actually decreases at lower shear rate ($\dot{\gamma} < 0.3\ s^{-1}$) but increases above the critical shear rate, resulting in the shear-thickening behavior. The charge screening effect alone is not sufficient in explaining such shear rate-dependent behavior, while the reasoning based on polarity, when coupled with the description regarding shift between intramolecular and intermolecular interactions at different shear rate (as is predicted in our modeling work), can satisfactorily explain such seemingly contradictory dual behavior. Briefly speaking, increase of salinity leads to higher solution polarity, discouraging the existence of individual hydrophobic chains in the solution and promotes their interaction and assembly. Whether such assembly is dominated by intramolecular or intermolecular interaction is largely dependent on their relaxation time constant relative to the shear rate. When intramolecular hydrophobic assembly dominates, we can observe decrease in solution viscosity, and when intermolecular assembly prevails, increase in viscosity is expected.

4.7.2 Effect of Surfactants

In order to solubilize the otherwise insoluble hydrophobic or amphiphilic monomers before the syntheses of hydrophobically modified PAM, surfactants are very often an essential ingredient for such polymerization, and due to the nature of gel polymerization and associated work−up, surfactants remain in the final polymer product. It has been suggested that surfactants can influence the rheological behaviors of polymer solutions[28,29], so it is sensible to investigate their specific role in shear-thickening polymer solutions as an important external contributing factor.

It has been reported that the concentration of surfactant with respect to their critical micelle concentration (CMC) can alter the rheology of solution of hydrophobically modified water-soluble polymers, and the concentration just below CMC will enhance the solution viscosity most significantly as the so-called "micellar bridging" which maximizes intermolecular interaction is most pronounced at this concentration (Figure 48). In the light of such statement, the maximum viscosification a surfactant can boost is determined by its CMC, so those surfactants with higher CMC are preferable as they are able to bridge more hydrophobic sidechains before they self-aggregate above CMC. Among common low-cost surfactants, sodium dodecyl sulfate (SDS) has the highest CMC due to its anionic nature and relatively short hydrocarbon chain (Table 4).

[28]S. Biggs, J. Selb, F. Candau. Effect of surfactant on the solution properties of hydrophobically modified polyacrylamide. *Langmuir***1992,***8,* 838 − 847.
[29]S. Biggs, J. Selb, F. Candau. Copolymers of acrylamide/N-alkylacrylamide in aqueous solution: the effects of hydrolysis on hydrophobic interactions. *Polymer***1993**, *34*, 580-591.

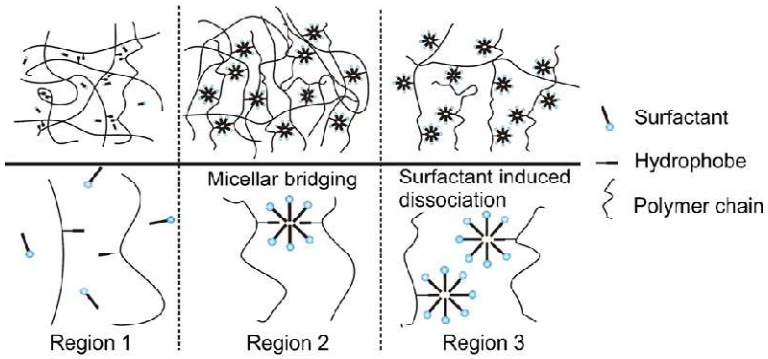

Figure 48. Illustration of surfactant-polymer interaction at various surfactant concentrations.[28]

Table 4. Parameters of common surfactants used in this study.

Surfactant	Abbr.	MW (g/mol)	SDS (M)	SDS (g/L)
Cetyltrimethylammonium chloride	CTAC	320	1.3×10^{-3}	0.416
Polyoxyethylene (23) lauryl ether	Brij L23	1199.8	6.0×10^{-5}	0.072
Sodium dodecyl sulfate	SDS	288.3	8.2×10^{-3}	2.36
Sodium dodecyl benzyl sulfonate	SDBS	348.4	1.2×10^{-3}	0.418
nonylphenol ethoxylate (9.5)	NP-9.5	639.0	8.5×10^{-5}	0.0543

Because the as-synthesized hydrophobically-modified PAM contains surfactants from the syntheses, we propose to remove them via dialysis first before further study. Experimentally, a bag made of dialysis membrane (cutoff MW ~14,000 Da) is filled with polymer solution containing surfactants and placed in a tank of deionized water. Small surfactant molecules diffuse into the tank due to differences in chemical potential, leaving large polymer coils behind thanks to size exclusion. At equilibrium, the surfactant concentration inside the bag is negligible due to large volumes of water in the tank (Figure 49). We have measured the surface tension of water in the tank after dialysis and have found out that it is indeed lower than that of pure water (69 dyn/cm *vs.* 72 dyn/cm), confirming the diffusion of surfactants.

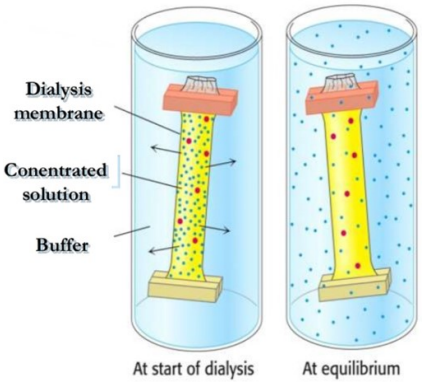

Figure 49. Removing surfactants from polymer solution via dialysis.

Rheology measurements offer further evidence that surfactants are indeed remove and this has affected the solution viscosity. Direct comparison indicates that solution viscosity of 2000 ppm SRM-1382 is slightly lowered after surfactants are removed (Figure 50, grey and indigo curves), suggesting that surfactants indeed play a role in interconnecting the polymers and viscosifying the solution. More interestingly, the salt effect of hydrophobically-modified PAM solution manifests itself quite differently when surfactants are largely absent from the system. Comparison of pristine (**Figure 43**) and surfactant-removed (Figure 50) SRM-1382 solutions under same salinity reveal thatthe surfactant-removed SRM-1382 solution is more "non-responsive" towards the increase of ionic strength, namely the solution viscosity decreases and does not show any shear-thickening property at lower NaCl concentrations (Figure 50, indigo, green and orange curves), similar to the behavior of regular HPAM without hydrophobes. Only at higher NaCl concentration (≥ 40 mM) does the surfactant-removed SRM-1382 solution start to become dilatant once again (Figure 50, pink curve). This is in contrast to the case of surfactant-containing SRM-1382, where viscosification and shear-thickening immediately occur even when only low concentration of NaCl (500 ppm, or 8.56 mM) is added. Such distinction further proves that surfactants facilitate the bridging of hydrophobic side chains, even though intermolecular assembly and viscosification can still be triggered by suitable salinity and shear rate in the absence of surfactants.

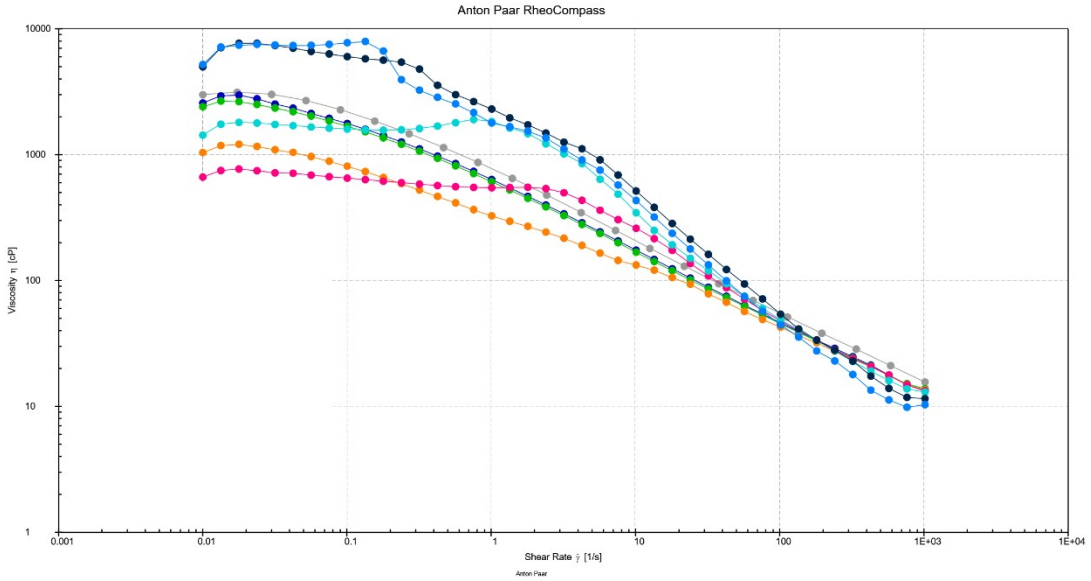

Figure 50. Rheology of pristine (grey curve) and surfactant-removed SRM-1382 polymer solution under various NaCl concentration (indigo - 0 mM; green - 10 mM; orange - 20 mM; pink - 40 mM; cyan - 100 mM; black - 200 mM; blue - 400 mM).

One of our motivations for investigating the effect of surfactants is the tunability of rheological

behaviors of functionalized polyacrylamides (FPAMs). Although the rheology of polymer solution is also partially influenced by the hydration of dissolved macromolecules, it is still fundamentally determined by polymer characteristics (composition, molecular weight, monomer distribution). Therefore, one cannot apply a single formulation of polymer to various scenarios where different rheological behaviors are desired. In order to introduce flexibility towards rheology tuning, it is highly desirable to add small amount of additive that can alter the associative behavior of FPAMs, and we have proven that surfactants can be an effective such additive due to its unique amphiphilicity. Although the research of rheological behaviors of various polymer-surfactant systems has been conducted for around three decades, most studies focus on only one species of surfactant, with the exception of a few reports,[30,31] and even these reports mainly investigate the discrepancy between surfactants carrying different charges (i.e., nonionic, anionic and cationic surfactants).

As such, we take advantage of a polymer synthesized during Task 4-2 of this project, namely N-benzylacrylamide-modified partially-hydrolyzed polyacrylamide (BAM-HPAM), and demonstrate how different species of surfactants, especially the ones carrying the same charge and resembling in structures, can affect the rheology of this BAM-HPAM solution in a somewhat surprisingly contrasting manner. We propose that besides the more obvious electrostatic factor, the dynamics of mixed micelles formed between surfactants and hydrophobic sections of polymers also significantly affect the rheological behavior of the polymer solution. We believe that as a factor long being neglected, the dynamics of micelles can actually be used as an effective tuning knob to achieve very different rheological characteristics for a single BAM-HPAM polymer.

In this study, the copolymer of acrylamide (AM), acrylic acid (AA) and N-benzylacrylamide (BAM), hereafter termed BAM-HPAM, is synthesized and used as the model polymer of hydrophobically-modified HPAM. The reasoning for designing such a polymer is two-fold. On one hand, benzyl group is a relatively small hydrophobic functional group compared with other more common hydrophobes (such as dodecyl group), so their self-association at concentration of 2000 ppm is minimal. As is seen in the viscosity-concentration plot (Figure 51), the viscosity of BAM-HPAM solution increases almost linearly with the concentration with no inflection point corresponding to the critical association concentration (CAC) observed, in contrast to the cases of many other hydrophobically-modified PAMs where such relationship is exponential, suggesting that the benzyl groups are too short to effectively bridge two polymer chains and facilitate the formation of polymer networks which are responsible for the viscosification of the solution. Consequently, all the changes in rheological characteristics in this polymer system can be unambiguously attributed to the addition of surfactants rather than the hydrophobes themselves. On the other hand, albeit being small, the benzyl group is still capable of inducing effective intermolecular interactions via dispersion forces, which leads to the interaction between benzyl

[30]Smith GL, McCormick CL (2001) Water-soluble polymers. 79 - Interaction of microblocky twin-tailed acrylamido terpolymers with anionic, cationic, and nonionic surfactants. Langmuir 17:1719–1725 . https://doi.org/10.1021/la001221l

[31]Penott-Chang EK, Gouveia L, Fernández IJ, Müller AJ, Díaz-Barrios A, Sáez AE (2007) Rheology of aqueous solutions of hydrophobically modified polyacrylamides and surfactants. Colloids Surfaces A Physicochem Eng Asp 295:99–106 . https://doi.org/10.1016/j.colsurfa.2006.08.038

groups and the hydrophobic tails of surfactant molecules and hence the facile formation of mixed micelles.

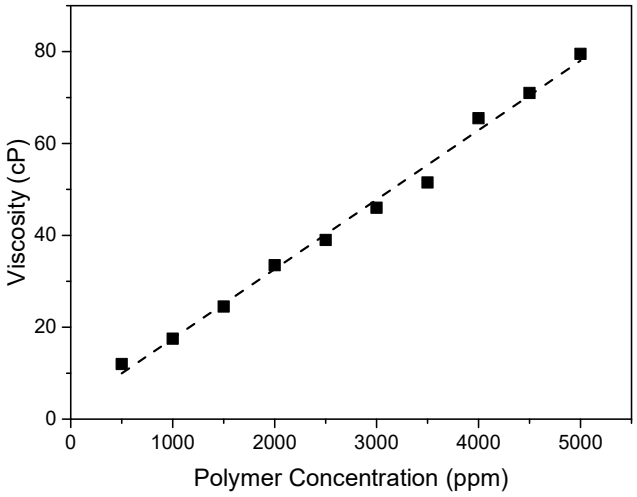

Figure 51. Viscosity-concentration relationship of BAM-HPAM solution measured at 7.92 s^{-1}.

Synthesis-wise, the BAM-HPAM copolymer is synthesized via the micelle polymerization in water which ends up with a hydrogel. Due to the fact that crude polymer product does not undergo precipitation or other separation methods before drying and pulverization, it contains extra surfactants, oligomers and possibly unreacted monomers, which need to be removed in order to confidently determine the rheological properties of BAM-HPAM alone without interference. To do so, we dissolved the pulverized polymer product in water and dialyzed the solution with several batches of large amount of deionized water using semi-permeable membrane with a cut-off molecular weight at 14,000 Da, which should effectively remove most small molecules and oligomers from the polymer solution.

The dialyzed polymer solutions are ready for investigation of their interactions with external surfactants. First, their intrinsic rheological property is examined (Figure 52), which shows pseudoplasticity typical to unmodified PAM and HPAM (Figure 52, black curve). An almost invisible hump appears at medium shear rate range (10-50 s^{-1}), which may indicate the very weak, if existent attraction between benzyl groups. Higher salinity (Figure 52, blue, red and grey curves) results in monotonically decreasing viscosity because of the charge screening effect in which the added electrolytes shields the negative charges carried by the acrylate groups on polymer chains, diminishes the electrostatic repulsion and extension of chains, promotes their coiling and structural collapse, and thus leads to lower viscosity. Such shear-thinning phenomenon is in sharp contrast to many hydrophobically-modified PAM solutions, where the addition of electrolytes leads to enhancement of interpolymeric hydrophobic interactions and higher viscosity, demonstrating that the interaction between benzyl groups is indeed minimum in the absence of additives.

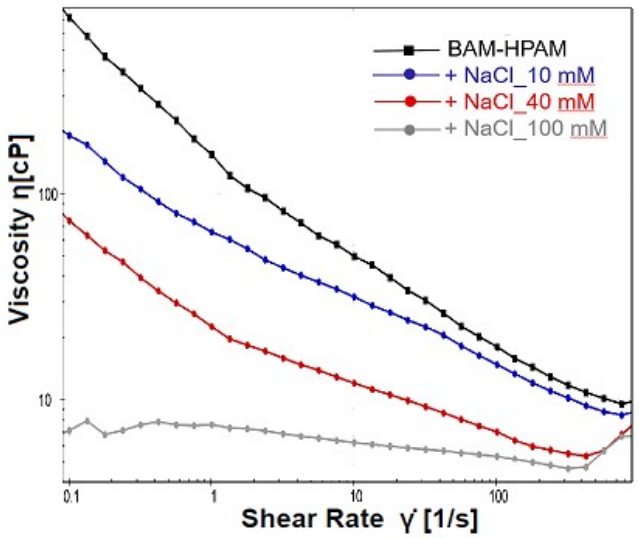

Figure 52. Rheology characteristics of 2000 ppm dialyzed BAM-HPAM solutions with 0 (black curve), 10 mM (indigo curve), 40 mM (red curve) or 100 mM (grey curve) NaCl.

Upon mixing dialyzed BAM-HPAM solutions with various concentrations of SDS, some interesting changes in the rheology of resultant solutions can be observed (Figure 53). At 0.05- and 0.10-times 2.36g /L, or the critical micelle concentration (CMC) of SDS (Figure 53, indigo and red dashed curves), the overall viscosity of BAM-HPAM solution decreases considerably, suggesting that the charge screening effect by sodium cations in SDS plays a dominant role in these scenarios. However, as the dose of SDS further increases to 0.15-, 0.20- and 0.25-times CMC (Figure 53, grey, green, orange and pink solid curves), the viscosity boosts significantly, suggesting the formation of hybrid micelles comprising SDS molecules and BAM blocks on the polymers that collectively bridge separate polymer chains to form networks. When the dose of SDS is raised to 0.35-, 0.40- (Figure 53, cyan and blue solid curves), 0.45- and 0.50-times CMC (Figure 53, dark turquoise and purple dashed curves), the viscosity again drops throughout the entire tested range of shear rate. Such decrease is attributed to the fact that as more SDS is added to the solution, the average percentage of BAM in a mixed micelle will reduce, which translates to weakened bridging between polymer chains and lower viscosity. In this particular combination of BAM-HPAM and SDS, the turning point seems to be between 0.25- to 0.30-times CMC of SDS, which may root from the fact that the drastic structural difference between phenyl group and dodecyl group as well as the diminished electrostatic repulsion significantly lowers the effective CMC when the mixed micelles are considered.

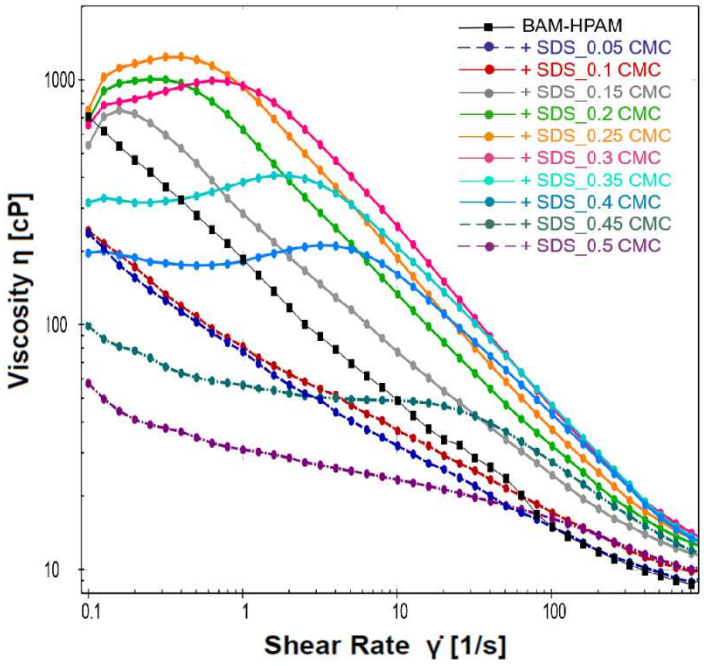

Figure 53. Rheology curve of 2000 ppm dialyzed BAM-HPAM solution with 0 (black solid curve), 0.05 (indigo dashed curve), 0.10 (red dashed curve), 0.15 (grey solid curve), 0.20 (green solid curve), 0.25 (orange solid curve), 0.30 (pink solid curve), 0.35 (cyan solid curve), 0.40 (blue solid curve), 0.45 (dark turquoise dashed curve), or 0.50 (purple dashed curve) times CMC of SDS surfactant.

Another notable rheological feature from this combination of polymer and surfactant is the emergence of Newtonian or even shear-thickening behavior at low to medium range of shear rate (0.1 - 30 s^{-1}) when the concentration of SDS is suitable. Particularly, when the dose of SDS is 0.35- or 0.40-times CMC (Figure 53, cyan and blue solid curves), there is a clear crossover between the rheological curves with the original one when SDS is absent (Figure 53, black solid curve), which unambiguously reveals that at least one factor with respect to the shear rate is not taken into account in the previous discussion. To the best of our knowledge, the mechanism behind such unusual crossover has not been explained in established literature, and we will elaborate on this topic in subsequent paragraphs as more results are revealed.

To elucidate the influence of structures of surfactants, surfactants other than SDS are added to the BAM-HPAM solution in order to observe their impacts on the rheology. Nonylphenol ethoxylate with an average number of repeating units of ethylene oxide equal to 9.5 (NP-9.5) is a widely used non-ionic surfactant, and when added to BAM-HPAM solution, a monotonical decrease in viscosity across the entire range of shear rate tested is observed as the dose of NP-9.5 reaches CMC. As NP-9.5 does not contribute to the ionic strength of the solution, it must have disrupted the original polymer configuration which results in the viscosity decrease. Compared with the anionic SDS, one distinction of NP-9.5 is that the lack of repulsion between surfactants and polymers render intrapolymeric bridging more likely, namely NP-9.5 molecules are prone to

form mixed micelles with various BAM blocks on a single polymer chain (especially when polymer solution is dilute or semi-dilute), which causes polymer coils to shrink and viscosity to drop. Another interesting feature of these rheological behaviors is that as the dose of NP-9.5 surpasses CMC and further rises, the overall viscosity largely remains constant, neither further decreases nor bounces back. One explanation for this is that the relatively large size of NP-9.5 does not allow formation of mixed micelles containing only one BAM block (i.e., the steric hinderance does not permit each BAM block to be "saturated" by NP-9.5 molecules, as opposed to the case of SDS), instead the bridging micelles always dominate no matter how high the concentration of NP-9.5 is.

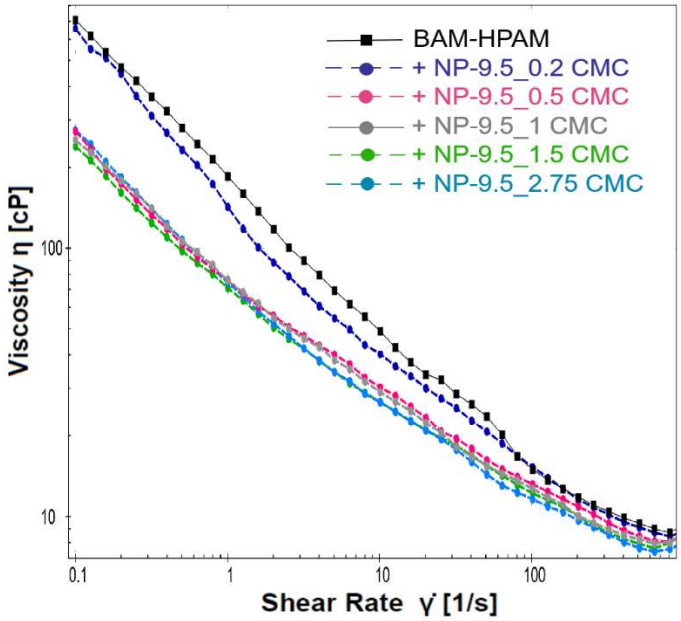

Figure 54. Rheology characteristics of 2000 ppm dialyzed BAM-HPAM solutions with 0 (black curve), 0.2 (indigo curve), 0.5 (pink curve), 1 (grey curve), 1.5 (green curve), or 2.75 (blue curve) times CMC of NP-9.5 surfactant.

Another structurally more relevant surfactant to be examined is the sodium dodecylbenzyl sulfonate (SDBS) (Figure 55). Similar to the case of SDS, as the dose of SDBS increases, the viscosity decreases initially due to charge screening effect (Figure 55, indigo and red dashed curves), then increases (Figure 55, grey, green and orange solid curves) and reaches maximum when the dose is 0.6-times CMC, after which the viscosity again decreases (Figure 55, cyan, blue and dark turquoise solid curves). However, one notable distinction in this set of data to the case of SDS is that throughout the range of concentration of SDBS, neither Newtonian or shear-thickening behavior nor crossover with the original viscosity curve is observed. In other words, these is no substantial differences between low shear rate range (0.1 - 1 s^{-1}) and medium shear rate range (1 - 10 s^{-1}) when the viscosity increases or decreases with the addition of SDBS, as opposed to the case of SDS in which the extent of viscosity change is clearly highly shear rate dependent.

We believe the underlying mechanism for such difference lies in the dynamics of micelles. Once formed in the solution by amphiphilic species, micelles are in dynamic equilibrium as they constantly exchange individual surfactant molecules with the environment as well as completely disintegrate and then reintegrate. The former process, involving fewer molecules, is known as the fast relaxation process (characterized by relaxation time τ_1), while the latter one is termed slow relaxation process (characterized by relaxation time τ_2) and is more important towards explaining the difference in rheological behaviors when the same polymer is mixed with different surfactants. Obviously, SDBS micelles possess larger τ_2 than SDS due to their structural bulkiness, so dynamic process to form and break apart the mixed micelles containing BAM-HPAM and SDBS is more sluggish than the one involving SDS. When the solution of BAM-HPAM and SDBS is subject to shear, the high spinning rate encountered does not permit the mixed micelles to reintegrate if they disintegrate, as the polymers are stretched and the system is constantly disturbed at a strain rate higher than $1 / \tau_2$. Therefore, the mixed micelles are virtually locked in a static state independent of the actual shear rate, and the entire system still manifests pseudoplasticity, behaving just like linear HPAM but with overall higher viscosity due to the bridging of mixed micelles.

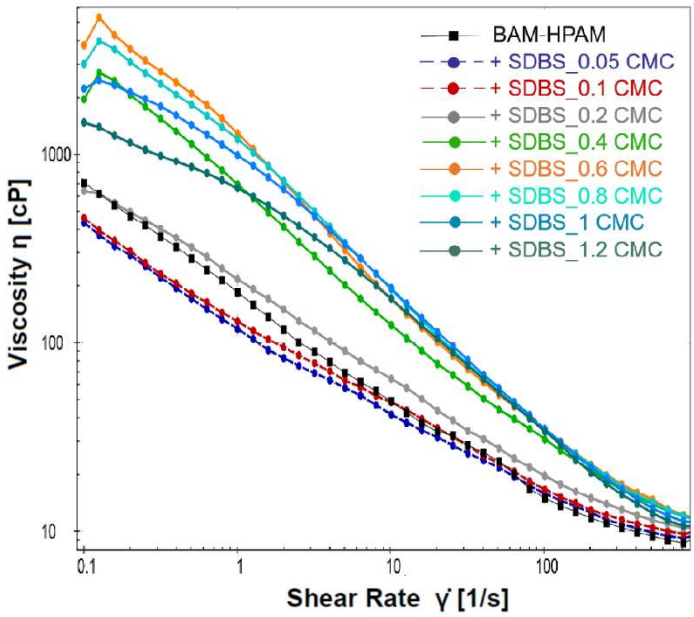

Figure 55. Rheology curve of 2000 ppm dialyzed BAM-HPAM solution with 0 (black solid curve), 0.05 (indigo dashed curve), 0.10 (red dashed curve), 0.20 (grey solid curve), 0.40 (green solid curve), 0.60 (orange solid curve), 0.80 (cyan solid curve), 1.0 (blue solid curve), and 1.2 (dark turquoise dashed curve) times CMC of SDBS surfactant.

On the other hand, the rheological phenomenon of the mixture of BAM-HPAM and SDS is dependent on the shear rate and thus more complicated (Figure 53). The slow relaxation time τ_2

of the mixed micelles involving SDS is much shorter, comparable to or even shorter than the typical timescale encountered during rotational shear. Consequently, it becomes possible for the mixed micelles to disintegrate and then reintegrate at the shear rates of interests, and when the shear rate changes, these mixed micelles are capable of reorganizing and adopting the most favorable configuration under that particular condition of deformation. Specifically, under lower shear rate where polymer chains are naturally twisted, more benzyl hydrophobes are buried inside the coils than exposed to the solvent, leading to the formation of more intrapolymeric mixed micelles than interpolymeric ones when SDS is introduced, which result in the overall decrease (or disproportionately low increase) of viscosity. As the shear rate increases and polymer chains are forced to stretch which exposes more benzyl hydrophobes, some SDS molecules discharged from the intrapolymeric micelles assemble around these exposed hydrophobes to form new interpolymeric micelles which bridge separate polymer chains, thus enhancing polymer networks and compensating for the viscosity loss due to forced polymer stretching, which ultimately manifest itself as Newtonian or even dilatant characteristics. Such transition between interpolymeric association and interpolymeric association when shear rate changes is not plausible in the case of SDBS due to the large τ_2 of the mixed micelles involving SDBS, which simply indicates the incapability of the micelles to disintegrate and then reintegrate in a different configuration given the timescale of the shear.

To summarize, we showcase that the rheological behaviors of hydrophobically-modified polyacrylamide can be rationally modulated through the addition of various surfactants. Besides the well-known electrostatic factor, dynamics of micelles formed between polymers and surfactants is demonstrated to be an effective but previously neglected parameter that can be utilized to attenuate or viscosify the hydrophobically-modified polyacrylamide solution in a shear-rate-dependent manner. Particularly, Newtonian and dilatant behaviors can be observed when such dynamics is fast, which bears significant technological implications. Although this study focuses on one model polymer (BAM-HPAM) and several surfactants (SDS, NP-9.5, SDBS), the conclusion can be generalized to many other polymer-surfactant systems. Further investigation will extend to the detailed quantification of micellar dynamics in order to achieve fine control of the rheological behaviors of polymers in the presence of surfactants, which may prove to be of great convenience towards industrial applications.

4.8 SRMs as Potential Flocculants for Special Wastewater

One of the niche applications our SRMs hold potential in is the treatment of special wastewaters. Most municipal, industrial and agricultural wastewaters are collected through sewage systems and treated collectively in water treatment plants, but some wastewaters from special origins such as dye houses, poultry farms and restaurants cannot be effectively treated via traditional approaches due to the presence of soluble or partially soluble organics (dye molecules, proteins, etc.), which are too small to be removed via physio-chemical methods, yet too large to be digested via biological methods. In this task, we divert a small portion of our resources to carry out a side project to preliminarily evaluate the efficacy of our SRMs as a potential flocculant for removing

soluble organics from special wastewaters. Our hypothesis is that the hydrophobically-modified HPAM in the SRM formulations not only inherits the properties such as high molecular weight and high degree of hydrolysis (i.e., high charge density) from regular HPAM which are proven to be advantageous in flocculating particles, but also possesses hydrophobic pendants which may offer additional attractive interactions with organics (i.e., van der Waals force) that facilitates their removal.

Table 5. Common Pollutants in Textile Effluents.[32]

Process	Compounds
Desizing	Sizes, enzymes, starch, waxes, ammonia.
Scouring	Disinfectants and insecticides residues, NaOH, surfactants, soaps, fats, waxes, pectin, oils, sizes, anti-static agents, spent solvents, enzymes.
Bleaching	H_2O_2, AOX, sodium silicate or organic stabiliser, high pH.
Mercerizing	High pH, NaOH
Dyeing	Colour, metals, salts, surfactants, organic processing assistants, sulphide, acidity/alkalinity, formaldehyde.
Printing	Urea, solvents, colour, metals.
Finishing	Resins, waxes, chlorinated compounds, acetate, stearate, spent solvents, softeners.

Among the aforementioned special wastewaters, we started with textile wastewaters (

Table 5), one of the most polluted wastewaters due to their characteristics, such as high chemical oxygen demand (COD) concentration, strong color, high pH and temperature, and low biodegradability. These effluents are complex in composition, especially due to the various dye molecules used during the dyeing process (Table 6), and can thus exhibit serious environmental problems and public health concerns if improperly disposed.

Table 6. Classification of textile dyes.

Type	Solubility	Chemistry	Application
Acid dye	Soluble	Anionic compound	silk, wool, nylon, acrylic fiber
Azoic dye	Soluble → Insoluble	Diazoic + coupling compounds	cotton
Basic dye	Soluble	Cationic compound	acrylic fiber
Direct dye	Soluble	Polycyclic Aromatic Compounds	cotton, paper, leather, wool, silk, nylon

[32] Z. Wang *et al.* Textile Dyeing Wastewater Treatment. in Advances in Treating Textile Effluent, P. Hauser (Ed.), InTech 2011, pp 91-116.

Dispersive dye	Insoluble	Azobenzene / Anthraquinone	polyester
Mordant dye	Insoluble	Chelating agent	wool
Reactive dye	Soluble	Chlorotriazine, etc.	cotton, wool, nylon
Sulfur dye	Soluble	Nitrophenol + (poly)sulfide	cotton
Vat dye	Insoluble	Oxidative neutral compound	cotton

Various treatment processes have been proposed and utilized to treat textile dyeing wastewater (**Table 7**), among which coagulation & flocculation is undoubtedly the most economic method in terms of both chemicals and equipment. This method can be further classified into combined coagulation & flocculation and direct flocculation[33]. In this task, our plan is to first synthesize several cationic and anionic PAM-based polymers with or without hydrophobes and then test their efficacy when used as flocculants alone or in conjunction with inorganic coagulant. The wastewater sample was acquired from a local dye house that uses reactive dye (**Table 6**), which is probably the most challenging type of dye as it is not only water-soluble but also possesses low charge density.

Table 7. Treatment processes of textile dyeing wastewater.

Non-biological Methods	Biological Methods	Emerging Techniques

• **Physical Methods**
  • Floatation
  • Sedimentation
• **Chemical Oxidation**
  • Fenton Reaction
  • Ozone Oxidation
• **Physicochemical Methods**
  • Adsorption
  • Coagulation & Flocculation
• **Membrane Process**
	• **Aerobic Treatment**
	  • Activated Sludge
	  • Biofilm
	• **Anaerobic Treatment**
		• **Combinatorial Processes**
		• **Chemical Methods**
		  • Photochemical Oxidation
		  • Electrochemical Oxidation
		  • High-Energy Physics Process
		• **Physical Methods**
		  • Ultrasonic Method

Our preliminary results of flocculation tests offer several insights. Firstly, filtration leads to more complete removal of flocs than sedimentation after the application of flocculant in all scenarios, as is revealed by the lower values of COD, indicating that the flocs is not yet large enough to settle quickly. However, this should not be an issue in industrial applications as the flocs would be allowed to settle for a much longer period of time (weeks vs. hours). Secondly, higher dosage of

[33]Lee CS, Robinson J, Chong MF (2014) A review on application of flocculants in wastewater treatment. Process Saf Environ Prot 92:489–508 . https://doi.org/10.1016/j.psep.2014.04.010

flocculants does not necessarily lead to lower COD values, which suggest that there is a limit for the electrostatic attraction effect and bridging effect, two major mechanisms of flocculation, and more flocculants soluble in water actually contribute to higher COD themselves. Thirdly, cationic polymer flocculants perform consistently better than their anionic counterparts, which is expected as many reactive dyes are water-soluble molecular or oligomeric anions.

Table 8. Effect of direct flocculation of reactive dye wastewater using various flocculants.

Flocculant Dosage	FlocculantType	Hydrophobe in Flocculant?	COD (supernatant)	COD (filtered)
-	-	-	209	217
40ppm	Cationic	No	212	193
80ppm	Cationic	No	203	191
40ppm	Cationic	Yes	185	156
80ppm	Cationic	Yes	162	155
40ppm	Anionic	No	299	253
80ppm	Anionic	No	367	288
40ppm	Anionic	Yes	290	253
80ppm	Anionic	Yes	317	275

Our final insight and the most important one is that charged PAMs functionalized with hydrophobes, the major component of our SRM formulations, outperform their counterparts without hydrophobes. This is a clear indication that our initial hypothesis that the pendant hydrophobes on polymer chains lead to enhanced attraction of soluble organics, in this case reactive dyes, through van der Waals force. We believe that such mechanism needs to synergize with electrostatic and bridging mechanisms in order to take effect and remove soluble organics effectively, as the van der Waals force is weak by itself and formation of large flocs through such attraction only is unlikely. In other words, a PAM-based polymer simultaneously possess higher molecular weight, appreciable charge density and pedant hydrophobes are imperative to function as a effective flocculant for aforementioned special wastewaters.

Based on such promising observation, we are setting out to test the efficacy of our new flocculants when used in conjunction with inorganic coagulant (such as aluminum sulfate) as well as use other types of wastewaters as testbeds. Our hope is to expand the application of the SRMs developed in this project and bring broader impacts.

4.9 Laboratorial Core-Flooding Tests

Following the system setup finished at the end of Quarter III (see previous progress report for details), core flooding tests are carried out as a major component of the work conducted during Quarter IV and Quarter V of this project.

4.9.1 Materials

Polymers: Two polymer samples were used in this study. The first one was SRM-1382, a functionalized PAM-based polymer developed during this DOE-STTR Phase II project by incorporating special monomer into HPAM backbone; the second one was 3630S, a commercially available high molecular weight, water-soluble regular HPAM.

Crude Oil: One crude oil from field is used. The oil contains substantial amount of waxy contents and the wax decomposition temperature is ~ 40 °C. Table 9 and Table 10 list some measured properties of this oil.

Table 9. API measurements of crude oil at Room Temperature (25 °C).

Sample	Mass	Volume	Density
Distilled Water	99.67 g	100.00 mL	0.9967 g/mL
Crude Oil	91.47 g	100.00 mL	0.9147 g/mL
Specific Gravity (SG) of the Crude Oil = 0.9147 g/ml ÷ 0.9967 g/ml = 0.9177			
$API\ of\ the\ Crude\ Oil = \frac{141.5}{SG} - 131.5 = \frac{141.5}{0.9177} - 131.5 = 154.2 - 131.5 = \mathbf{22.7}$			

Table 10. Viscosity of crude oil under various shear rates and temperatures.

Temperature	Viscosity at Different RPM and Shear Rates		
	6 rpm or 7.94 sec^{-1}	12 rpm or 15.9 sec^{-1}	30 rpm or 39.7 sec^{-1}
25 °C	Crude oil not flowable, viscosity not measurable.		
35 °C	101 cP	76.5 cP	56.0 cP
50 °C	11.0 cP	12.0 cP	11.2 cP

Core Sample: Coreplugs with distinguishable permeability were used. The low-perm Bentheimercoreplug had an air permeability of ~ 800 mD and fluid permeability of ~ 600 mD, while the high-perm Bentheimercoreplug had an air permeability of ~ 3000 mD and fluid permeability of ~ 2000 mD. Their properties are listed in Table 11.

Table 11. Bentheimer Core Properties.

Core Sample	Low Permeability	High Permeability	Unit
Rock Type	Bentheimer	Bentheimer	
Estimated k	600	2000	mD
Diameter	3.661	3.661	cm
Length	24.72	24.72	cm
Mass	442.58	515.42	g
Mass (Left side)	206.69	239.68	g
Mass (Right side)	235.89	275.74	g
Bulk vol.	260.22	260.22	cm^3
Porosity	0.266	0.229	
Area	10.53	10.53	cm^2
PV	69.27	59.70	cm^3
Temperature	50	50	°C

Brines: Brines used are synthetic, produced by mixing the chemicals and deionized water according to the geochemical analysis of water samples from candidate fields. Various smart brines were prepared for coreflooding by using synthetic seawater (SW) with different dilution factors and optimization of calcium ions. Phase behaviors of different polymer concentrations under various brine conditions were studied. The final brine solution used in the coreflood experiments contains monovalent ions with TDS ~ 8000ppm with no divalent cations added. Nevertheless, the phase behavior studies suggested the presence of certain amounts of divalent cations (e.g., Ca^{2+}) could even enhance the shear-thickening performance of the SRM-1382 polymer, as is discussed in detail in Section 4.4 of this report.

4.9.2 Methods

Engineered Brines: Multiple engineered brines were analyzed, prepared, and selected as precondition fluids to enhance the compatibility and longevity of the special polymers in the harsh reservoir formation. The coreplugs were flooded with the selected engineered brines with each of the two tested polymer formulations, to establish impact on oil displacement efficiency as a function of pore volumes injected. This involved screening and short-listing multiple combinations of polymer-in-brine samples. These shortlisted formulations were further tested

under reservoir pressure, temperature, oil saturation and wettability conditions.

Multi-permeability Core Flood: One important innovation in this experiment is the side-by-side multi-permeability core flood. The tested coreplugs were assembled by placing two semi-cylindrical coreplugs to form one cylindrical coreplug. One semi-cylindrical part comes from the high-perm coreplugs, which is pre-saturated with brine only, whereas another semi-cylindrical part comes from the low-perm coreplugs, which is pre-saturated with crude oil. Consequently, such an assembled multi-permeability coreplug has three zones with distinguishable permeability, namely, the low-perm zone (~ 600 mD), the high-perm zone (~ 2000 mD), and the middle large channel.

This allowed the generation of two near identical assembled multi-perm coreplugs used for the two coreflood - one with the regular HPAM polymer flood, and another one with shear-thickening SRM-1382 polymer flood.

Procedure for Core Preparation:

1. Select 2 Bentheimer core with different fluid permeability (~2000 mD vs. ~600 mD) and similar physical size, use a 10" industrial tile/brick saw to cut the cores to the same length;

2. Cut the coreplugs into 2 pieces along their axes. Mark the core cuts as:

"Low L": The left side of the core with lower permeability,

"Low R": The right side of the core with lower permeability,

"High L": The left side of the core with higher permeability,

"High R": The right side of the core with higher permeability,

3. Place the coreplugs in the oven with 105 °C for 24 hours to remove any water inside;

4. Cool down the coreplugs in a vacuum oven with room temperature, measure the weight of each piece of the coreplugs;

5. Place the coreplugs into 2 core holders respectively with confining pressure 650 psi, vacuum the core with negative 13 psi for 24 hours;

6. Saturate the coreplugs with the synthetic softened injection brine (SSIB) for 24 hours;

7. Measure the weights of the coreplugs with brine and the density of the brine at this temperature, calculate the pore volumes of the coreplugs;

8. Place the coreplugs into the core holder in the oven with 500 psi confining pressure and 150 psi backpressure at reservoir temperature 50 °C;

9. Inject synthetic softened brine with 500 ppm dithionite at three different injection rates to measure absolute permeability of the coreplugs to water.

Oil Saturation in the Core with Lower Permeability:

1. Filter the crude oil from candidate oilfield at reservoir temperature 50 °C in an oven under 70 psi pressure by use of 0.45 μm cellulose acetate filters;

2. Place both "Low L" and "Low R" core cuts in the core holder for saturation with the crude oil;

3. Saturate the coreplugs with the lower permeability with the oil at 70 °C, aging the core with dead oil at 70 °C for 7 days with confining pressure 500 psi and back pressure 150 psi;

4. Bring down the temperature to reservoir temperature of 50 °C, calculate the OOIP and the initial oil saturation based the amount of brine displaced and collected.

Polymer Flood on the Mixed Combined Cores:

1. Filter all polymer solution through a nitrocellulose membrane with 5.0 μm pore size under 20 psi nitrogen pressure;

2. Combine "High L" and "Low R" to assemble a new coreplugs "Core A"; combine "Low L" and "HighR" to assemble a new coreplugs "Core B";

3. Conduct polymer flood with SRM-1382 for "Core A" and HPAM polymer 3630S for "CoreB" at flow rate of 1 ft/day (0.06 mL/min) for ~ 4 PV;

4. Adjust the flow rate to 2 ft/day, 3 ft/day, 4 ft/day for ~1 each PV injection;

5. For "Core A" and "Core B", compare the oil cut (V%), cumulative oil recovery (V%) and remaining oil saturation (V%).

4.9.3 Results

The effluents collected during the flooding of SRM fluid is shown in Figure 56(a) while those collected during flooding of HPAM fluid is shown in Figure 56(b). For each coreflood test, 70 plastic tubes were used for the effluent collection. Figure 56(a) shows considerable amount of crude oil was recovered by use of SRM-1382 polymer at 1000 ppm and 50 °C, while there was no oil recovered by regular HPAM polymer3630S as shown in Figure 56(b).

(a) (b)

Figure 56. Comparison of oil recovery from side-by-side core flood test: (a) By use of 1000 ppm SRM-1382; (b) by Use of 1000 ppm 3630S regular HPAM polymer.

This indicates that the injected SRM-1382 polymer has been diverted from the fault zone to the high permeability zone and successfully diverted into the low-perm core, where oil actually resided. This provides direct evidence that SRM-1382 polymer could slow down flow in the high-perm zone and divert the fluid to the low-perm zone, whereas the regular PAM-based polymers did not exhibit that capability. Details of the oil recovery by SRM-1382 are shown in Figure 57.

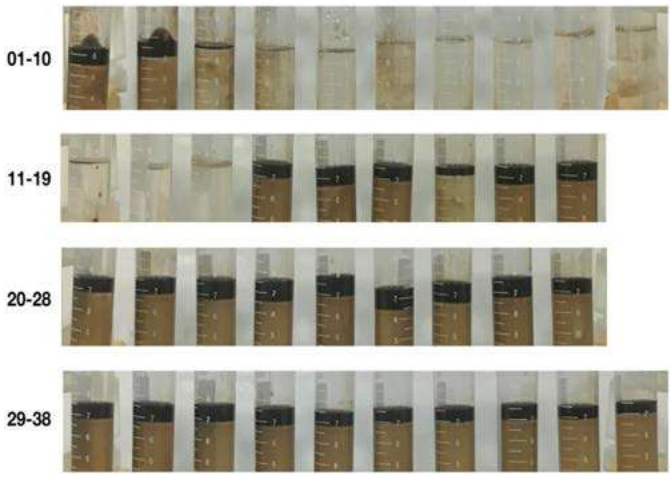

Figure 57. Tubes containing crude oil recovered by SRM-1382. Tube# 01-10: collected at flow rate = 0.06 mL/min (~ 1 ft/day, 1.1 PV); Tube# 11-19: collected at flow rate = 0.12 mL/min (~ 2 ft/day, 1.0 PV); Tube# 20-29: collected at flow rate = 0.18 mL/min (~ 3 ft/day, 1.0 PV); Tube# 29-38: collected at flow rate = 0.24 mL/min (~ 4 ft/day, 1.1 PV).

The experimental data and cumulative oil recovery calculated based on the effluent collection shown in Figure 56(a) and Figure 57 are listed in Table 12.

Table 12. Cumulative Oil Recovery, Remaining Oil Saturation by SRM-1382 Polymer Flooding.

Mass Balance								
Flow rate	Tube	Cumulative Volume	Cumulative PV	Oil Volume	Oil Cut	Cumulative Oil	cum oil recovered	So
[ml/min]	#	[ml]	[PV]	[ml]	%	[ml]	[%]	[%]
	1	5.93	0.11	0.43	7.30%	0.43	1.69%	68.13%
	2	12.36	0.22	0.42	6.57%	0.86	3.34%	66.98%
	3	19.36	0.33	0.00	0.00%	0.86	3.34%	66.98%
	4	26.36	0.44	0.00	0.00%	0.86	3.34%	66.98%
0.06	5	33.36	0.56	0.00	0.00%	0.86	3.34%	66.98%
	6	40.36	0.67	0.00	0.00%	0.86	3.34%	66.98%
	7	47.36	0.78	0.00	0.00%	0.86	3.34%	66.98%
	8	54.36	0.89	0.00	0.00%	0.86	3.34%	66.98%
	9	61.36	1.00	0.00	0.00%	0.86	3.34%	66.98%
	10	68.36	1.11	0.00	0.00%	0.86	3.34%	66.98%
	11	75.36	1.22	0.00	0.00%	0.86	3.34%	66.98%
	12	82.36	1.33	0.00	0.00%	0.86	3.34%	66.98%
	13	89.36	1.44	0.00	0.00%	0.86	3.34%	66.98%
	14	96.54	1.55	0.29	4.02%	1.14	4.47%	66.20%
0.12	15	103.74	1.67	0.60	8.33%	1.74	6.81%	64.58%
	16	111.06	1.78	0.41	5.62%	2.16	8.41%	63.47%
	17	118.19	1.89	0.13	1.87%	2.29	8.93%	63.11%
	18	125.16	2.00	0.37	5.26%	2.66	10.36%	62.12%
	19	132.44	2.11	0.59	8.08%	3.24	12.66%	60.53%
	20	139.56	2.22	0.21	2.97%	3.46	13.48%	59.96%
	21	146.84	2.33	0.49	6.71%	3.94	15.39%	58.63%
	22	154.02	2.44	0.38	5.26%	4.32	16.86%	57.61%
	23	161.13	2.55	0.61	8.59%	4.93	19.25%	55.96%
0.18	24	168.60	2.66	0.57	7.59%	5.50	21.46%	54.43%
	25	175.77	2.78	0.77	10.70%	6.27	24.45%	52.35%
	26	182.91	2.89	0.54	7.62%	6.81	26.57%	50.88%
	27	190.16	3.00	0.44	6.13%	7.26	28.31%	49.68%
	28	197.33	3.11	0.28	3.87%	7.53	29.39%	48.93%
	29	204.42	3.22	0.29	4.08%	7.82	30.52%	48.15%
	30	211.76	3.33	0.53	7.27%	8.36	32.60%	46.71%
	31	218.84	3.44	0.19	2.65%	8.54	33.34%	46.20%
	32	225.93	3.55	0.29	4.08%	8.83	34.46%	45.41%
0.24	33	233.01	3.66	0.28	3.92%	9.11	35.55%	44.66%
	34	240.22	3.77	0.21	2.93%	9.32	36.37%	44.09%
	35	247.58	3.89	0.36	4.83%	9.68	37.76%	43.13%
	36	254.83	4.00	0.26	3.52%	9.93	38.76%	42.44%
	37	261.93	4.11	0.20	2.82%	10.13	39.54%	41.90%
	38	269.22	4.22	0.29	3.95%	10.42	40.66%	41.12%

Figure 58 summarizes the cumulative oil recovery (%) and Sor (%) from collected tubes with respect to PV of injected fluid. Because the shear stress is related to the injection flow rate, we also varied the flow rate of injection. Although 1 ft/day is commonly used as a standard flow rate in core flood experiments, we have only recovered a relatively small amount of OOIP with this flow rate. One possible explanation is that under this flow rate, the shear stress acting on the injection fluid is below the maximum shear rate. With increasing flow rate, thus increasing shear stress, the viscosity of polymer solution increased in the high-perm zone, consequently the solution was successfully diverted into the low-perm zone to push out oil from low-perm coreplug. The overall oil recovery from core-A by SRM-1382 was over 40% OOIP, whereas no oil was recovered by using the regular HPAM 3630S polymer as shown in Figure 59. Further investigation

will be carried out in our upcoming experiments to confirm this hybrid EOR formulation at various levels of heterogeneity and reservoir conditions.

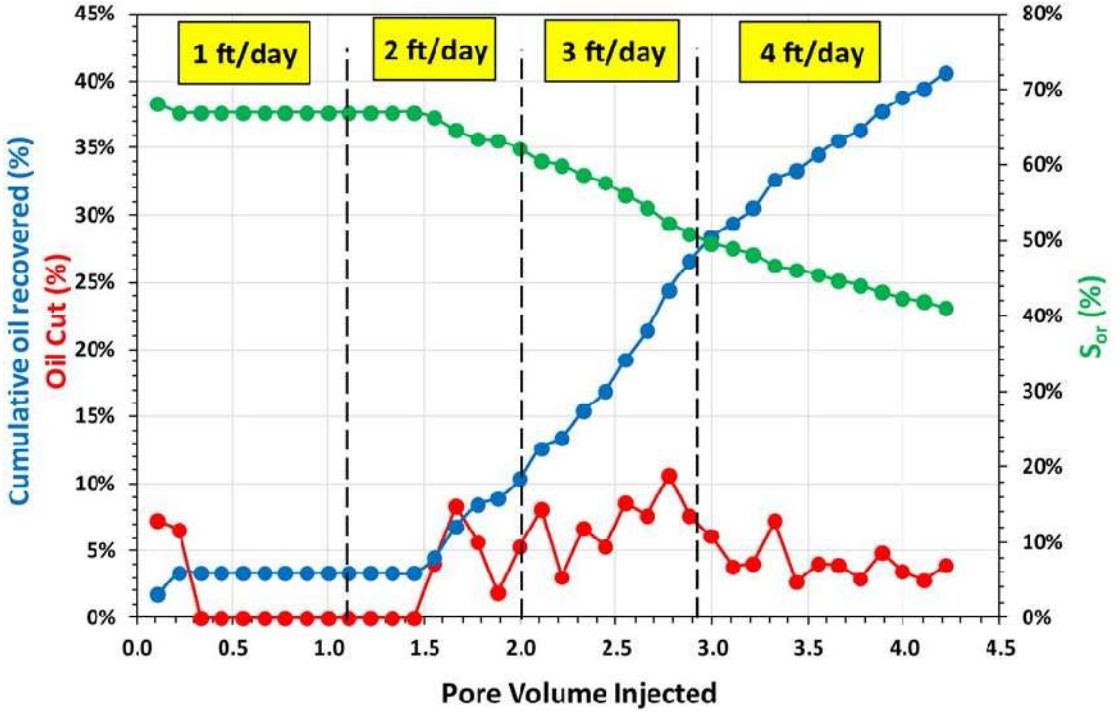

Figure 58. Cumulative oil recovered (blue line), oil cut (red line) during the SRM-1382 flooding at different injection rates and remaining oil saturation in the core (green line).

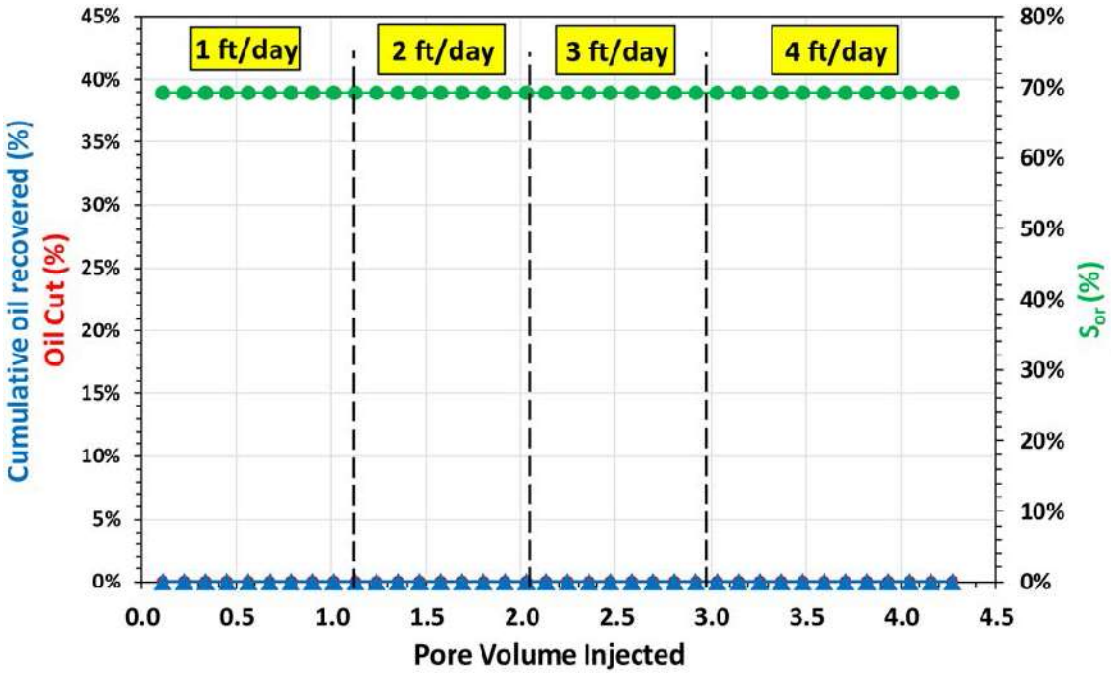

Figure 59. Curves of cumulative oil recovered (blue line), oil cut (red line) during the 3630Sflooding at different injection rates and remaining oil saturation in the core (green line).

Figure 60 demonstrates the oil was substantially swept in the case of the novel SRM-1382 fluid, whereas "Core B" did not show evidence of successful sweep from the hybrid EOR formulation with HPAM. The oil in "Core B" was resident in the plug with an indication that some of it was moving towards the outlet without breaking through into the effluent stream.

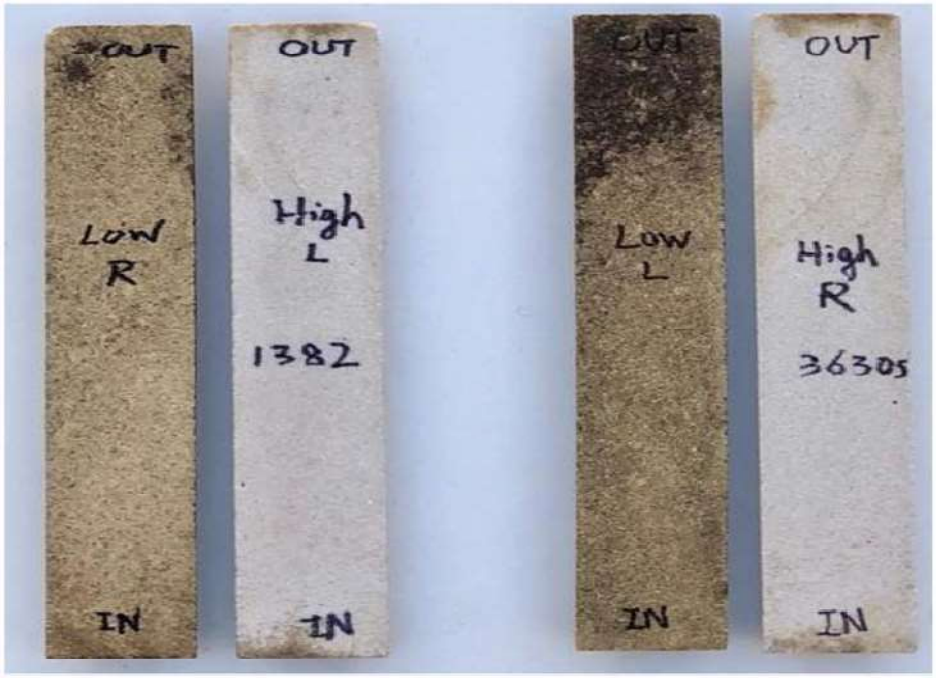

(a) (b)

Figure 60. Comparison of the Bentheimer core samples after oil recovery by use of the two polymers without alkaline and surfactant: (a) 40% (v/v) of OOIP recovered by use of 1000 ppm SRM-1382; (b) Zero OOIP recovered by use of 1000 ppm EOR workhorse HPAM 3630S.

4.10 Digital Core Flooding Studies

As is stated in the work plan, major tool for the digital core flooding studies conducted during this Phase II project will be MATLAB Reservoir Simulation Toolbox (MRST), a free open-source software package for reservoir modeling and simulation, developed by the Computational Geosciences group in the Department of Mathematics and Cybernetics at SINTEF Digital, and Heriot-Watt University, NTNU, TNO and TU Delft. The software consists of a minimal core module offering basic data structure and functionality, as well as different add-on modules for various specific purposes. Another advantage of MRST is that it is compatible with ECLIPSE, an industry-reference simulator that offers the industry's most complete and robust set of numerical solutions for fast and accurate prediction of dynamic behavior for all types of reservoirs and

development schemes. In other words, MRST directly accepts parameter input files in ECLIPSE-compatible formats.

4.10.1 Protocol for Simulation

A simulation model for digital core flooding studies can be considered to consist of two main parts; the first part describes the reservoir rock and the second part describes the mathematical laws that govern fluid behavior. Aquifers and natural petroleum reservoirs consist of a subsurface body of sedimentaryrock having sufficient porosity and permeability to store and transmit fluids. All sedimentary rocks consist of a solid matrix with an interconnected void. The void pore space allows the rocks to store and transmit fluids. The ability to store fluids is determined by the volume fraction of pores (the rock porosity), and the ability to transmit fluids (the rock permeability) is given by the interconnection of the pores. As the first step in MRST setup, such rocks that contain hydrocarbons or aquifer systems are modelled to become part of a simulation model. Rock formations found in natural petroleum reservoirs are typically heterogeneous at all length scales, from the micrometer scale of pore channels between the solid particles making up the rock to the kilometer scale of a full reservoir formation.To obtain a description of the reservoir geology, one builds models that attempt to reproduce the true geological heterogeneity in the reservoir rock at the macroscopic scale by introducing macroscopic petrophysical properties that are based on a continuum hypothesis and volume averaging over a sufficiently large representative elementary volume (REV).

The basic geological description of a petroleum reservoir or an aquifer system will typically consist of two sets of surfaces. Geological horizons are lateral surfaces that describe the bedding planes that delimit the rock strata, whereas faults are vertical or inclined surfaces along which the strata may have been displaced by geological processes. This basic geological description can be turned into a discrete model used to formulate various computational methods via “grid”, a tessellation of a planar or volumetric object by a set of contiguous simple shapes referred to as cells. Grids can be described and distinguished by their geometry (the shape of the cells that form the grid) and their topology (the way individual cells are connected). In a structured grid, only one basic shape is allowed and this basic shape is laid out in a regular repeating pattern so that the topology of the grid is constant in space. The most typical structured grids are based on hexahedron cells in 3D.

Once the models for porous media are set, the next step is to mathematically model the flow of fluids through the porous media, and this includes establishing forcing terms and fluid properties and connecting them with several well-known equations. Besides the fundamental Darcy’s Law, the Laplace’s Equation, or more generally the Poisson’s Equation is the important partial differential equation (PDE) that govern fluid dynamics in porous media. To solve this PDE numerically, we adopt the simplest example of a finite-volume discretization, the two-point flux-approximation (TPFA) scheme, which is used extensively throughout industry and also is the default discretization method in MRST. As inputs to the TPFA scheme, forcing terms (with the exception of gravity) and fluid properties are introduced as data objects in MRST.On one hand,

forcing terms are represented similarly using objects with data structures that are specific to boundary conditions, (volumetric) source terms, and models of injection and production wells. On the other hand, fluid properties include parameters such as density, viscosity, and compressibility. In MRST, the fluid behavior is represented as a fluid object that describes basic fluid properties. In addition, it is convenient to introduce a state object holding the reservoir states (primary unknowns and derived quantities) like pressure, fluxes, face pressures, etc.

Furthermore, for most applications of reservoir simulation, one is interested in modeling how one fluid phase displaces one or more other fluid phases. In petroleum recovery, typical examples will be water or gas flooding in which injected water or gas displaces the resident hydrocarbon phase(s). multiple phases will flow simultaneously throughout the porous medium when viewed from the scale of a representative elementary volume, even if the fluids are immiscible and do not mix on the microscale. To model this flow, three new physical properties of multiphase models, namely saturation, relative permeability, and capillary pressure are introduced.

Multiphase flow is generally governed by a number of physical effects. For simple flows, fluids can be moved by pressure differentials, by gravity segregation, capillary forces, or fluid and rock compressibility. More advanced models also involve dissolution effects, hysteresis, and molecular diffusion, to name a few. Multiphase flow equations can therefore give rise to very different behavior depending upon what are the main physical effects. In the recovery of petroleum resources, the predominant force is viscous advection caused by pressure differential. Here, pressure disturbances will in most cases propagate much faster through the porous medium than the material waves that transport fluid phases and chemical components. This means that the mathematical equations describing multiphase flow will have a mixed character. However, in the special case of incompressible rock and immiscible and incompressible fluids, the system of PDEs can be reformulated so that it consists of an elliptic equation for fluid pressure and one or more transport equations, which could be discretized and solved numerically. In MRST, a different fluid object is also implemented to reflect multiphase flow. The most basic multiphase fluid model in MRST implements a simplified version of the Corey model.

4.10.2 Setup of Models

Pursuant to the aforementioned protocol to simulate the flooding processes, we first set up grids with properties such as size, porosity, permeability, depth, etc. Initial oil saturation level as well as injection and production wells are also incorporated to picture the complete initial state (Figure 61). Next, we import the ECLIPSE-compatible data object of fluids. Specifically, this type of data object contains important parameters such as the polymer concentration-viscosity relationship, polymer concentration-absorption relationship, Todd-Longstaff mixing parameter, etc. With these components in place, we also set up several operational conditions including the injected polymer concentration, a constant flow rate at the injection well, a constant pressure at the production well, duration of each timestep and number of total timesteps. Information of the well to be simulated, for example the location, depth and size, is also record if any. The parameters applied for the following digital core with example are:

- The digital core is designed according to the real core size and properties;
- The core is standing vertically and the flow direction is from the bottom to the top, which is the case for the real coreflood experiment and the field situation;
- Cross-sectional area: 10.53 cm^2, Length: 24.72 cm;
- Number of grids: 6x5x46;
- Size of each grid: 0.540832x0.64900x0.53739 (cm);
- Porosity: 0.229;
- Pore Volume: 59.7 cm^3;
- Permeability of grids: 600 mD (left) and 2000 mD (right);
- Initial oil saturation: 0.6813 in the lower perm half, 0 in the higher perm half;
- Back pressure: 1 MPa;
- Viscosity of fluid @ 62 ^oC: oil 15cP, water: 0.46 cP; polymer 50 cP;
- Polymer injected: 2500 ppm with 50 cP viscosity, can be changed according to the viscosity vs. concentration curve;
- Injection rate: 0.06 ml/min;
- The simulation contains 100 steps, 0.2 hours for each step.

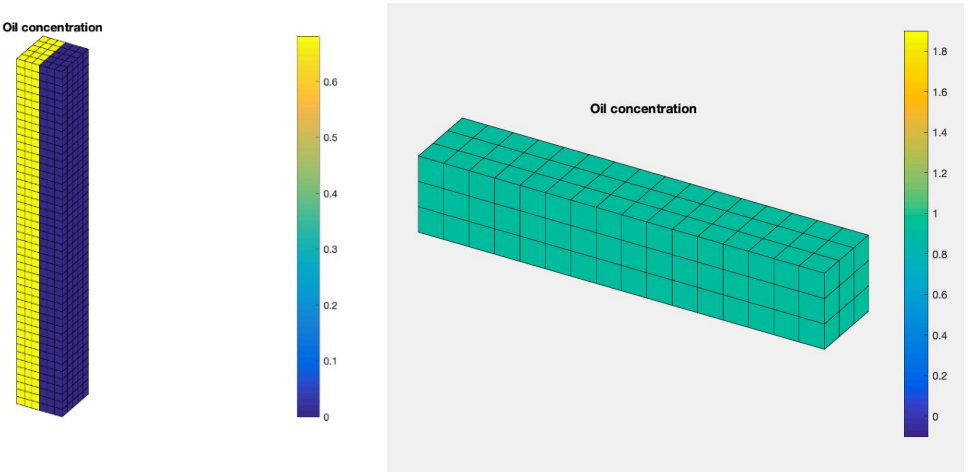

Figure 61. Initial state of a digital core.

The properties of each grid at each time step are simulated and recorded. The coreflood give rise to expected results in terms of the final gradient of pressure (Figure 62), water saturation level (Figure 63), oil saturation level (Figure 64) and polymer concentration (Figure 65). This digital core experiment shows that the normal polymer tends to flow in the channel with higher permeability. In the next stage, we will further refine our current models, including the fluid model to incorporate the rheological behavior of shear-thickening polymers.

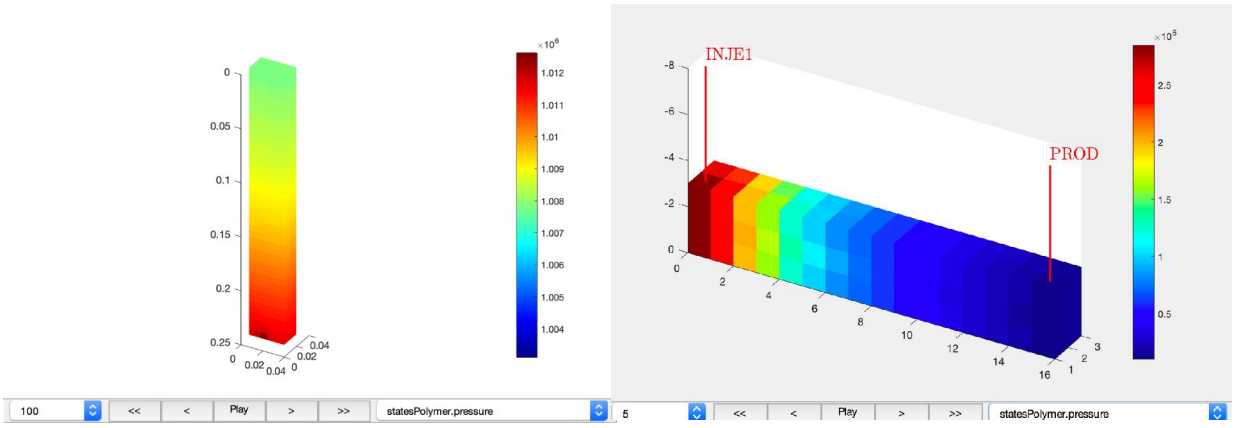

Figure 62. Gradient of pressure at the end of the simulation.

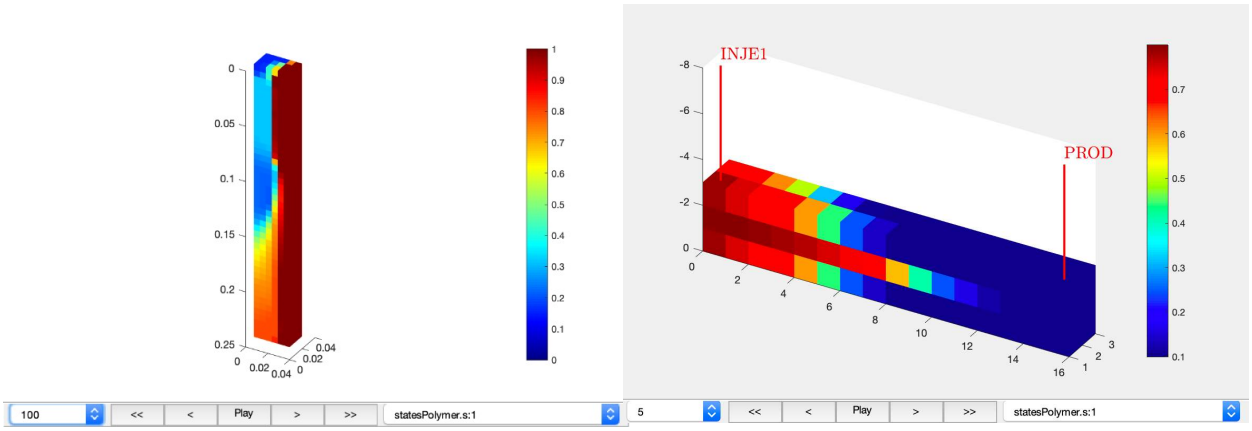

Figure 63. Gradient of water saturation level at the end of the simulation.

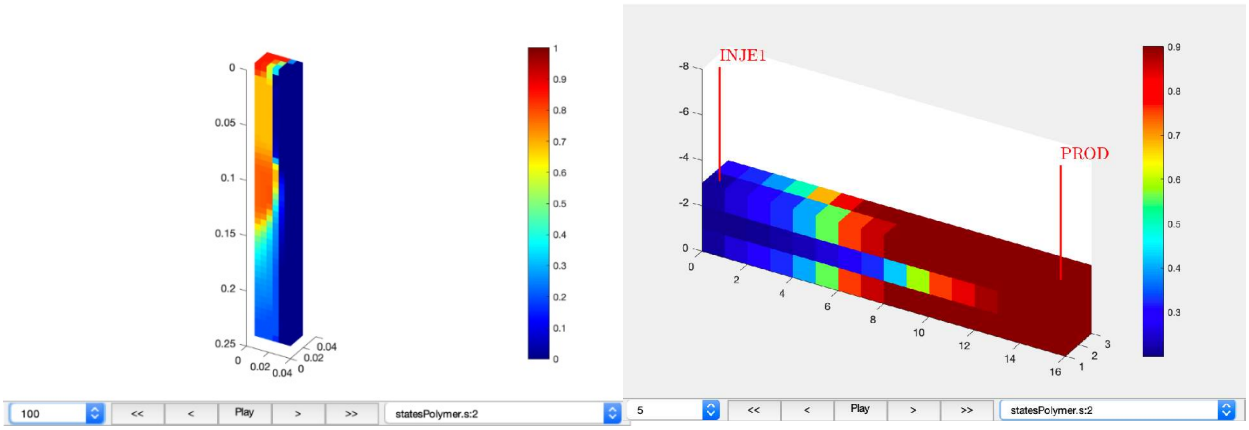

Figure 64. Gradient of oil saturation level at the end of the simulation.

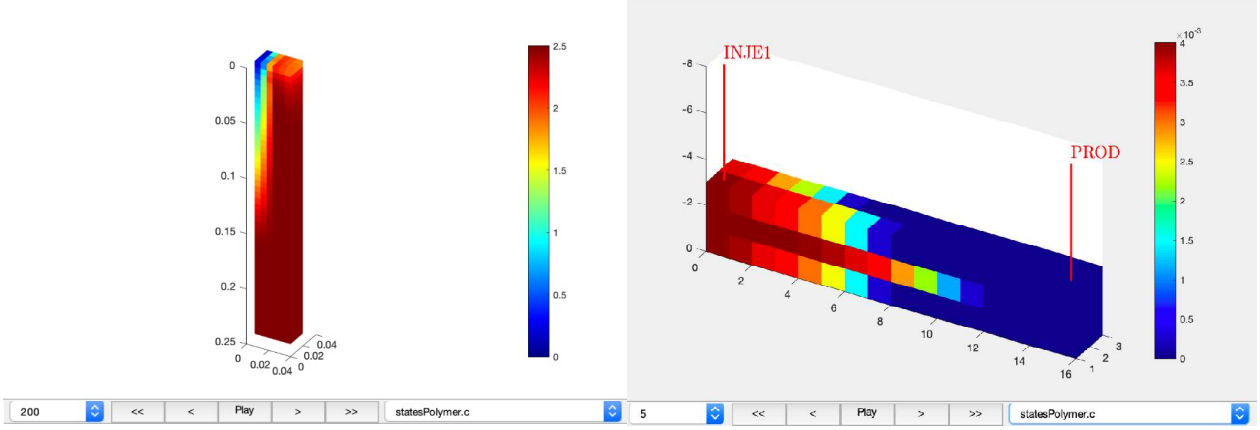

Figure 65. Gradient of polymer concentration at the end of the simulation.

4.11Reservoir Selection Criterion for the SRM-flooding Process

Criteria for reservoir selection include at least the following items: reservoir conditions (temperature, pressure, lithology, porosity, permeability, connectivity, etc.); oil conditions (OOIP, composition, viscosity, water-cut, etc.), and typical injection water and produced water information (composition, salinity, hardness, total dissolved solids, etc.). During Quarter V of this project, we start to collaborate with our industrial partner, Paladin Geological Services, to investigate several oil-producing zones throughout the US, especially the Illinois Basin, which is a 400 miles by 200 miles elongated Paleozoic depositional and structural basin, centered in and underlying most of the state of Illinois, and extending into southwestern Indiana and western Kentucky (Figure 66). The rocks in the Illinois Basin are known for being sources of coal, petroleum and nonfuel minerals. Particularly, the Illinois Basin has produced more than four billion barrels of petroleum up to date. Oil production peaked in 1940 at 140 million barrels per year, after which production declined steadily. Waterflooding of old reservoirs caused another peak of oil production in the 1950s. To this day, there are more than 1000 oilfields with about 14.1 billion barrels Original Oil in Place (OOIP) in the Illinois Basin, and only 20~40% of OOIP is recovered by the previous primary and the secondary recoveries. Therefore, the Illinois Basin hold great potential for chemically enhanced oil recovery, especially with the shear-thickening polymers developed in the current project. Further information within the scope of reservoir selection criteria will be revealed in the next progress report as it becomes available.

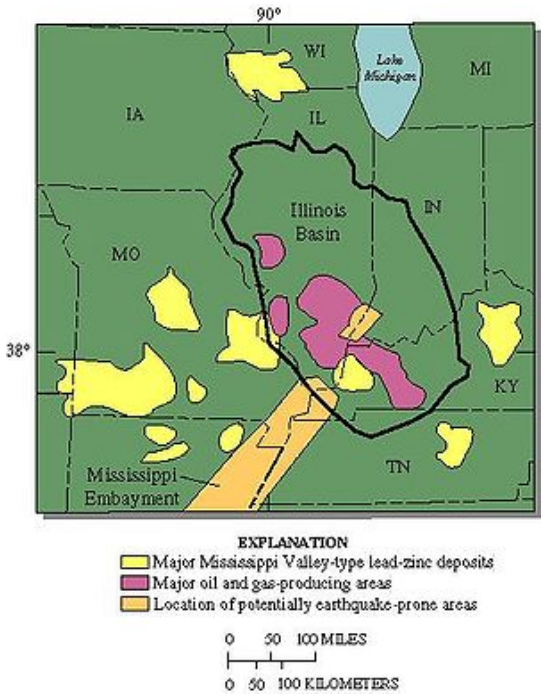

Figure 66. Location of the Illinois Basin (from U.S. Geological Survery).

The comparison of the reservoir selection criterion of our newly developed SRM-flooding process with other commonly used tertiary EOR processes are shown in Table 13. Besides aqueous-based chemical EOR processes which often involve addition of chemicals such as polymers (i.e., polymer (P) flooding), surfactants (i.e., surfactant-polymer (SP) flooding) and alkalines (i.e., alkaline-surfactant-polymer (ASP) flooding), gas injections (either miscible or immiscible) with nitrogen-based gas (air or flue-gas), hydrocarbon gases, and CO_2 have also been commercially practiced. From many years of studies, a number of reservoir selection standards have been established as are specified in SPE 113269, SPE 170695, and SPE 187576. Taber J. J. *et al.* from New Mexico Petroleum Recovery Research Center had conducted a thorough revisit on these criteria and provided a so-called "Taber's Table for EOR" summary (SPE 35383 and SPE 39234). Because our SRM-flooding EOR process is meaned to be an advanced chemicals EOR process, we focus on some detailed comparisons with the micelle P/SP/ASP flooding as follows:

1. Oil properties

The proper mobility ratio between the injected gas/fluid and the residual oil has been identified as one of the most important factors towards the success of an EOR process. Because of the low density of gases, light oil composition is generally desired. Even with the CO_2 flooding which can be in its supercritical form under high-pressure/high-depth reservoir conditions, the lower-viscosity (< 10 cP) residual oil is required. On the other hand, the aqueous-based chemical EOR processes can be applied to more viscous oil, in which the high viscosity of injection fluid is achieved by adding polymers with ultrahigh molecular weight. The role of thumb for the design of polymer-flooding is that the viscosity of the polymer solution should match the viscosity of oil

under reservoir conditions, such that a sufficiently steady sweeping can be achieved. For regular PAM-based polymer fluid, the fluid viscosity is controlled by the concentration of the polymer, which in turn, is affected by a number of factors such as the designed pumping power and budgeted chemical cost. For the SRM-flooding, an additional fluid viscosity can be generated from the shear-thickening effect. Therefore, we speculate that the SRM flooding process can be applied to reservoirs with the residual oils are more viscous.

2. Reservoir conditions

Compared to gas injections, aqueous-based chemical flooding processes often have more strict requirements on the reservoir conditions in term of formation type, reservoir temperature, brine salinity, hardness and so on. Basically, the SRM-flooding is a polymer-based flooding, so it follows similar requirements on the reservoir conditions as for the P/SP/ASP flooding. However, one superiority of the SRM-flooding is its ability to deal with reservoirs of high heterogeneity, e.g., non-uniform permeability, which often leads to early breakthrough of the injected gas/fluids and hence poor oil recovery. On the other hand, one drawback is the thermal stability of the SRM formulation, which is one direction of our further improvements. Due to the higher lability of the SRM formulation than the traditional PAM polymers, we foresee stricter requirement on the reservoir conditions to ensure thermal stability of the polymer solutions during operation. As a result, we set a lower reservoir temperature (< 165°F) for the SRM-flooding.

3. Additional Notes

In addition to the oil and reservoir properties, we also compare the SRM-flooding to individual P/SP/ASP flooding process as follows:

- Compared to P-flooding, a higher sweeping efficiency can be achieved because of the improved controls of the rheological properties;
- Compared to SP/ASP-flooding, there is no chromatographic separation issue in the SRM-flooding (even if additional surfactants are added to the SRM formulation, the system will still be kept integral at large due to the formation of mixed micelles).
- Like SP/ASP-flooding which involves the use of the surfactants, SRM might also experience similar issues such as adsorption loss and demulsification.

Table 13. Comparison of reservoir selection criteria of SRM-flooding with other tertiary EOR processes

	Nitrogen and Flue-Gas Flooding	**Hydrocarbon-Miscible Flooding**	**CO_2 Flooding**	**Micelle/P/SP/ASP Flooding**	**SRM Flooding**
Oil Properties					
Gravity, °API	> 35	> 23	> 22	> 20	> 18
Viscosity, cP	< 0.4	< 3	< 10	< 35	< 37

Composition	High percentage of light hydrocarbons	High percentage of light hydrocarbons	High percentage of intermediate hydrocarbon	Light to Intermediate; Organic acid for ASP	Light, intermediate to more viscous
Reservoir Conditions					
Oil saturation, % PV	> 40	> 30	> 20	> 35	> 30
Formation Type	Sandstone/Carbonate with few fractures and high permeability stacks	Sandstone/Carbonate with few fractures and high permeability stacks	Sandstone/Carbonate with few fractures and high permeability stacks	Sandstone preferred	Sandstone preferred
Net Thickness	Relatively thin unless formation is dipping	Relatively thin unless formation is dipping	Relatively thin unless formation is dipping	Not Critical	Not Critical
Average permeability, mD	Not critical if uniform	Not critical if uniform	Not critical if uniform	> 10	> 100, Non-Uniform
Depth, ft	> 6000	> 4000	Depth, Temp, and Oil API are related	< 9000	< 7500
Temperature, °F	Not Critical	Effect on minimum miscibility pressure (MMP)		< 200	< 165
Additional Notes					
Applicability	Light Oil, Deep reservoir with high pressure	High pressure for LPG, steeply dipping formation is desirable	Low-cost CO_2 source	> 50% sweep efficiency; Low concentration of divalent cations	Control of fluid rheology
Problems	Viscous fingering, product separation, corrosion problems.	Viscous fingering, large quantities of HC gases, Solvent recovery issue	Corrosion problems, early breakthrough	Complex and expensive system, chromatographic separation, Adsorption and degradation of chemicals, early breakthrough	Adsorption on carbonate or high-clay content reservoirs, demulsification issues?

4.12 Engineering Processing

Our laboratorial core flooding studies (Section 4.5) offer exciting results with respect to engineering considerations. First of all, no pressure accumulation was observed throughout the flooding process, suggesting that the association of shear-thickening polymer did not block pores and channels that are vital to oil production. Secondly, polymer solution recovered from the core flooding process shows viscosity profiles very close to the original one (Figure 67), excluding the

possibility of several polymer adsorption onto solid surfaces of rocks. Last but not least, recovered oil-water mixtures are clearly phase separated (Figure 57), thus circumventing any tricky demulsification processes. These engineering aspects will be constantly monitored as we move forward.

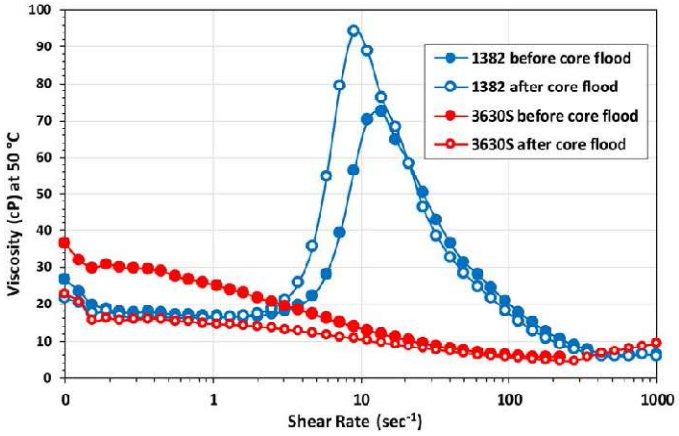

Figure 67. Rheology of solutions of shear-thickening polymer (blue curves) and HPAM (red curves) before and after core flooding processes at 50°C.

The engineering processing of the SRM flooding procedure will be very similar to that of the traditional polymer flooding (P-flooding), which has been well developed and commercialized. In general, as a polymer-augmented water flooding process, P-flooding is a sequential flooding after the regular water flooding (secondary recovery). It has been found that the P-flooding is more effective in the early stages of a waterflood while the mobile oil saturation is still high. Once the oil saturation becomes lower, additional chemicals such as surfactant or surfactant + alkaline will be needed, leading to the more complex engineering designs and process costs.

One of the main processing designs in polymer flooding is the slug design which was widely practiced in 1960's (SPE 7043). Polymer slugs were injected at constant concentration during field operations. As a polymer bank propagates through porous media, the front edge gradually is stripped of polymer, which is adsorbed onto the rock. The concept of programming a polymer slug is an attempt to more effectively match the mobility of the fluids ahead of and behind the slug. The slug starts at the relatively high concentration and declines to a fairly low concentration. The variation in polymer concentration circumvents two disadvantages of using constant concentration polymer slugs. Currently, the programmed slug is used in almost all polymer and surfactant-polymer flooding field operations. An intermediate mobility-control slug of constant polymer concentration may be injected between the initial and terminal slugs. The initial slug is smaller than the terminal slug.

In principle, the SRM-flooding is an improved polymer flooding operation, so its engineering process will be very similar to that of the polymer flooding. Besides, the SRM polymer slugs can either be used standalone, or be combined with regular PAM polymer flooding at different stages to enhance the overall ability in oil recovery.

4.13Economic Assessment

There are several major factors that affect the overall economics of SRM flooding. Most of the non-technical factors cannot be easily quantified in an exact manner because of the many uncertainties related to global and regional policies, economic development, reservoir characteristics and technology advancement. Therefore, we only focus on the economic assessments associated with technology, processes and materials rather than the uncontrollable factors.

The polymer costs are determined by at least two factors: (1) the amount of polymer needed; and (2) the unit price of polymer manufactured. Currently, at least two main types of polymers are being used in the polymer-based EOR flooding, namely the synthetic polyacrylamide (PAM) and its derivatives and xanthan gum-based biopolymers. PAMs are derived from petroleum products, so their costs are more associated with the crude oil price. Other costs, such as those for oxygen scavenger, biocide, and quality water, also are significant to the polymer flooding, as they are often be included in the polymer slug. Depending on reservoir and brine conditions, different types of the PAMs are manufactured, such as the ultrahigh molecular weight products, high-temperature-resistant products and high-salinity-resistant products. Costs of PAMs vary, and the typical average price is at $1.30 per lb. Xanthan gums are polysaccharide-based biopolymers which are mainly manufactured by the fermentation of glucose and sucrose. Xanthan gums can also be used in food additives as viscosifiers and thickeners. Despite of its extensive developments in recent decades, the manufacturing cost of the xanthan gum is still very high, nearly twice of that of PAMs, at the average cost of $2.5 per lb. However, because xanthan gums are produced biologically, their cost will be less sensitive to the to the crude oil price. In addition, with the development of the advanced biological and biochemical processes, the manufacturing cost of xanthan gum could be constantly reduced. For example, more and more non-food-grade bio-waste or bio-mass raw materials can be utilized for the xanthan gum productions; highly-efficient purification and separation processes are also being developed to further reduce the manufacturing cost.

The manufacture process of SRM polymer should be very similar to that of the conventional PAMs, because the two share same molecular backbones and major chemical ingredients. The only noticeable difference between SRM and PAM is the addition of the special monomers, typically at 1~5 wt%, to SRM polymers to improve their rheological performances. Consequently, we foresee that the overall manufacturing cost of SRM when the process is scaled up and becomes more mature, will be at the level of $1.5 to $1.7 per lb, i.e., about 10-20% higher than that of PAM.

The operational cost of PAM-based, xanthan-gum-based, and SRM-based flooding will also be similar. However, the chemical treatment such as filtration for xanthan gum will be more costly than for PAMs, because of its inherent branched structure. This usually increases the operational cost for xanthan-gum-based flood by as high as $0.50/bbl of oil produced. On the other hand, the requirement of fresh water supply for xanthan gum is not as critical as for PAMs, because xanthan gum is normally more salt tolerant than PAMs. In some regions, the treatment costs of the surface

water and produced water for PAMs will be more significant than for xanthan gum biopolymers. SRM polymers are in nature synthetic polymers (PAM-like) but also possess high viscosity (Xanthan-like), so we expect certain increments of the operation cost of the SRM-flooding than conventional PAM-based flooding.

The potential economic advantage of the SRM-flooding is the possibility to use the lower concentration of chemicals when compared to the traditional PAM-based flooding, in which case the key factor in maintaining a favorable mobility ratio between the injected fluid and the residual crude oil under reservoir conditions is to use higher concentration of polymer on the surface, such that the viscosity of the polymer fluid could match the oil viscosity underground after certain viscosity loss after the initial injection and transportation in the matrix. One unique feature of our SRM formulation is its ability to modify the fluid viscosity according to the change of the shear stress, i.e., it possesses lower viscosity at very low shear rate (during storage) or very high shear rate (during injection), but switch to high-viscosity form at moderate shear rate. This uniqueness of SRM formulations enables the better design to use substantial lower chemical concentration in the polymer slug than regular PAMs. Conventionally, in order to achieve favorable mobility ratio, the minimum polymer concentration in the polymer slug is in the range of 250 to 2500 ppm, depending on the oil viscosity. We expect that for the SRM-flooding, the required concentration would be significantly lowered (by 40-60%), so the typical range of usage will be 150 to 1000 ppm. This cost reduction might well compensate the manufacturing and operational costs of the SRM-flooding.

5. Summary and Outlook

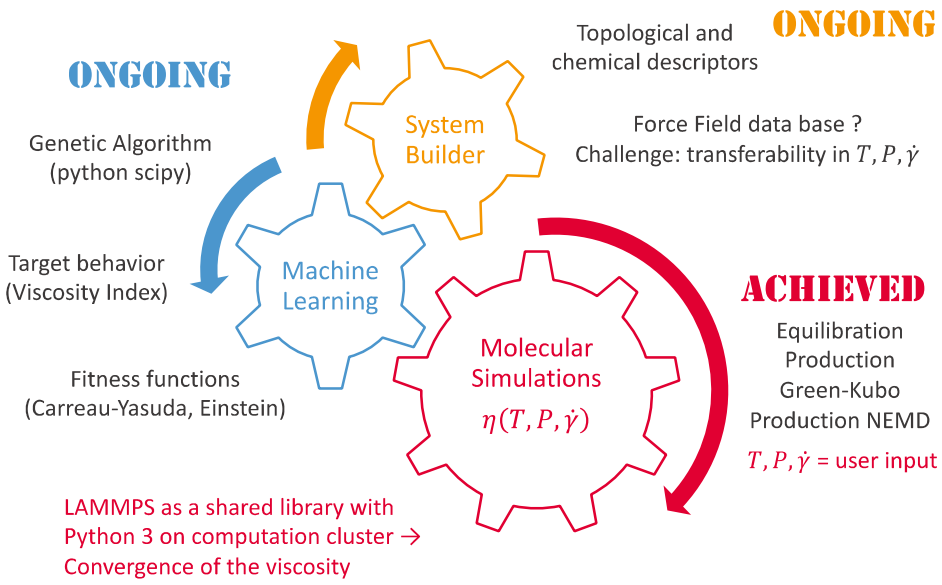

Figure 68. Schematic to represent state of progress in computational work.

During this Phase II program, our progress in computational work (depicted graphically in Figure 68) includes:

1. Connected Machine Learning scheme (Genetic Algorithm) to molecular simulations (atomistic and CG levels).

2. Improved automated and systematic convergence criteria for viscosity computation, which requires interpolation of the average viscosity as a function of time, and calculation of the slope of the viscosity as a function of shear rate.

3. Developed new and chemically accurate Coarse-grain Force Fields for polyethylene (PE), polyethylene glycol (PEO) and PAM (with polar and non-polar interactions) over different T and P ranges.

Quantum mechanical optimization with dispersion corrections, temperature (up to 1kilo K) and pressure fitting up to 1GPa of the non-bond terms in new coarse-grain force fields for PE, PEO, and PAM force fields. Conventional coarse-grain force field are trained to one specific set of TP conditions, which renders them useless for applications to EOR, involving significant changes in both. Our PAAM CG force field has also been trained to include polar interactions. We are currently advancing in integrating to optimized valence terms for 2 and 3 body terms of the force fields.

4. Systematic polymer builder. We currently have a systematic coarse-grain model builder capable of topological descriptors, as described in our previous report, including Additive length (AL), Degree of branching (DB), Branching frequency (BF), Branch length (BL). We are now working to add chemical descriptors.

Our ML test platform uses the Distributed Evolutionary Algorithms in Python (DEAP), the Scikit-Learn, and the Atomic Simulation Environment (ASE) Genetic Algorithm (GA) module libraries in python to drive the lower level calculations, performed mostly under the LAMMPS parallel molecular simulations package.

We now have preliminary CG force field non-bond components for PE, PEO and PAAM and validated for our polarizable force fields Rexpon. We expect to have the full framework operational within Phase II, in order to steer experimental synthesis of polymer mixtures based on PE, PEO and PAM. Furthermore, since we've guaranteed by design that the results are matching our atomistic reactive and polarizable force field Rexpon, this will allow us to do further characterization of the best performers via chemometrics directly at the rexpon level; after performing the corresponding CG-atomistic mapping.

Technical feasibility of our proposed approach has also been further demonstrated experimentally. In this Phase II program, we have proposed two experimental work packages, namely (1) syntheses and characterization of a series of potentially shear-thickening polyacrylamide-based polymers as candidates of SRMs and (2) coreflooding tests and digital coreflooding simulations with SRMs. Significant progress has been achieved in both work

packages, building solid technical foundations towards the commercialization of our proposed technology.

Back in Phase I, we demonstrated the possibility of achieving shear-thickening behavior by incorporating a special hydrophobic or amphiphilic monomer into the PAM/HPAM backbone. In our ongoing Phase II project, we further compile a database with commercially available or conveniently synthesizable vinyl and acrylyl monomers as entries and categorize these entries according to a variety of features (charge, hydrophobicity, reactivity, synthesizability or cost, etc.). It is worth mentioning here that molecular modeling of monomers in the database coupled with suitable machine learning techniques is proven to be useful in assisting us to decide key properties of new monomers, another demonstration of the technical feasibility of our proposed route for materials discovery. For example, our CG models have predicted the importance of polymer linearity (Figure 4), chain entanglement and possible transient crosslinking due to electrostatic or other forces, and all such factors have inspired the design of polymers that potentially possess shear-thickening properties. On the other hand, the structural features and associated rheological behaviors of model polymers are fed back to the predictive models for their refinement and improvement of accuracy.

Syntheses of polymer candidates are performed with combinations of monomers whose selection is inspired by our predictive high-throughput screening models. We pay special attention to the cost of monomers, the robustness of our syntheses (ensuring variation of environmental factors and experimental conditions beyond our control) and the scalability of our process (ensuring each procedure is cost-effective and compatible with industrial setups). Up to now, we have successfully synthesized several PAM-based functional polymers with gel polymerization method featuring high conversion rate of monomers, smooth temperature profile curve (which is particularly important when the polymerization is scaled up), good reproducibility and facile workup procedures. A patent application has been filed to protect the innovative aspects of our synthetic route (US63/018,799).

Synthesized polymers are then subject to scrutiny of their rheological behaviors in aqueous solution and their applicability as SRM components. In Phase II, we have systematically investigated various factors that could affect the flowing characteristics of polymers, especially the manifestation of shear-thickening behaviors of SRMs, including method of solution preparation, concentration, ionic strength, type of electrolytes, temperature and some additives. Such experimental study is imperative towards the applications of SRMs as the optimal condition is specific to individual SRM and cannot be precisely predicted by theoretical models yet. In short, we have demonstrated in the current phase that the rheological behavior of SRMs is highly dependent on and can be controlled by various parameters.

To evaluate the feasibility of using SRM candidates to boost oil recovery rate, we have performed novel coreflooding experiments in Phase II to compare our SRMs with a commercial HPAM. Specifically, two cores with different permeabilities are combined, and only the core with the lower permeabilities are saturated with oil. When HPAM-based fluid is injected via two channels into the two semi-cylinders simultaneously, almost all of fluid goes through the core

with higher permeability and flood out no oil at all. However, if the same experiment is performed with SRM, the polymer can partially go through the core with lower permeability and recover approximately 40% of the initial saturated oil. This is strong evidence that our predictive-model-inspired SRM formulations not only possess shear-thickening properties, but also are actually capable of dramatically boosting the oil recovery rate in zones with low permeability. Our result has been presented in Society of Petroleum Engineers Gas & Oil Technology Showcase and Conference (SPE-198557-MS).